Calhoun: The NPS Institutional Archive

DSpace Repository

Theses and Dissertations | 1. Thesis and Dissertation Collection, all items

2001

Modeling of shipboard smoke propagation with a forced counter-flow air supply

Farman, Garrett J.

http://hdl.handle.net/10945/10938

This publication is a work of the U.S. Government as defined in Title 17, United States Code, Section 101. Copyright protection is not available for this work in the United States.

Downloaded from NPS Archive: Calhoun

http://www.nps.edu/library

Calhoun is the Naval Postgraduate School's public access digital repository for research materials and institutional publications created by the NPS community. Calhoun is named for Professor of Mathematics Guy K. Calhoun, NPS's first appointed -- and published -- scholarly author.

Dudley Knox Library / Naval Postgraduate School
411 Dyer Road / 1 University Circle
Monterey, California USA 93943

NAVAL POSTGRADUATE SCHOOL
Monterey, California

THESIS

MODELING OF SHIPBOARD SMOKE PROPAGATION WITH A FORCED COUNTER-FLOW AIR SUPPLY

by

Garrett J. Farman

June 2001

Thesis Advisor: M.D. Kelleher

Approved for public release; distribution is unlimited

20010905 136

REPORT DOCUMENTATION PAGE			Form Approved OMB No. 0704-0188
Public reporting burden for this collection of information is estimated to average 1 hour per response, including the time for reviewing instruction, searching existing data sources, gathering and maintaining the data needed, and completing and reviewing the collection of information. Send comments regarding this burden estimate or any other aspect of this collection of information, including suggestions for reducing this burden, to Washington headquarters Services, Directorate for Information Operations and Reports, 1215 Jefferson Davis Highway, Suite 1204, Arlington, VA 22202-4302, and to the Office of Management and Budget, Paperwork Reduction Project (0704-0188) Washington DC 20503.			
1. AGENCY USE ONLY *(Leave blank)*	**2. REPORT DATE** June 2001	**3. REPORT TYPE AND DATES COVERED** Master's Thesis	
4. TITLE AND SUBTITLE: Title (Mix case letters) Modeling of Shipboard Smoke Propagation with a Forced Counter-Flow Air Supply		**5. FUNDING NUMBERS** N0002400WR10669	
6. AUTHOR(S) Garrett J. Farman			
7. PERFORMING ORGANIZATION NAME(S) AND ADDRESS(ES) Naval Postgraduate School Monterey, CA 93943-5000		**8. PERFORMING ORGANIZATION REPORT NUMBER**	
9. SPONSORING / MONITORING AGENCY NAME(S) AND ADDRESS(ES) NAVSEA		**10. SPONSORING / MONITORING AGENCY REPORT NUMBER**	
11. SUPPLEMENTARY NOTES The views expressed in this thesis are those of the author and do not reflect the official policy or position of the Department of Defense or the U.S. Government.			
12a. DISTRIBUTION / AVAILABILITY STATEMENT Approved for public release; distribution is unlimited		**12b. DISTRIBUTION CODE**	

13. ABSTRACT

The propagation of fire-generated smoke with a counter-flow air supply in a horizontal arrangement of shipboard compartments and passageways was modeled using a computational fluid dynamics program generated by Computational Fluid Dynamics Research Corporation. This study was based on a large-scale live fire experiment performed by Naval Research Laboratory on the ex-USS SHADWELL. All simulations were evaluated at steady state conditions. A constant velocity counter-flow air supply was introduced into the model structure. The counter-flow air velocities used were 0.5, 1, and 2 m/s. This study used a computational fluid dynamics combustion module to simulate a 620 kW fire generated by the complete combustion of propene gas from a burn pan in the space. Carbon dioxide from the fire was tracked throughout the structure to model smoke propagation. Seven simulations were performed with adiabatic and isothermal bulkhead, deck and overhead boundary conditions. Simulation smoke propagation results were consistent with experimental observations. Figures depicting temperature distribution, carbon dioxide distribution and mixture flow patterns at specified locations are provided in the report. The goal of this study is to evaluate the effectiveness of computational fluid dynamics modeling of smoke propagation in a shipboard space with a counter-flow air supply.

14. SUBJECT TERMS Smoke, Smoke Modeling, Smoke Propagation, Smoke Spread, Smoke Movement, Computational Fluid Dynamics, Control Shipboard Smoke, Fire Induced Flow, Fire Spread, Field Modeling, Damage Control, Convection, Forced Air Supply			**15. NUMBER OF PAGES** 170
			16. PRICE CODE
17. SECURITY CLASSIFICATION OF REPORT Unclassified	**18. SECURITY CLASSIFICATION OF THIS PAGE** Unclassified	**19. SECURITY CLASSIFICATION OF ABSTRACT** Unclassified	**20. LIMITATION OF ABSTRACT** UL

NSN 7540-01-280-5500

Standard Form 298 (Rev. 2-89)
Prescribed by ANSI Std. 239-18

THIS PAGE INTENTIONALLY LEFT BLANK

Approved for public release; distribution is unlimited

MODELING OF SHIPBOARD SMOKE PROPAGATION WITH A FORCED COUNTER-FLOW AIR SUPPLY

Garrett J. Farman
Lieutenant Commander, United States Navy
B.S., University of Rochester, 1990

Submitted in partial fulfillment of the
requirements for the degree of

MASTER OF SCIENCE IN MECHANICAL ENGINEERING

from the

NAVAL POSTGRADUATE SCHOOL
June 2001

Author: 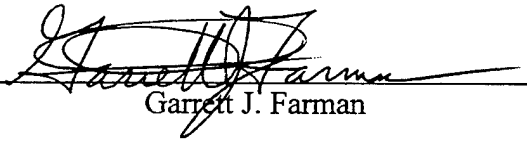
Garrett J. Farman

Approved by: 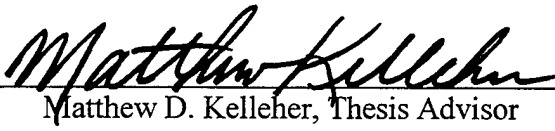
Matthew D. Kelleher, Thesis Advisor

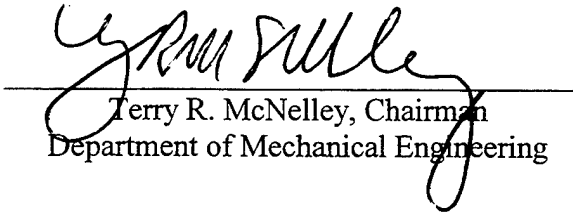
Terry R. McNelley, Chairman
Department of Mechanical Engineering

THIS PAGE INTENTIONALLY LEFT BLANK

ABSTRACT

The propagation of fire-generated smoke with a counter-flow air supply in a horizontal arrangement of shipboard compartments and passageways was modeled using a computational fluid dynamics program generated by Computational Fluid Dynamics Research Corporation. This study was based on a large-scale live fire experiment performed by Naval Research Laboratory on the ex-USS SHADWELL. All simulations were evaluated at steady state conditions. A constant velocity counter-flow air supply was introduced into the model structure. The counter-flow air velocities used were 0.5, 1, and 2 m/s. This study used a computational fluid dynamics combustion module to simulate a 620 kW fire generated by the complete combustion of propene gas from a burn pan in the space. Carbon dioxide from the fire was tracked throughout the structure to model smoke propagation. Seven simulations were performed with adiabatic and isothermal bulkhead, deck and overhead boundary conditions. Simulation smoke propagation results were consistent with experimental observations. Figures depicting temperature distribution, carbon dioxide distribution and mixture flow patterns at specified locations are provided in the report. The goal of this study is to evaluate the effectiveness of computational fluid dynamics modeling of smoke propagation in a shipboard space with a counter-flow air supply.

THIS PAGE INTENTIONALLY LEFT BLANK

TABLE OF CONTENTS

I. INTRODUCTION 1
A. BACKGROUND 1
B. PREVIOUS WORK 3
C. PROBLEM DESCRIPTION 7
II. GEOMETRY AND BOUNDARY CONDITION DESCRIPTION 9
A. MODEL GEOMETRY 9
B. CALCULATIONS FOR INLET CONDITIONS 12
1. Combustion Module Input Calculations 13
2. Simulated Combustion Calculations 15
C. BOUNDARY AND VOLUME CONDITIONS 16
D. SIMULATION MATRIX 17
III. RESULTS 19
IV. CONCLUSIONS 27
V. RECOMMENDATIONS 29
LIST OF REFERENCES 31
BIBLIOGRAPHY 33
APPENDIX A: SIMULATION 1 37
APPENDIX B: SIMULATION 2 45
APPENDIX C: SIMULATION 3 53
APPENDIX D: SIMULATION 4 61
APPENDIX E: SIMULATION 5 69
APPENDIX F: SIMULATION 6 77
APPENDIX G: SIMULATION 7 85
INITIAL DISTRIBUTION LIST 93

THIS PAGE INTENTIONALLY LEFT BLANK

LIST OF FIGURES

Figure 1. Plan view of horizontal experiment test space from Reference 13. 9
Figure 2. Plan view of CFD model 10
Figure 3. Model volume blocks 11
Figure 4. Plan view section identification. 20
Figure 5. Elevation view section identification. 20
Figure 6. Plot of elevation versus CO_2 for all simulations at the centerline of the longitudinal passageway. 22
Figure 7. Plot of elevation versus CO_2 for all simulations at the centerline of the stateroom door. 22
Figure 8. Plot of elevation versus temperature at the centerline of the longitudinal passageway door. 23
Figure 9. Plot of elevation versus temperature at the centerline of the stateroom door. The scattered data near the deck for simulations 2, 3, 4 and 5 are caused by the isothermal deck boundary condition. 24
Figure 10. Simulation 1, partial elevation view (A-A) depicting temperature (K) distribution and fluid circulation pattern at the centerline of the longitudinal passageway in the vicinity of the watertight door. 38
Figure 11. Simulation 1, partial elevation view (A-A) depicting CO_2 (mass fraction) distribution along the centerline of the longitudinal passageway in the vicinity of the watertight door 38
Figure 12. Simulation 1, elevation view (A-A) depicting CO_2 (mass fraction) distribution along the centerline of the longitudinal passageway. 39
Figure 13. Simulation 1, partial elevation view (B-B) depicting temperature (K) distribution and fluid circulation pattern along the centerline of the transverse passageway on the port side of the structure. 39
Figure 14. Simulation 1, elevation view (B-B) depicting CO_2 (mass fraction) distribution along the centerline of the transverse passageway. 40
Figure 15. Simulation 1, partial elevation view (C-C) depicting temperature (K) distribution and fluid circulation pattern through the centerline of the stateroom door from the transverse passageway. 40
Figure 16. Simulation 1, partial elevation view (C-C) depicting CO_2 (mass fraction) distribution at the centerline of the stateroom door. 41
Figure 17. Simulation 1, partial plan view (D-D) depicting temperature (K) distribution and fluid circulation pattern from the transverse passageway through the door into the stateroom. 41
Figure 18. Simulation 1, partial plan view (E-E) depicting temperature (K) distribution and fluid circulation pattern from the transverse passageway through the door into the stateroom. 42
Figure 19. Simulation 1, partial plan view (D-D) depicting CO_2 (mass fraction) distribution in the stateroom and transverse passageway. 42
Figure 20. Simulation 1, partial plan view (E-E) depicting CO_2 (mass fraction) distribution in the stateroom and transverse passageway. 43

Figure 21. Simulation 1, plan view (D-D) depicting CO_2 (mass fraction) distribution throughout the structure. 43
Figure 22. Simulation 1, plan view (E-E) depicting CO_2 (mass fraction) distribution throughout the structure. 44
Figure 23. Simulation 2, partial elevation view (A-A) depicting temperature (K) distribution and fluid circulation pattern at the centerline of the longitudinal passageway in the vicinity of the watertight door. 46
Figure 24. Simulation 2, partial elevation view (A-A) depicting CO_2 (mass fraction) distribution along the centerline of the longitudinal passageway in the vicinity of the watertight door....46
Figure 25. Simulation 2, partial elevation view (A-A) depicting CO_2 (mass fraction) distribution at the centerline of the longitudinal passageway....47
Figure 26. Simulation 2, partial elevation view (B-B) depicting temperature (K) distribution and fluid circulation pattern along the centerline of the transverse passageway on the port side of the structure. 47
Figure 27. Simulation 2, elevation view (B-B) depicting CO_2 gas (mass fraction) distribution at the centerline of the transverse passageway. 48
Figure 28. Simulation 2, partial elevation view (C-C) depicting temperature (K) distribution and fluid circulation pattern through the centerline of the stateroom door from the transverse passageway. 48
Figure 29. Simulation 2, partial elevation view (C-C) depicting CO_2 (mass fraction) distribution at the centerline of the stateroom door. 49
Figure 30. Simulation 2, partial plan view (D-D) depicting temperature (K) distribution and fluid circulation pattern from the transverse passageway through the door into the stateroom. 49
Figure 31. Simulation 2, partial plan view (E-E) depicting temperature (K) distribution and fluid circulation pattern from the transverse passageway through the door into the stateroom. 50
Figure 32. Simulation 2, partial plan view (D-D) depicting CO_2 (mass fraction) distribution in the stateroom and transverse passageway. 50
Figure 33. Simulation 2, partial plan view (E-E) depicting CO_2 (mass fraction) distribution in the stateroom and transverse passageway. 51
Figure 34. Simulation 2, plan view (D-D) depicting CO_2 (mass fraction) distribution throughout the structure. 51
Figure 35. Simulation 2, plan view (E-E) depicting CO_2 (mass fraction) distribution throughout the structure. 52
Figure 36. Simulation 3, partial elevation view (A-A) depicting temperature (K) distribution and fluid circulation pattern at the centerline of the longitudinal passageway in the vicinity of the watertight door. 54
Figure 37. Simulation 3, partial elevation view (A-A) of CO_2 gas (mass fraction) propagation at the centerline of the longitudinal passageway in the vicinity of the watertight door....54
Figure 38. Simulation 3, elevation view (A-A) of CO_2 gas (mass fraction) propagation at the centerline of the longitudinal passageway. 55

Figure 39. Simulation 3, partial elevation view (B-B) depicting temperature (K) distribution and fluid circulation pattern along the centerline of the transverse passageway on the port side. 55
Figure 40. Simulation 3, elevation view (B-B) of CO_2 gas (mass fraction) propagation at the centerline of the transverse passageway. 56
Figure 41. Simulation 3, elevation view (C-C) depicting the temperature (K) distribution and fluid circulation pattern through the centerline of the stateroom door from the transverse passageway. 56
Figure 42. Simulation 3, elevation view (C-C) depicting CO_2 (mass fraction) distribution at the centerline of the stateroom door. 57
Figure 43. Simulation 3, partial plan view (D-D) depicting temperature (K) distribution and fluid circulation pattern from the transverse passageway through the door into the stateroom. 57
Figure 44. Simulation 3, partial plan view (E-E) depicting temperature (K) distribution and fluid circulation pattern from the transverse passageway through the door into the stateroom. 58
Figure 45. Simulation 3, partial plan view (D-D) depicting CO_2 (mass fraction) distribution in the stateroom and transverse passageway. 58
Figure 46. Simulation 3, partial plan view (E-E) depicting CO_2 (mass fraction) distribution in the stateroom and transverse passageway. 59
Figure 47. Simulation 3, plan view (D-D) depicting CO_2 (mass fraction) distribution throughout the structure. 59
Figure 48. Simulation 3, plan view (E-E) depicting CO_2 (mass fraction) distribution throughout the structure. 60
Figure 49. Simulation 4, partial elevation view (A-A) depicting temperature (K) distribution and fluid circulation pattern at the centerline of the longitudinal passageway in the vicinity of the watertight door. 62
Figure 50. Simulation 4, partial elevation view (A-A) of CO_2 gas (mass fraction) propagation at the centerline of the longitudinal passageway in the vicinity of the watertight door. 62
Figure 51. Simulation 4, elevation view (A-A) of CO_2 gas (mass fraction) propagation at the centerline of the longitudinal passageway. 63
Figure 52. Simulation 4, partial elevation view (B-B) depicting temperature (K) distribution and fluid circulation pattern along the centerline of the transverse passageway on the port side. 63
Figure 53. Simulation 4, elevation view (B-B) of CO_2 gas (mass fraction) propagation at the centerline of the transverse passageway. 64
Figure 54. Simulation 4, elevation view (C-C) depicting the temperature (K) distribution and fluid circulation pattern through the centerline of the stateroom door from the transverse passageway. 64
Figure 55. Simulation 4, elevation view (C-C) depicting CO_2 (mass fraction) distribution at the centerline of the stateroom door. 65
Figure 56. Simulation 4, partial plan view (D-D) depicting temperature (K) distribution and fluid circulation pattern from the transverse passageway through the door into the stateroom. 65

Figure 57. Simulation 4, partial plan view (E-E) depicting temperature (K) distribution and fluid circulation pattern from the transverse passageway through the door into the stateroom. 66
Figure 58. Simulation 4, partial plan view (D-D) depicting CO_2 (mass fraction) distribution in the stateroom and transverse passageway. 66
Figure 59. Simulation 4, partial plan view (E-E) depicting CO_2 (mass fraction) distribution in the stateroom and transverse passageway. 67
Figure 60. Simulation 4, plan view (D-D) depicting CO_2 (mass fraction) distribution throughout the structure. 67
Figure 61. Simulation 4, plan view (E-E) depicting CO_2 (mass fraction) distribution throughout the structure. 68
Figure 62. Simulation 5, partial elevation view (A-A) depicting temperature (K) distribution and fluid circulation pattern at the centerline of the longitudinal passageway in the vicinity of the watertight door. 70
Figure 63. Simulation 5, partial elevation view (A-A) of CO_2 gas (mass fraction) propagation at the centerline of the longitudinal passageway in the vicinity of the watertight door. 70
Figure 64. Simulation 5, elevation view (A-A) of CO_2 gas (mass fraction) propagation at the centerline of the longitudinal passageway. 71
Figure 65. Simulation 5, partial elevation view (B-B) depicting temperature (K) distribution and fluid circulation pattern along the centerline of the transverse passageway on the port side. 71
Figure 66. Simulation 5, elevation view (B-B) of CO_2 gas (mass fraction) propagation at the centerline of the transverse passageway. 72
Figure 67. Simulation 5, elevation view (C-C) depicting the temperature (K) distribution and fluid circulation pattern through the centerline of the stateroom door from the transverse passageway. 72
Figure 68. Simulation 5, elevation view (C-C) depicting CO_2 (mass fraction) distribution at the centerline of the stateroom door. 73
Figure 69. Simulation 5, partial plan view (D-D) depicting the temperature (K) distribution and fluid circulation pattern from the transverse passageway through the door into the stateroom. 73
Figure 70. Simulation 5, partial plan view (E-E) depicting the temperature (K) distribution and fluid circulation pattern from the transverse passageway through the door into the stateroom. 74
Figure 71. Simulation 5, partial plan view (D-D) depicting CO_2 (mass fraction) distribution in the stateroom and transverse passageway. 74
Figure 72. Simulation 5, partial plan view (E-E) depicting CO_2 (mass fraction) distribution in the stateroom and transverse passageway. 75
Figure 73. Simulation 5, plan view (D-D) depicting CO_2 (mass fraction) distribution throughout the structure. 75
Figure 74. Simulation 5, plan view (E-E) depicting CO_2 (mass fraction) distribution throughout the structure. 76

Figure 75. Simulation 6, partial elevation view (A-A) depicting temperature (K) distribution and fluid circulation pattern at the centerline of the longitudinal passageway in the vicinity of the watertight door. 78
Figure 76. Simulation 6, partial elevation view (A-A) of CO_2 gas (mass fraction) propagation at the centerline of the longitudinal passageway in the vicinity of the watertight door. 78
Figure 77. Simulation 6, elevation view (A-A) of CO_2 gas (mass fraction) propagation at the centerline of the longitudinal passageway. 79
Figure 78. Simulation 6, partial elevation view (B-B) depicting temperature (K) distribution and fluid circulation pattern along the centerline of the transverse passageway on the port side. 79
Figure 79. Simulation 6, elevation view (B-B) of CO_2 gas (mass fraction) propagation at the centerline of the transverse passageway. 80
Figure 80. Simulation 6, elevation view (C-C) depicting the temperature (K) distribution and fluid circulation pattern through the centerline of the stateroom door from the transverse passageway. 80
Figure 81. Simulation 6, elevation view (C-C) depicting CO_2 (mass fraction) distribution at the centerline of the stateroom door. 81
Figure 82. Simulation 6, partial plan view (D-D) depicting the temperature (K) distribution and fluid circulation pattern from the transverse passageway through the door into the stateroom. 81
Figure 83. Simulation 6, partial plan view (E-E) depicting the temperature (K) distribution and fluid circulation pattern from the transverse passageway through the door into the stateroom. 82
Figure 84. Simulation 6, partial plan view (D-D) depicting CO_2 (mass fraction) distribution in the stateroom and transverse passageway. 82
Figure 85. Simulation 6, partial plan view (E-E) depicting CO_2 (mass fraction) distribution in the stateroom and transverse passageway. 83
Figure 86. Simulation 6, plan view (D-D) depicting CO_2 (mass fraction) distribution throughout the structure. 83
Figure 87. Simulation 6, plan view (E-E) depicting CO_2 (mass fraction) distribution throughout the structure. 84
Figure 88. Simulation 7, partial elevation view (A-A) depicting temperature (K) distribution and fluid circulation pattern at the centerline of the longitudinal passageway in the vicinity of the watertight door. 86
Figure 89. Simulation 7, partial elevation view (A-A) of CO_2 gas (mass fraction) propagation at the centerline of the longitudinal passageway in the vicinity of the watertight door. 86
Figure 90. Simulation 7, elevation view (A-A) of CO_2 gas (mass fraction) propagation at the centerline of the longitudinal passageway. 87
Figure 91. Simulation 7, partial elevation view (B-B) depicting temperature (K) distribution and fluid circulation pattern along the centerline of the transverse passageway on the port side. 87
Figure 92. Simulation 7, elevation view (B-B) of CO_2 gas (mass fraction) propagation at the centerline of the transverse passageway. 88

Figure 93. Simulation 7, elevation view (C-C) depicting the temperature (K) distribution and fluid circulation pattern through the centerline of the stateroom door from the transverse passageway. 88
Figure 94. Simulation 7, elevation view (C-C) depicting CO_2 (mass fraction) distribution at the centerline of the stateroom door. 89
Figure 95. Simulation 7, partial plan view (D-D) depicting the temperature (K) distribution and fluid circulation pattern from the transverse passageway through the door into the stateroom. 89
Figure 96. Simulation 7, partial plan view (E-E) depicting the temperature (K) distribution and fluid circulation pattern from the transverse passageway through the door into the stateroom. 90
Figure 97. Simulation 7, partial plan view (D-D) depicting CO_2 (mass fraction) distribution in the stateroom and transverse passageway. 90
Figure 98. Simulation 7, partial plan view (E-E) depicting CO_2 (mass fraction) distribution in the stateroom and transverse passageway. 91
Figure 99. Simulation 7, plan view (D-D) depicting CO_2 (mass fraction) distribution throughout the structure. 91
Figure 100. Simulation 7, plan view (D-D) depicting CO_2 (mass fraction) distribution throughout the structure. 92

LIST OF TABLES

Table 1. Species mass fractions for combustion module. 15
Table 2. Species mass fractions for simulated combustion. 16
Table 3. Volume initial conditions 17
Table 4. Simulation summary matrix 18
Table 5. Simulation 1, inlet, burn pan, vent and bulkhead boundary conditions 37
Table 6. Simulation 1, inlet, burn pan and vent mixture definition. 37
Table 7. Simulation 2, inlet, burn pan, vent and bulkhead boundary conditions 45
Table 8. Simulation 2, inlet, burn pan and vent mixture definition. 45
Table 9. Simulation 3, inlet, burn pan, vent, bulkhead boundary conditions. 53
Table 10. Simulation 3, inlet, burn pan and vent mixture definition. 53
Table 11. Simulation 4, inlet, burn pan, vent and bulkhead boundary conditions 61
Table 12. Simulation 4, inlet, burn pan and vent mixture definition. 61
Table 13. Simulation 5, inlet, burn pan, vent, bulkhead boundary conditions. 69
Table 14. Simulation 5, inlet, burn pan and vent mixture definition. 69
Table 15. Simulation 6, inlet, burn pan, vent, bulkhead boundary conditions. 77
Table 16. Simulation 6, inlet, burn pan and vent mixture definition. 77
Table 17. Simulation 7, inlet, burn pan, vent, bulkhead boundary conditions. 85
Table 18. Simulation 7, inlet, burn pan and vent mixture definition. 85

THIS PAGE INTENTIONALLY LEFT BLANK

I. INTRODUCTION

A. BACKGROUND

Presently, in the United States Navy, there is a drive to reduce the manning on naval ships. This movement is driven by several issues such as reduced total ownership costs and the desire to minimize exposure of shipboard personnel to the combat environment. To compensate for the crew size reduction, machines will automate numerous shipboard functions that formerly required human interface. While the reduction of shipboard personnel has many attractive advantages, it also has several potential drawbacks and uncertainties. One area of great uncertainty is the effect of reduced manning on damage control efforts in response to a casualty.

Shipboard fires have always been extremely hazardous to both the crew and the vessel. This fact is vividly evident in the USS STARK incident. On 17 May 1987, the USS STARK (FFG 31) was struck by two Iraqi Exocet missiles, disabling the ship and killing 37 sailors. The ensuing fire from unexpended missile propellant produced temperatures in excess of 1400-1500 degrees Fahrenheit within a minute and engulfed the affected spaces in flames. The burning missile propellant, electrical cables, berthing mattresses, personal effects, etc., produced a dense, toxic smoke that propagated throughout the ship. This intense fire, toxic smoke, and damage to fire fighting equipment inhibited the crew's effectiveness in combating the conflagration. [Ref 1]

In dealing with a shipboard casualty, or any other casualty, the actions taken within the first 3-5 minutes by watch standers determine how effectively the casualty will be controlled. A poor or slow response can allow an easily controllable situation to cascade into a severe, catastrophic, out-of-control casualty. On the other hand, swift and

correct actions can neutralize a potentially catastrophic situation, thus minimizing personnel losses and ship damage while maintaining the operational effectiveness of the vessel.

Historically, warships have had a sufficient number of personnel available to man damage control parties to combat 'worst case' casualties. On a reduced manned ship, personnel resources will be stretched to the edge of their capabilities, therefore the crew must heavily rely on automated damage control responses to ensure that their capabilities to control any casualty are not exceeded. [Ref 2]

The United States Navy has been exploring several new technologies and options to address damage control issues on reduced manned ships. The Damage Control Automation for Reduced Manning (DC-ARM) Project has a technical objective of performing damage control functions "with 50% fewer personnel and in at least 75% less time while maintaining the offensive capability of the ship." [Ref 3]

Remote manual operation of advanced damage control systems was successfully used in a demonstration conducted on 18-22 September 2000 at the Navy full-scale Research, Development, Testing and Evaluation (RDT&E) facility, the ex-USS-*Shadwell*, located in Mobile, AL. The demonstration included the Early Warning Fire Detection (EWFD) system, water mist suppression system, automated firemain control system and smoke control system. [Ref 4]

For an automated smoke control system to be effective, a thorough understanding of smoke movement in a highly compartmented structure is required. Smoke movement is very complex in a shipboard structure because of the complex arrangement of

passageways and compartments, combustion dynamics, forced ventilation effects, highly conductive bulkheads, deck and overhead, etc. Computational Fluid Dynamics (CFD) models of shipboard spaces can provide the insight required to effectively evaluate smoke propagation in a particular arrangement of ship spaces or evaluate the effectiveness of a shipboard smoke control system. At a relatively low cost and resource investment, CFD models can test many scenarios and space configurations to evaluate a vessel's arrangement and the correct smoke control response for a given casualty scenario. A minimal number of costly large-scale experiments still must be performed to validate the CFD models' accuracy. The combination of CFD modeling and large-scale experiments can be a powerful design tool for evaluating future ship designs and proposed damage control configurations. This study evaluates the use of CFD models to evaluate smoke propagation in a shipboard environment.

B. PREVIOUS WORK

Historically, knowledge of fire and smoke behavior was gained through large-scale experiments. Over the last 10 years, the computing capability, processor speed and memory capacity of the desktop computer has increased significantly. Additionally, software programs have become more capable and easy to use. With these expanded capabilities, the desktop computer has become a powerful tool in evaluating smoke movement scenarios.

Presently, there are two general models used to predict smoke propagation in complex structures, zone models and field models. Several different types of zones models have been applied to simulating fire and smoke environments.

Most commonly, the zone model represents the system as two distinct

> compartment gas zones: an upper volume and a lower volume resulting from thermal stratification due to buoyancy. This type of model is therefore also termed a two-zone model. Conservation equations are applied to each zone and serve to embrace the various transport and combustion processes that apply. The fire is represented as a source of energy and mass, and manifests itself as a plume which acts as a "pump" of mass from the lower zone to the upper zone through a process called entrainment. [Ref 5: p. 258]

During the last 15 years, zone models have been used extensively in the study of smoke propagation in compartmented structures. Zone models generally are less computationally intensive, hence faster than other methods. Zone models may have limited effectiveness in certain structure geometries such as structures "with a large length-to-width ratio or rooms where the horizontal length to vertical length ratio is very large or very small." [Ref 5: p. 268] Further degradation of a zone model solution occurs in areas within the modeled structure where very strong turbulence causes thorough mixing of the hot and cold gas masses yielding a relatively uniform temperature distribution. [Ref 5: p. 269]

Jones and Walton [Ref 6] used a zone model to study the effectiveness of using a computer model to predict fire growth and smoke propagation in a highly compartmented shipboard structure. The model simulated a 1 MW fire consisting of unspent missile fuel and bedding material in the forward berthing compartment of an FFG 7 class ship with initial conditions provided by the Ship Vulnerability Model at the David W. Taylor Naval Ship Research and Development Center. The simulation results demonstrated that the model provided an accurate prediction of the spread of fire and smoke and that the model could be used to evaluate alternative ship designs and configurations.

In recent years, as described by Jones and Forney [Ref 7], zone models, like the Consolidated Fire Growth and Smoke Transport (CFAST) model, have improved algorithms that include horizontal momentum, radiation exchange and forced flow. Bailey and Tatem [Ref 8] compared CFAST predictions to a full-scale live fire experiment conducted on the ex-USS SHADWELL as part of the Internal Ship Conflagration Control (ISCC) program.

> The ISCC program was chartered to provide guidance to the Fleet on the control of fire spread in both the vertical and horizontal directions. An additional objective was the development of new ship design criteria to address the devastation that occurred on the USS STARK as a result of missile induced fires. [Ref 8: p. 1]

The CFAST model predictions with the vertical heat transfer algorithm included correlated reasonably well with the live fire data.

A field model or Computational Fluid Dynamics (CFD) model is "based on a complete, time-dependent (or time independent), three-dimensional solution of the fundamental conservation laws. The volume under consideration is therefore divided into a very large number of sub-volumes and the basic laws of mass, momentum, and energy conservation are applied to each of these." [Ref 5: p. 269]

CFD models are computationally intense, therefore the computational time and resources required are greater than that required of the zone model. CFD models simulating smoke propagation have increased significantly in the last few years because of computing capability gains and lower hardware and software costs. A CFD model provides more detailed information than the zone model. It provides velocity vectors,

isotherms, molecular species concentration, temperature distribution, pressure distribution, density distribution, wall heat transfer rates, etc.

Chow [Ref 9] modeled the effect of forced-ventilation on smoke layer stability and the burning process in a single room using the CFD package PHOENICS. Chow found that when the vent was located near the ceiling, the smoke layer was well defined. When the vent was located near the floor, a "short-circuiting" effect occurred that directed hot air out the vent causing mixing to occur within the room, thus the smoke layer became unstable and the temperature of the layer was much lower.

Mehls [Ref 10] simulated smoke dissipation in a shipboard space using a CFD model. This model studied steady state smoke distribution in a DDG 51 shipboard space with the smoke entering one door and exiting out another door located on the adjacent bulkhead towards the other side of the space.

Abaya [Ref 11] simulated steady state smoke propagation in a DDG 51 shipboard space with a geometric interference using a CFD model. As with Mehls, this model simulated smoke entering through a door from an adjacent space and exited another door on the other side of the space. The results demonstrated that the CFD model realistically modeled smoke propagation in the presence of a geometric interference.

Vegara [Ref 12] simulated steady state smoke propagation in a relatively large DDG 51 shipboard space using a CFD model. This model simulated smoke entering through a door from an adjacent space and exited another door on the other side of the space. The results confirmed Mehl's findings that a heated deck did not significantly

affect smoke propagation within the space and that Mehl's work also applied to a larger and more complex space.

C. PROBLEM DESCRIPTION

Williams, Forsell, DiNenno, Beyler and Lain [Ref 13] performed a live fire experiment, at the Navy full-scale RDT&E facility, the ex-USS *Shadwell*, to investigate shipboard smoke control using a forced counter-flow air supply. The experiment evaluated smoke propagation in horizontal passageways and vertical trunks for several different fire intensities and forced counter-flow air velocities. A propene gas fire was used to simulate a shipboard fire. Shipboard ventilation supply fans along with exhaust vent flow regulation were used to control the forced counter-flow air velocity. The experiment found that "relatively modest air velocities were able to limit the migration of smoke in either the horizontal corridor or the vertical trunk." [Ref 13: p. 63]

The purpose of this study is to evaluate a CFD model of smoke propagation in a shipboard space similar to the space geometry used in the full-scale experiment of Reference 13. This structure was selected because the data presented in Reference 13 could be used as a benchmark to compare the CFD model results. This study concentrates on modeling the effect of a forced counter-flow air supply on smoke propagation from a 620 kW fire. The data obtained from the model was then compared to the live fire experimental data to verify that the model results were realistic.

CFD-ACE version 6.4, commercial CFD program produced by the Computational Fluid Dynamics Research Corporation (CFDRC), was used for analysis. The software was last updated February 21, 2001. The modeling and simulations for this study were

performed on a Micron Client Pro Desktop computer, with a 400 MHz processor, 384 megabytes of RAM and a 12 gigabyte internal hard drive.

II. GEOMETRY AND BOUNDARY CONDITION DESCRIPTION

A. MODEL GEOMETRY

The structure modeled for CFD analysis was based on the horizontal structure described in Reference 13. Figure 1 is a plan view of the horizontal space used in the large-scale live fire experiment.

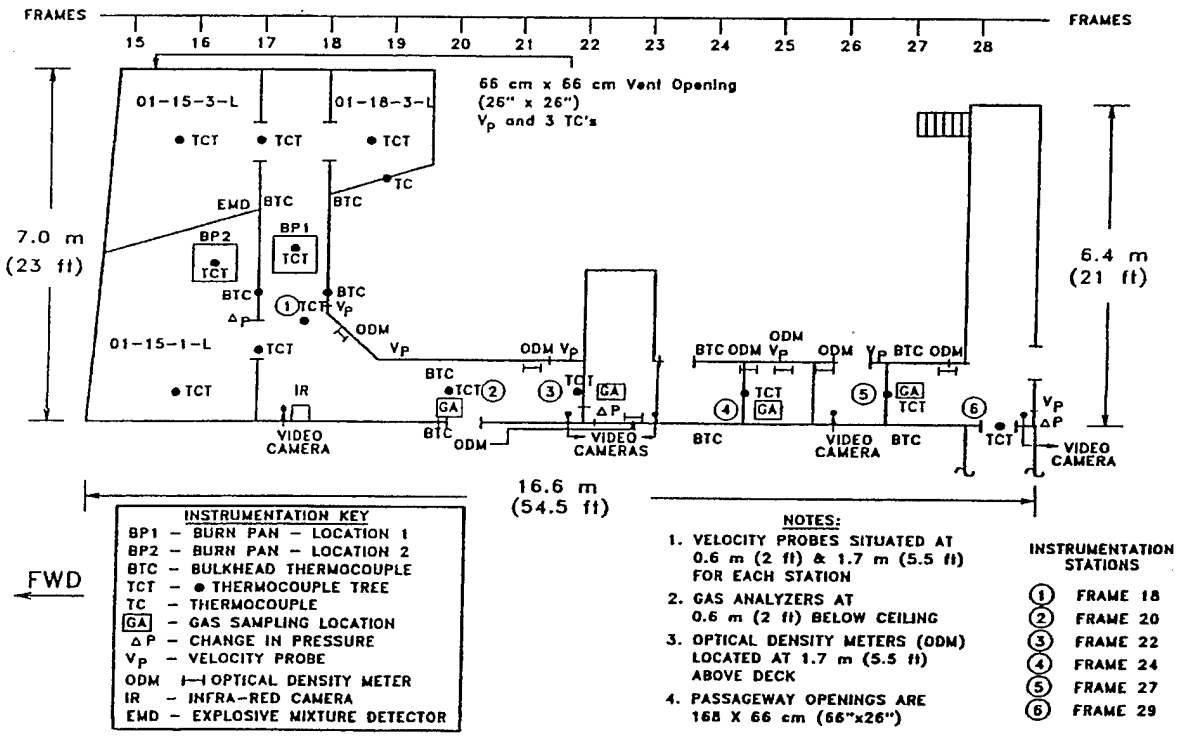
FRAMES
15 16 17 18 19 20 21 22 23 24 25 26 27 28
FRAMES
66 cm x 66 cm Vent Opening
(26" x 26")
V_P and 3 TC's
01-15-3-L
01-18-3-L
01-15-1-L
7.0 m
(23 ft)
6.4 m
(21 ft)
16.6 m
(54.5 ft)
FWD
VIDEO CAMERA
VIDEO CAMERAS
INSTRUMENTATION KEY
BP1 - BURN PAN - LOCATION 1
BP2 - BURN PAN - LOCATION 2
BTC - BULKHEAD THERMOCOUPLE
TCT - THERMOCOUPLE TREE
TC - THERMOCOUPLE
GA - GAS SAMPLING LOCATION
ΔP - CHANGE IN PRESSURE
V_P - VELOCITY PROBE
ODM - OPTICAL DENSITY METER
IR - INFRA-RED CAMERA
EMD - EXPLOSIVE MIXTURE DETECTOR
NOTES:
1. VELOCITY PROBES SITUATED AT 0.6 m (2 ft) & 1.7 m (5.5 ft) FOR EACH STATION
2. GAS ANALYZERS AT 0.6 m (2 ft) BELOW CEILING
3. OPTICAL DENSITY METERS (ODM) LOCATED AT 1.7 m (5.5 ft) ABOVE DECK
4. PASSAGEWAY OPENINGS ARE 168 X 66 cm (66"x26")
INSTRUMENTATION STATIONS
1 FRAME 18
2 FRAME 20
3 FRAME 22
4 FRAME 24
5 FRAME 27
6 FRAME 29

Figure 1. Plan view of horizontal experiment test space from Reference 13.

Figure 2 shows the CFD model plan view of the test structure. The model consists of a single rectangular stateroom and an L-shaped passageway. There are two watertight doors located in the longitudinal portion of the L-shaped passageway. One watertight door is located at the end of the longitudinal passageway and the other is located in the middle of the longitudinal passageway, 8.3 m from the aft end of the

passageway. For simplicity, the watertight doors are modeled as rectangles (0.6 m x 1.8 m) with the base of the door located 0.2 m above the deck. The stateroom door is also modeled as a rectangle (0.6 m x 2.0 m) with the base of the door located at the deck. The stateroom door and the watertight doors are modeled as fully open during each simulation.

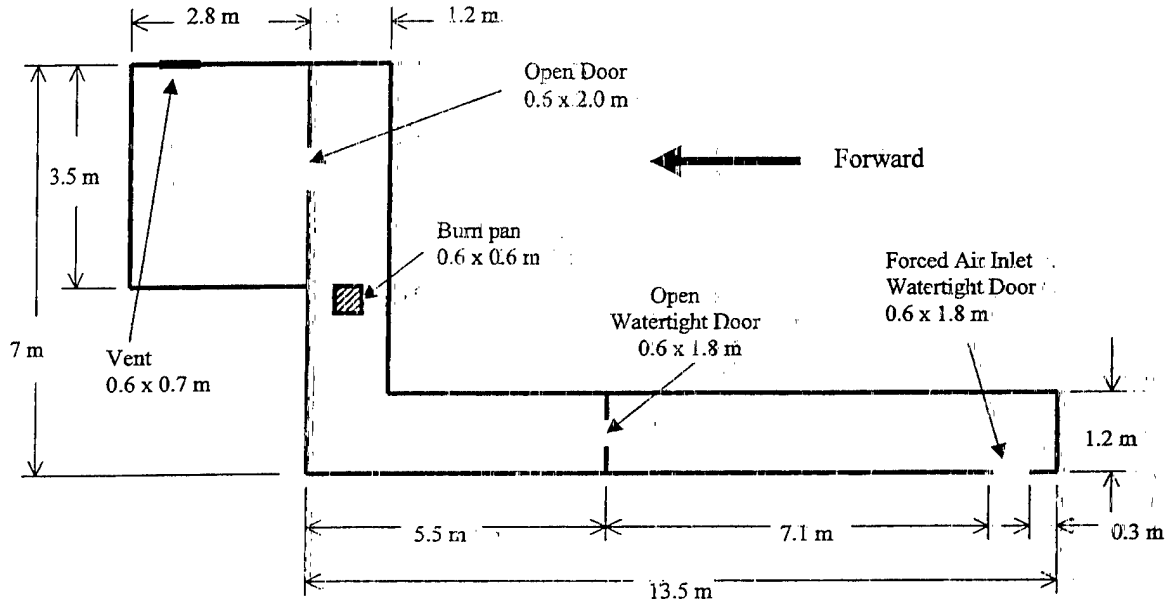

Figure 2. Plan view of CFD model.

In the original live fire experiment of Reference 13, a 0.66 m x 0.66 m natural vent was located in the stateroom on the outboard bulkhead. For simplicity, the vent dimensions are modified to 0.6 m x 0.7 m. These dimensions allow for the construction of a structured grid. The overboard vent is placed 0.5 m above the deck and 0.5 m aft of the forward stateroom bulkhead.

A 0.6 m x 0.6 m burn pan is located flush with the deck in the middle of the transverse passageway and the center of the burn pan is located 3.2 m from the port bulkhead as shown in Figure 2.

The model is divided into 4 blocks as depicted in Figure 3. Block 1 is the stateroom, the rectangular space where the vent is located. Block 2 is the transverse passageway where the burn pan is located. Block 3 is located forward of the watertight door that divides the longitudinal passageway. Block 4 is located aft of the watertight door that divides the longitudinal passageway. Grid spacing is every 5 cm in the vertical and transverse directions and every 10 cm in the longitudinal direction except for the longitudinal section of the burn pan where the grid spacing is set at 5 cm between grid points. The grid is comprised of 373,086 nodes and 345,184 elements. Further refinement of the grid is limited because of computer memory constraints.

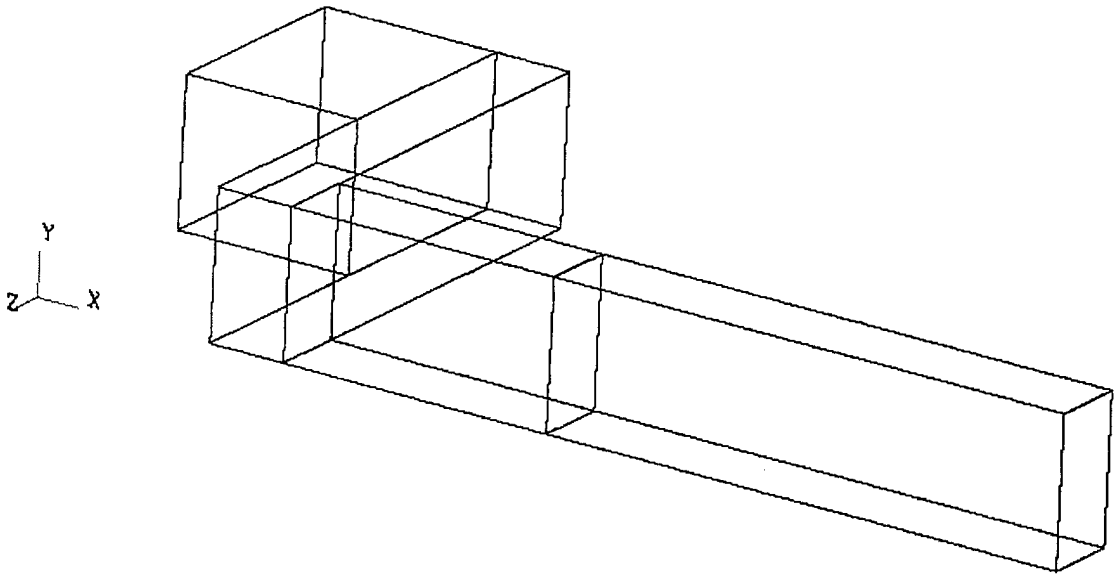

Figure 3. Model volume blocks.

B. CALCULATIONS FOR INLET CONDITIONS

For this study, instantaneous combustion of propene (C_3H_6) gas with air forming products of water vapor (H_2O) and carbon dioxide (CO_2) is assumed. Instantaneous combustion is a stoichiometric chemical reaction of reactants transforming to final products and heat release with no intermediate chemical reactions. [Ref 14]

This assumption introduced some simulation difficulties that must be addressed. Specifically, the instantaneous combustion process produces extremely high temperatures near the burn pan of approximately 2200 - 2300 K with all the energy released during combustion absorbed by the combustion products. In reality, temperatures exceeding 2000 K will result in significant dissociation of water vapor and carbon dioxide, an endothermic reaction, thus suppressing the actual combustion temperature. [Ref 14: p. 27-28] Equilibrium equations for the dissociation of water vapor and carbon dioxide are provided below:

$$H_2O \Leftrightarrow H^+ + OH^-$$

$$H_2O \Leftrightarrow H_2 + \frac{1}{2}O_2 \qquad \text{[Ref 15: p.27]}$$

$$CO_2 \Leftrightarrow CO + \frac{1}{2}O_2$$

For this study, dissociation of water vapor and carbon dioxide is neglected. As stated before, the purpose of this study is to model the effect of a forced counter-flow air supply on smoke propagation from a 620 kW fire. Therefore, emphasis is placed on modeling the energy input into the system and not the particular combustion process itself. Future models can focus on both modeling the combustion process and the effect of the particular combustion process on smoke propagation in the structure.

1. Combustion Module Input Calculations

The CFD model simulations require a 620 kW fire. CFD-ACE contains a combustion module that simulates instantaneous and complete combustion of propene, the fuel used in the live fire experiment of Reference 13. Information required by the CFD program includes the stoichiometric chemical reaction, mass fractions of mixture species, and burn pan mixture inlet velocity. For simplicity, the burn pan mixture is set as a stoichiometric balance of air and propene such that all the oxygen and propene is consumed during combustion. The stoichiometric reaction is provided below:

$$2C_3H_6 + 9O_2 + 30N_2 \rightarrow 6CO_2 + 6H_2O + 30N_2 \qquad (1)$$

This model can be thought of as a Bunsen burner type of setup. The enthalpy of combustion, $|\Delta H_C|$, for propene is:

$$|\Delta H_C| = 45780 \text{ kJ/kg}$$

The required mass flow rate, $\dot{m}$, in kg/s, of propene is given by:

$$\dot{m}_{C_3H_6} = \frac{Q}{|\Delta H_C|}$$

where: Q= Fire intensity (kW)

The mole flow rate, $\dot{M}$, in kmol/s, is obtained by:

$$\dot{M}_{C_3H_6} = \frac{\dot{m}_{C_3H_6}}{MW_{C_3H_6}}$$

where: $MW_{C_3H_6}$ = Molecular weight of propene (C_3H_6)

Using ratios of the stoichiometric coefficients from equation (1), the mole flow rate of propene and the molecular weight of O_2, the required O_2 mass flow rate is obtained by:

$$\dot{m}_{O_2} = \frac{9}{2}\dot{M}_{C_3H_6} MW_{O_2}$$

For the entire model, air composition is assumed to be 21% O_2 and 79% N_2 by volume. Therefore, for each kmol of O_2 in air, there is approximately 3.76 kmol of N_2. The mass flow rate of N_2 is then determined from the following relation:

$$\dot{m}_{N_2} = 3.76\dot{M}_{O_2} MW_{N_2}$$

The Ideal Gas Law is used to determine the density, ρ, of O_2 and N_2 at a pressure of 100 kPa and a temperature of 300 K. The volume flow rate, $\dot{V}$, in m^3/s, for C_3H_6, O_2 and N_2 are determined by the following relation:

$$\dot{V} = \frac{\dot{m}}{\rho}$$

The burn pan mixture velocity, v, in m/s, required to generate a 620 kW fire is determined by the following relation:

$$v = \frac{\dot{V}_{C_3H_6} + \dot{V}_{O_2} + \dot{V}_{N_2}}{A}$$

where: A = Burn pan area (m^2)

The required burn pan mixture inlet velocity is 0.500 m/s. The required species mass fraction information for each mixture is provided in Table 1.

	C_3H_6	O_2	N_2
Burn Pan Mixture Mass Fractions	0.06363	0.21822	0.71815
Air Mixture Mass Fractions	0	0.233	0.767

Table 1. Species mass fractions for combustion module.

2. Simulated Combustion Calculations

A second method of simulating a 620 kW fire is also used. This method also assumes complete stoichiometic combustion of propene as indicated by equation (1). Assuming the combustion products and N_2 absorbed all heat of combustion, the hot gasses are expelled into the space through the burn pan opening. In order to use this method in the CFD program, the combustion product gas stream temperature and velocity are required. The combustion products gas stream temperature was obtained from the following relation:

$$Q = \left[\left(\dot{m}C_p\right)_{N_2} + \left(\dot{m}C_p\right)_{H_2O} + \left(\dot{m}C_p\right)_{CO_2}\right]\left(T - T_{amb}\right) \qquad (2)$$

where: Q = Fire intensity (kW)

$\dot{m}$ = Mass flow rate of molecular species (kg/s)

C_p = Specific heat constant (kJ/kg-K)

T_{amb} = Ambient temperature = 300 K

T = Gas temperature (K)

The specific heat, C_p (kJ/kg-K), of each molecular species are given by [Ref 16: p. 651]:

$$N_2: \qquad C_p = \frac{39.060 - 512.79\theta^{-1.5} + 1072.7\theta^{-2} - 820.40\theta^{-3}}{MW_{N_2}}$$

$$CO_2: \quad C_p = \frac{-3.7357 + 30.529\theta^{0.5} - 4.1034\theta + 0.024198\theta^2}{MW_{CO_2}}$$

$$H_20: \quad C_p = \frac{143.05 - 183.54\theta^{0.25} + 82.751\theta^{0.5} - 3.6989\theta}{MW_{H_2O}}$$

where: $\theta = \frac{T}{100}$ T is given in Kelvin

Substituting the C_3H_6, O_2 and N_2 mass flow rates, calculated in section II.B.1, into equation (2) yields a temperature of approximately 2307 K. Additionally, the required burn pan mixture velocity is calculated to be 4.08 m/s. The required species mass fraction information for each mixture is provided in Table 2.

	CO2	H2O	N_2	O_2
Burn Pan Mixture Mass Fractions	0.20006	0.08186	0.71808	0
Air Mixture Mass Fractions	0	0	0.767	0.233

Table 2. Species mass fractions for simulated combustion.

C. BOUNDARY AND VOLUME CONDITIONS

Two wall boundary conditions are evaluated, adiabatic and isothermal. In the isothermal condition, the outer bulkheads, overhead and deck are maintained at 300 K. Interior bulkheads are designated as adiabatic for all simulations. A uniform wall roughness of 0.0005 m is used for the overhead, deck and bulkheads.

For all simulations, the reference pressure and gravitational acceleration are set at 100 kPa and -9.81 m/s, respectively.

For the volume conditions, the evaluation methods for density, viscosity and specific heat are the ideal gas law, mixed Sutherland's law and the mix Joint Army, Navy, NASA and Air Force (JANNAF) method respectively. The Prantl number and Schmidt number were set at 0.707 and 0.7 respectively.

The initial volume conditions for all simulations are provided in Table 3.

Location	U Velocity (m/s)	V Velocity (m/s)	W Velocity (m/s)	Relative Pressure (Pa)	Temperature (K)
Block 1	0	0	0	0	300
Block 2	0	0	0	0	300
Block 3	0	0	0	0	300
Block 4	0	0	0	0	300

Table 3. Volume initial conditions.

D. SIMULATION MATRIX

Table 4 provides a summary of the model simulations evaluated in this study. Each simulation is evaluated at steady state.

Simulation Identification	Watertight Door Inlet Velocity (m/s)	Fire Simulation Method	Exterior Bulkhead Boundary Condition
1	1	CFD Chemistry module	Adiabatic
2	1	CFD Chemistry Module	Isothermal
3	1	Hot Combustion Products	Isothermal
4	0.5	CFD Chemistry Module	Isothermal
5	2	CFD Chemistry Module	Isothermal
6	0.5	CFD Chemistry Module	Adiabatic
7	2	CFD Chemistry Module	Adiabatic

Table 4. Simulation summary matrix.

III. RESULTS

For each variable, such as velocity components, enthalpy, pressure, etc., residuals are calculated for each cell, weighted by the cell volume, and then summed over the entire model. A residual reduction of five orders of magnitude is desired to ensure that solution convergence is achieved. [Ref 17] For all simulations in this study, each variable attains a residual reduction of three to four orders of magnitude. To achieve a residual reduction of at least five orders of magnitude, a finer model grid is required, however, this study is limited by available computer memory. The variable with the largest residual is enthalpy. Although the variables for each simulation only achieve a minimum of three orders of magnitude residual reduction, the results are sufficient to evaluate smoke movement in the structure.

Figures 4 and 5 present the representative section views used to analyze the data. Section A-A is an elevation view along the centerline of the longitudinal passageway. Section B-B is an elevation view along the centerline of the transverse passageway. Section C-C is an elevation view that bisects the stateroom door. Section D-D is a plan view located 0.5 m above the deck. Section E-E is a plan view located 1.75 m above the deck.

Results for simulations 1-7 are presented in Appendices A-G respectively. For this study, CO_2 is the molecular species selected to represent smoke. The figures in the appendices concentrate on the temperature distribution, CO_2 mass fraction distribution and the total gas mixture (CO_2, H_2O, O_2 and N_2) circulation pattern.

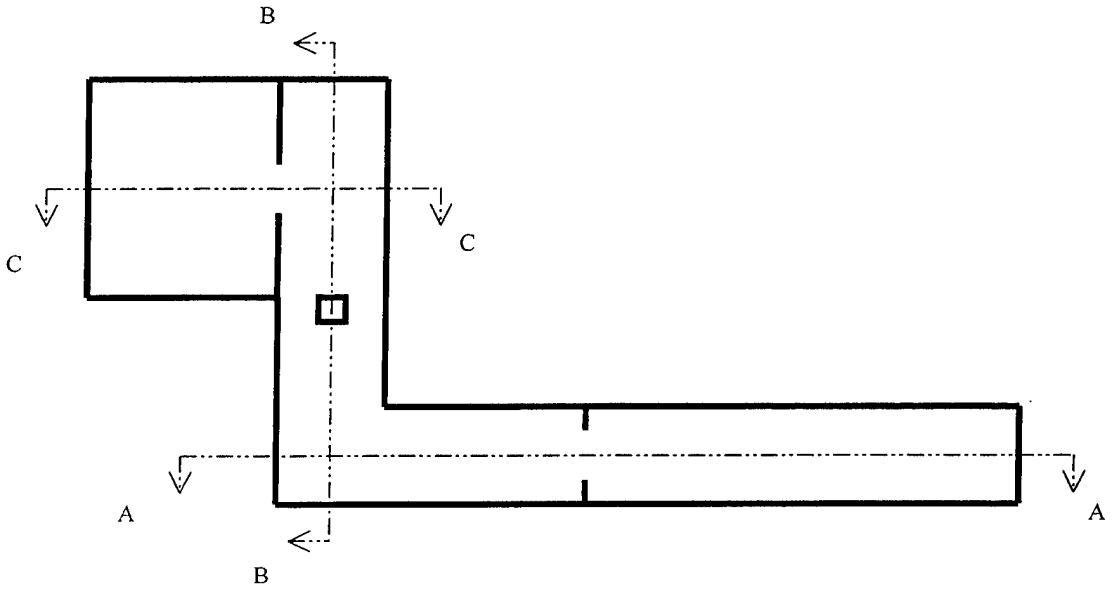

Figure 4. Plan view section identification.

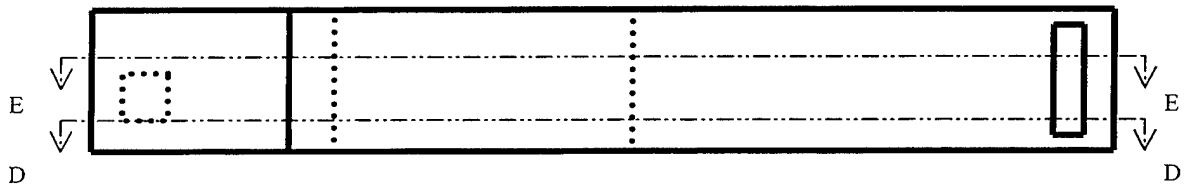

Figure 5. Elevation view section identification.

Given the geometry modifications of the CFD model as compared to the experimental structure of Reference 13 and the isothermal/adiabatic boundary condition assumptions for the overhead, deck and bulkheads, all simulation results compare reasonably well with the experimental smoke propagation distance reported in Reference 13 for a 620 kW fire. Figures 6 and 7 show that the CO_2 gas mass fraction distributions at the longitudinal passageway and stateroom doors are very similar. In Figure 6,

simulations 5 and 7 show that for an air inlet velocity of 2.0 m/s, the CO_2 mass fraction distribution is nearly zero for the isothermal and adiabatic bulkhead boundary conditions indicating that CO_2 propagation is significantly decreased downstream from the door. As the air inlet velocity decreases, the CO_2 mass fraction distributions diverge slightly as the top of the door is approached. Figure 6 also shows that the CO_2 gas mass fraction values for simulations 1 and 2 at an elevation of 1.75 m at the centerline of the longitudinal passageway door are within approximately 13% of each other. Additionally, the CO_2 gas mass fraction values for simulations 4 and 6 at an elevation of 1.75 m at the centerline of the longitudinal passageway door are within approximately 10% of each other. The CO_2 gas mass fraction value at an elevation of 1.75 m for simulation 3 is within approximately 40% of the value for simulation 1. Additionally, for a given air inlet velocity, comparison of the effect of bulkhead boundary condition (isothermal/adiabatic) on CO_2 mass fraction distribution in the longitudinal passageway reveals very similar patterns and are displayed in Figures 12, 25 (1 m/s inlet velocity), Figures 51, 77 (0.5 m/s inlet velocity) and Figures 64, 90 (2.0 m/s inlet velocity).

The air inlet velocity has a strong effect on the thickness of the CO_2 layer passing through the door. As observed in Figures 11, 24, 37, 50, 63, 76 and 89, the flow area reduction (39% area reduction) formed by the longitudinal passageway door restricted CO_2 propagation against the forced air flow from the inlet. Additional insight into the gas flow pattern for varying counter–flow velocities at the longitudinal passageway door are provided in Figures 10, 23, 36, 49, 62, 75 and 88. These flow patterns are consistent with experimental smoke propagation in the presence of a constriction against an airflow and is briefly described by Klote and Fothergill. [Ref 18: p. 22-23]

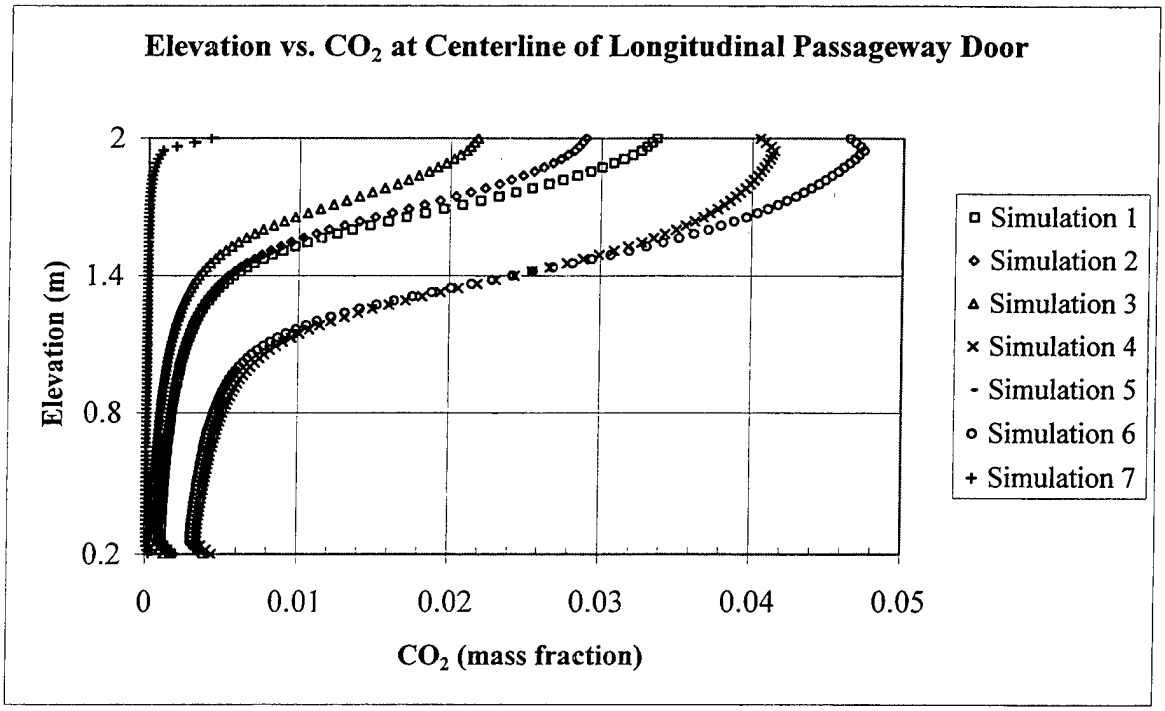

Figure 6. Plot of elevation versus CO_2 for all simulations at the centerline of the longitudinal passageway.

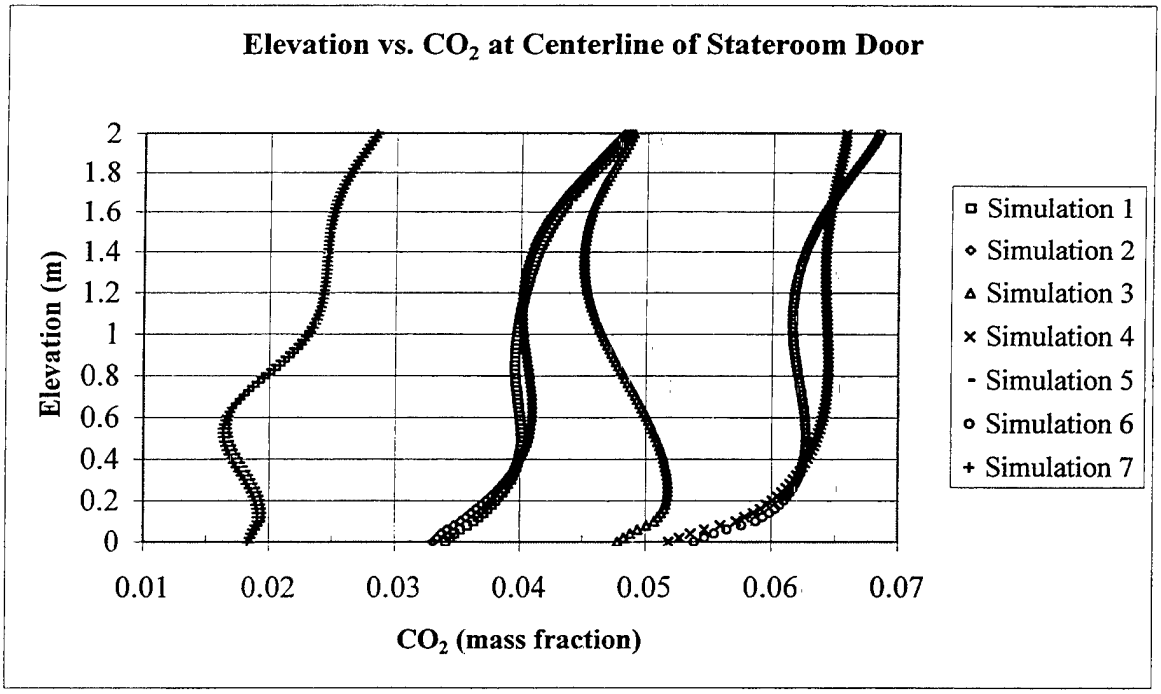

Figure 7. Plot of elevation versus CO_2 for all simulations at the centerline of the stateroom door.

Figure 7 shows that the CO_2 mass fraction distribution at the stateroom door is nearly identical for both the isothermal and adiabatic bulkhead boundary condition for all simulations using the CFD combustion module.

Figures 8 and 9 show the temperature profile at the longitudinal passageway door and the stateroom door for all simulations. With the exception of simulation 5 and 7, simulations using the CFD combustion module display a significant disparity in temperatures throughout the model because of the different overhead, deck and bulkhead boundary conditions. Simulations 5 and 7 show no difference in temperature because the air inlet velocity is sufficient to prevent the thermal layer from propagating towards the forced air inlet.

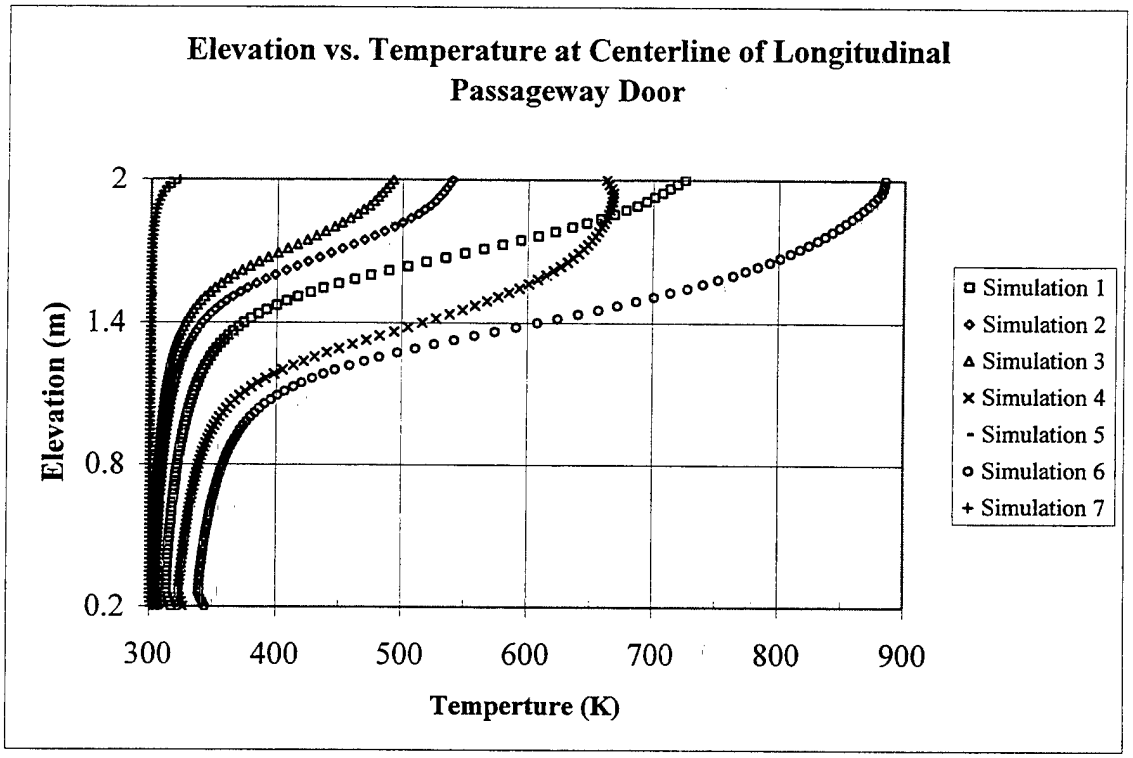

Figure 8. Plot of elevation versus temperature at the centerline of the longitudinal passageway door.

The CFD combustion model is not used in simulation 3 and yields different results. CO_2 propagation against the forced inlet air supply is not as pronounced as it is in simulations 1 and 2. Simulation 3 space temperatures are lower at the longitudinal passageway door, yet the temperatures are higher at the stateroom door than those found in simulation 2. Simulation 3 results do not compare as well as simulations 1 and 2 do with the experimental results reported in Reference 13 in terms of smoke propagation distance and temperature distribution.

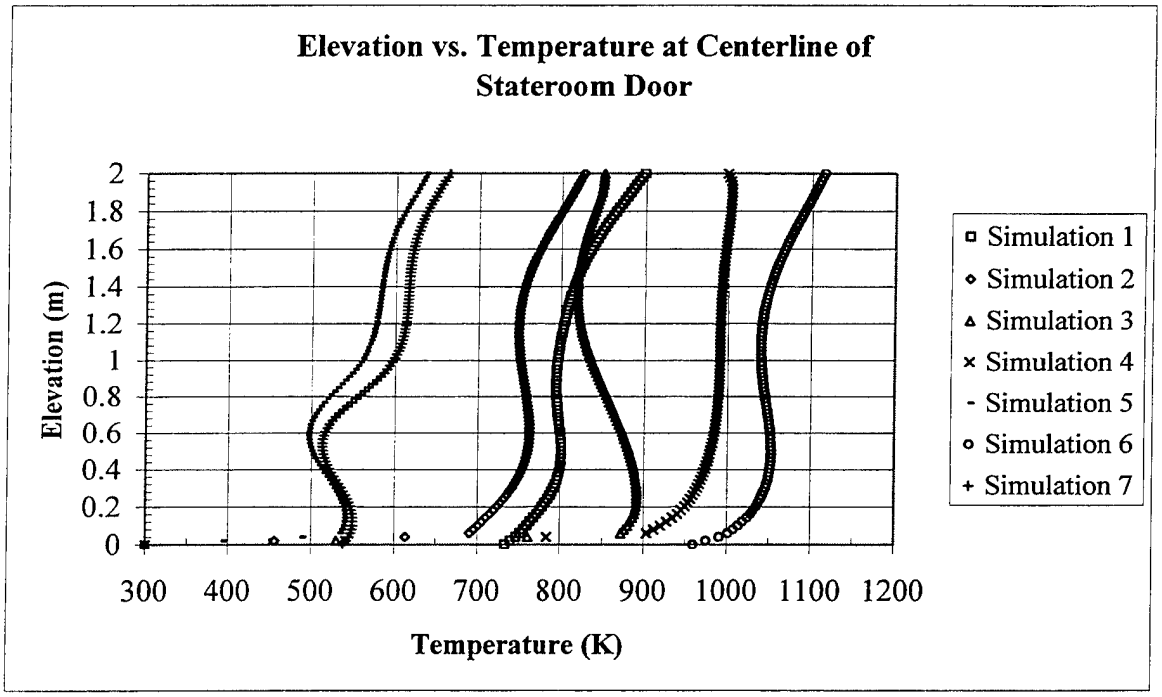

Figure 9. Plot of elevation versus temperature at the centerline of the stateroom door. The scattered data near the deck for simulations 2, 3, 4 and 5 are caused by the isothermal deck boundary condition.

The average temperature using 100 data points at two locations for simulations 5 and 7 are calculated and compared to the average temperature reported at the same general location in the experimental structure of Reference 13. The model average

temperatures at the centerline of the stateroom door and the centerline of the longitudinal passageway door for simulation 5 are 275 C and 27.6 C respectively. The model average temperatures at the centerline of the stateroom door and the centerline of the longitudinal passageway door for simulation 7 are 310 C and 28.1 C respectively. The average temperatures reported in the experimental structure at approximately the same locations were 356 C and 71 C respectively. The average temperatures for both simulations are lower than the average temperatures observed in the live fire experiment.

As seen in Appendices A-G, the CFD models produce many interesting flow patterns. As mentioned before, the flow pattern observed at the centerline of longitudinal passageway door is consistent with experimental observations. Another interesting flow pattern develops at the stateroom door. Figures 17, 18, 30, 31, 43, 44, 56, 57, 69, 70, 82, 83, 95 and 96 display a shear flow at the stateroom door that grows in intensity with increasing inlet velocity. The D-D section view shows that the lower flow is directed towards the vent while the E-E section view shows that the upper flow is directed away from the vent.

Figures 15, 28, 41, 54, 67, 80 and 93 show for all simulations that temperature stratification of the gas mixture in the stateroom is nonexistent and results in a relatively uniform temperature distribution. The CO_2 distribution, depicted in Figures 16, 29, 42, 55, 68, 81 and 94, is also relatively uniform indicating that strong turbulence is present in the stateroom. With the breakdown of two-layer temperature stratification, a zone model will experience problems in providing accurate results in the stateroom.

THIS PAGE INTENTIONALLY LEFT BLANK

IV. CONCLUSIONS

Computational fluid dynamics modeling of fire generated smoke propagation in a compartmented shipboard structure against an air flow provides results such as fluid circulation patterns, smoke propagation distances and structure temperature distributions, that are consistent with experimental data of Reference 13. Sufficient information of smoke movement in the structure is obtained without dedicating significant time and effort to modeling the exact experimental structure geometry and to realistically modeling the overhead, deck and bulkhead heat transfer rates. If fire spread or heat transfer to adjacent spaces is to be studied, detailed modeling of the structure geometry and accurate information of boundary heat transfer rates are required to obtain realistic predictions.

A zone model of smoke propagation in the structure used in this study would provided inaccurate results in the transverse passageway and the stateroom because of the breakdown of thermal stratification. Computational fluid dynamics modeling does not encounter this problem because it provides results based on the solution of the fundamental conservation laws.

The CFD combustion module used to simulate instantaneous combustion of propene gas yields results that are consistent with the experimental results of Reference 13.

A CFD program is computationally intensive; therefore, it is very demanding on computer resources. Each simulation in this study required 4-5 days to generate results while only achieving a 3-4 order of magnitude residual reduction. Although adequate

results were obtain, a finer mesh of the structure was required to ensure that a minimum of 5-6 orders of magnitude residual reduction was obtained for all variables. With a finer mesh, a faster processor and a larger RAM capability is required to keep the computation time within reason. Generally, for every 100,000 elements, 100 MB of RAM was required.

Based on the findings of this study, computational fluid dynamics modeling can be a powerful design tool for evaluating smoke and fire movement in current and future ship designs and proposed damage control configurations.

V. RECOMMENDATIONS

The following recommendations are made in continuation of this study:

- Develop a more realistic model for the combustion process. The combustion process is a very complex problem. Better knowledge of the process will allow engineers to design reliable sensors to rapidly identify a particular fire and develop fire suppressions systems that quickly and effectively extinguish fires.
- Model the effect of forced counter-flow ventilation on fire growth and intensity.
- Vary vent parameters such as vent location and boundary conditions (back pressure, fixed exit velocity simulating an operating fan, etc.) to study the effect on smoke propagation in a compartmented structure. Smoke control plans and/or systems must be integrated into future designs of collective protection systems. Knowledge of smoke propagation under the influence of shipboard ventilation systems is required to properly develop these systems.
- Study the effects of varying the location of the burn pan and fire intensity on smoke propagation. Knowledge of anticipated casualty indications will allow engineers to design automated damage control systems that respond quickly and correctly to a specific casualty.
- Modify the bulkhead, overhead and deck boundary conditions to more closely simulate reality. Explore the use of conjugate heat transfer to simulate conduction through the overhead, deck and bulkheads. Flashover of spaces adjacent to a fire is an issue of great concern to shipboard personnel.

- Use transient time step calculations to predict bulkhead, overhead and deck temperatures, and smoke propagation behavior throughout the structure. Knowledge of transient smoke behavior is important in the design and placement of smoke sensors, the development of smoke control plans and/or systems and the protection of shipboard personnel.
- Study smoke propagation and heat conduction in a multi-level compartmented structure.
- Include radiation heat transfer in the model.

LIST OF REFERENCES

1. Levinson, J.L. and Edwards, R.L., *Missile Inbound*, Naval Institute Press, 1997.

2. Scott, R., *Ship Manpower: How Low Can We Go?*, Jane's Defence Weekly, Volume 033, Issue 015, April 12, 2000.

3. http://www.chemistry.nrl.navy.mil/dcarm/objectives.html

4. http://www.chemistry.nrl.navy.mil/dcarm/remotemanualtest.html

5. Karlsson, B. and Quintiere, J.G., *Enclosure Fire Dynamics*, CRC Press LLC, 2000.

6. Jones, W.W. and Walton, W.D., *Spread of Smoke in an FFG 7,* Proceedings of the First NATO Conference on Fire Propagation Onboard Warships Ottawa, 1983.

7. Building and Fire Research Laboratory, NISTIR 4872, *Modeling Smoke Movement through Compartmented Structures*, by Jones, W.W. and Forney, G.P., 08 July 1992.

8. Naval Research Laboratory, NRL/MR/6180—95-7781, *Validation of Fire/Smoke spread Model (CFAST) using Ex-USS SHADWELL Internal Ship Conflagration control (ISCC) Fire Tests*, by Bailey, J.L. and Tatem, P.A., 30 September 1995.

9. Chow, W.K., *Studies On The Stability Of Thermal Stratified Layer In a Forced Ventilation Fire Using Computational Fluid Dynamics*, Journal of Applied Fire Science, v. 6(1), 1996.

10. Mehls, M., *Propagation of Fire Generated Smoke in Shipboard Spaces*, M.S. Thesis, Naval Postgraduate School, Monterey, California, March 2000.

11. Abaya, A.F., Jr., *Propagation of Fire Generated Smoke in Shipboard Spaces with Geometric Interferences*, Master's Thesis, Naval Postgraduate School, Monterey, California, September 2000.

12. Vegara, B.J., *Propagation of Fire Generated Smoke and Heat Transfer in Shipboard Spaces with a Heat Source*, Master's Thesis, Naval Postgraduate school, Monterey, California, September 2000.

13. Naval Research Laboratory, NRL/MR/6180—94-7616, *Shipboard Smoke Control Tests Using Forced Counterflow Air Supply*, by Williams, F.W., Forssell, E.W., DiNenno, P.J., Beyler, C.L. and Lain, P., 16 September 1994.

14. CFD-ACE(U), *Modules*, Version 6.4, CFD Research Corporation, January 2001.

15. Drysdale, D., *An Introduction to Fire Dynamics*, 2nd ed., John Wiley & Sons, Ltd., 1998.

16. Sonntag, R.E., Borgnakke, C. and Van Wylen, G.J., *Fundamentals of Thermodynamics*, 5th ed., John Wiley & Sons, Inc., 1998.

17. CFD-ACE(U), *User's Manual*, Version 6.4, CFD Research Corporation, January 2001.

18. Klote, J.H. and Fothergill, J.W., Jr., *Design of Smoke Control Systems for Buildings*, NBS Handbook 141, U.S. Department of Commerce, Washington D.C, July 1983.

BIBLIOGRAPHY

Abaya, A.F., Jr., *Propagation of Fire Generated Smoke in Shipboard Spaces with Geometric Interferences*, Master's Thesis, Naval Postgraduate School, Monterey, California, September 2000.

Building and Fire Research Laboratory, NISTIR 4872, *Modeling Smoke Movement through Compartmented Structures*, by Jones, W.W. and Forney, G.P., 08 July 1992.

Building and Fire Research Laboratory, NISTIR 5516, *Method of Predicting Smoke Movement in Atria Wing Application of Smoke Management*, by Klote, J.H., November 1994.

CFD-ACE(U), *User Manual*, Version 6.4, CFD research Corporation, January 2001.

Chemical Engineers' Handbook, 3rd ed., McGraw-Hill Book Company, Inc., 1950.

Chow, W.K., *Studies On The Stability Of Thermal Stratified Layer In a Forced Ventilation Fire Using Computational Fluid Dynamics*, Journal of Applied Fire Science, v. 6(1), 1996.

Cox, G. and Kumar, S., *Field Modeling of fire in Forced Ventilated Enclosures*, Combustion Science and Technology, v. 52, 1987.

Drysdale, D., *An Introduction to Fire Dynamics*, 2nd ed., John Wiley & Sons, Ltd., 1998.

Emmons, H.W., *The Prediction of Fires in Buildings*, 17th Symposium (International) on Combustion, The Combustion Institute, 1978.

Jones, W.W. and Walton, W.D., *Spread of Smoke in an FFG 7,* Proceedings of the First NATO Conference on Fire Propagation Onboard Warships Ottawa, 1983.

Jones, W.W. and Forney, G.P., Improvement in Predicting Smoke Movement in Compartmental Structures, Fire Safety Journal, 21, 269, 1993.

Jones, W.W., A Multicompartment Model for the Spread of Fire, Smoke and Toxic Gases, Fire Safety Journal, 9, 55, 1985.

Karlsson, B. and Quintiere, J.G., *Enclosure Fire Dynamics*, CRC Press LLC, 2000.

Kay, D., Morris, M., *The Role of Fire and Smoke Movement Modelling,* The Institute of Marine Engineers Conference on Fire Safety on Ships: Developments into the 21st Century, 26-27 May 1994.

Klote, J.H. and Fothergill, J.W., Jr., *Design of Smoke Control Systems for Buildings*, NBS Handbook 141, U.S. Department of Commerce, Washington D.C, July 1983.

Klote, J. H., *An Overview of Smoke Control Research*, ASHRAE Transactions: Symposia, v. 101, no. 1, 1995.

Klote, J. H. and Nelson, H.E., *Smoke Movement in Buildings*, Fire Protection Handbook, 18th ed., Section 7, Chapter 6, National Fire Protection Association, Quincy, MA, 1997.

Klote, J. H., *Smoke Control*, SFPE Handbook of Fire Protection Engineering. 2nd ed., Chapter 12, Section 4, p. 230-245.

Levinson, J.L. and Edwards, R.L., *Missile Inbound*, Naval Institute Press, 1997.

Mehls, M., *Propagation of Fire Generated Smoke in Shipboard Spaces*, M.S. Thesis, Naval Postgraduate School, Monterey, California, March 2000.

Milke, J.A. and Mowrer, F.W., *Computer Aided Design for Smoke Management*, ASHRAE Journal, August 1995.

National Fire Protection Association, NFPA 92A, *Recommended Practice for Smoke Control Systems*, NFPA, Quincy, MA, 1988.

Naval Research Laboratory, NRL/MR/6410—00-8428, *Advanced Simulation Tool for Improved Damage Assessment 10 A Multiblock technique for Simulating Fire and Smoke Spread in large Complex Enclosures*, by Prasad, K., Patniak, G. and Kailasanath, K., 21 February 2000.

Naval Research Laboratory, NRL/MR/6180--00-8446, *Modeling Missile Propellant Fires In Shipboard Compartments*, by Tatem, P.A., Williams, F.W., White, D.A., Beyler, C.L., 30 March 2000.

Naval Research Laboratory, NRL/MR/6180—94-7616, *Shipboard Smoke Control Tests Using Forced Counterflow Air Supply* , by Williams, F.W., Forssell, E.W., DiNenno, P.J., Beyler, C.L. and Lain, P., 16 September 1994.

Naval Research Laboratory, NRL/MR/6180—95-7781, *Validation of Fire/Smoke spread Model (CFAST) using Ex-USS SHADWELL Internal Ship Conflagration control (ISCC) Fire Tests*, by Bailey, J.L. and Tatem, P.A., 30 September 1995.

Null, G., *Computer Simulation Of The Thermal Effects On A Concentric Canister Missile Launcher With a Fire In An Adjacent Compartment*, Master's Thesis, Naval Postgraduate School, Monterey, California, September 1997.

Peacock, R.D. Jones, W.W., and Burkowski R.W., *Verification of a Model of Fire Growth and Smoke Transport*, Fire Safety Journal 21, 89, 1993.

Quintiere, J.G., *Principles of fire Behavior*, Delmar Publishers, 1998.

Sonntag, R.E., Borgnakke, C. and Van Wylen, G.J., *Fundamentals of Thermodynamics*, 5th ed., John Wiley & Sons, Inc., 1998.

Stroup, D.W., and Madrzykowski, D., *Modeling Smoke Flow in Corridors*, International Conference on Fire Research and Engineering, 10-15 September 1995.

Tabarra, M., Kenrick, B., and Matthews, R.D., *CFD Validation of Natural Smoke Movement in a Model Tunnel*, ASME Fluids Engineering Division Conference, FED-Vol. 238, 1996.

Thomas, P.H., *The Movement of Smoke in Horizontal Passages Against an Air Flow*, Fire Research Note No. 723, Fire Research Station, Borehamwood, Herts, England, 1968.

Vegara, B.J., *Propagation of Fire Generated Smoke and Heat Transfer in Shipboard Spaces with a Heat Source*, Master's Thesis, Naval Postgraduate school, Monterey, California, September 2000.

Versteeg, H.K. and Malalasekera, W., *An Introduction to Computational Fluid Dynamics*, Longman Group LTD., 1995.

THIS PAGE INTENTIONALLY LEFT BLANK

APPENDIX A: SIMULATION 1

Simulation 1 uses the CFD combustion module to simulate a 620 kW fire. The overhead, deck and bulkheads of the structure are adiabatic. The inlet, burn pan, vent and bulkhead conditions are presented in Table 5. The gas mixtures for the inlet, burn pan and vent are shown in Table 6.

Inlet/ Outlet Boundary Conditions					
Location	U Velocity (m/s)	V Velocity (m/s)	W Velocity (m/s)	Relative Pressure (Pa)	Temperature (K)
Watertight Door Inlet	0	0	-1	0	300
Burn Pan	0	0.5	0	0	300
Vent	0	0	0	0	300
Bulkhead Boundary Conditions					
Location	U Velocity (m/s)	V Velocity (m/s)	W Velocity (m/s)	Wall Roughness (m)	Adiabatic / Isothermal
Interior Bulkheads	0	0	0	0.0005	Adiabatic
Exterior Bulkheads, Overheads, Deck	0	0	0	0.0005	Adiabatic

Table 5. Simulation 1, inlet, burn pan, vent and bulkhead boundary conditions.

	Inlet	Burn Pan	Vent
Mixture	Air	Propene/Air	Air

Table 6. Simulation 1, inlet, burn pan and vent mixture definition.

CFD program default solvers, inertial and linear relaxations, and variable limits are used to evaluate the model.

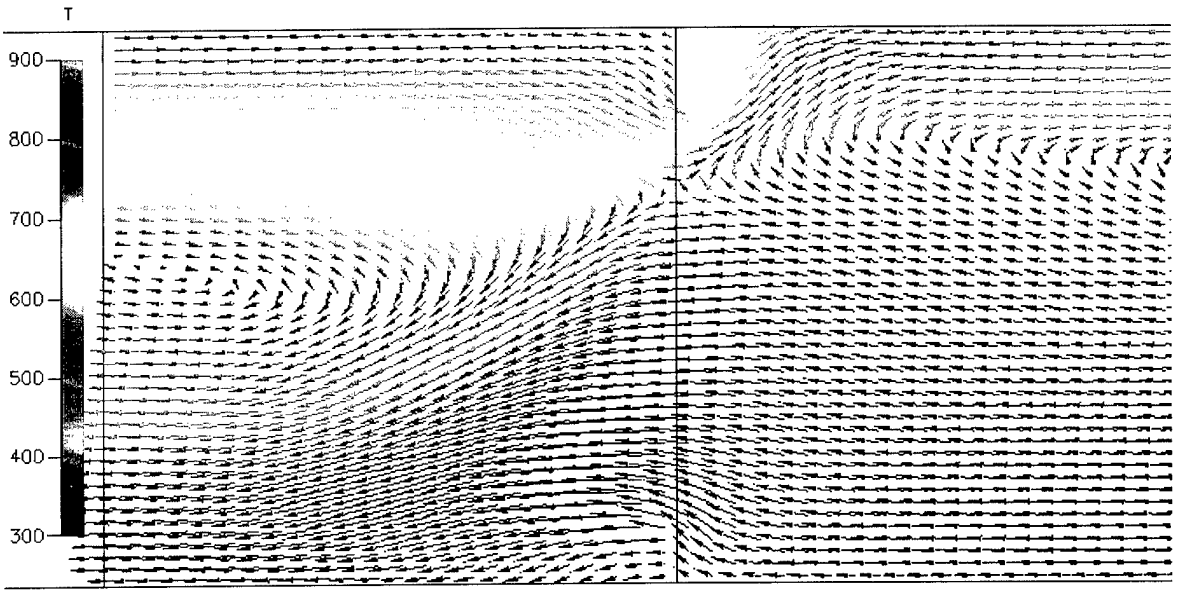

Figure 10. Simulation 1, partial elevation view (A-A) depicting temperature (K) distribution and fluid circulation pattern at the centerline of the longitudinal passageway in the vicinity of the watertight door.

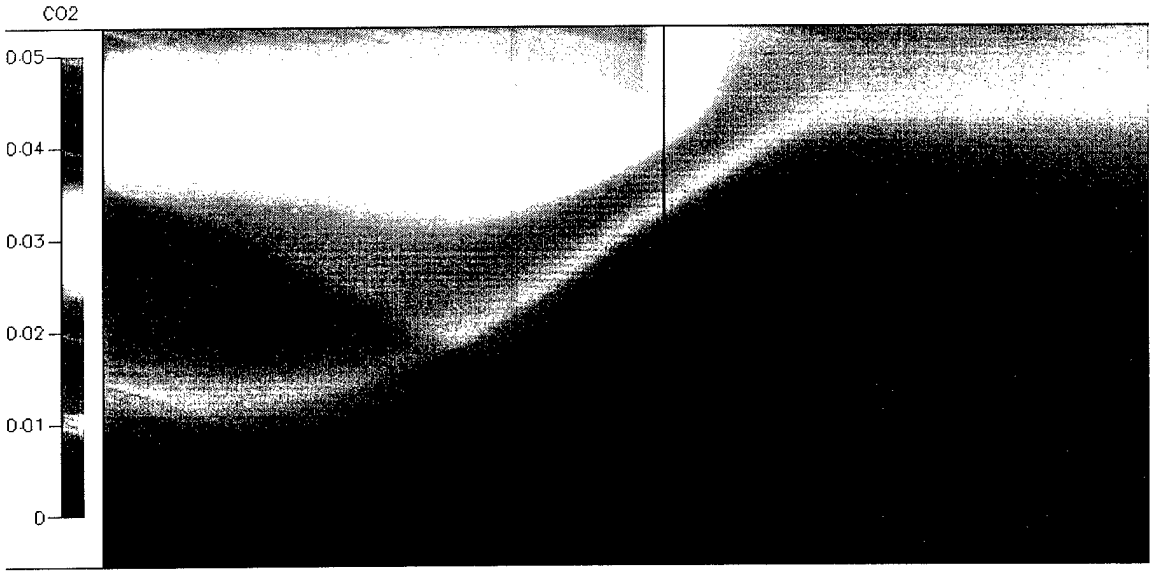

Figure 11. Simulation 1, partial elevation view (A-A) depicting CO_2 (mass fraction) distribution along the centerline of the longitudinal passageway in the vicinity of the watertight door.

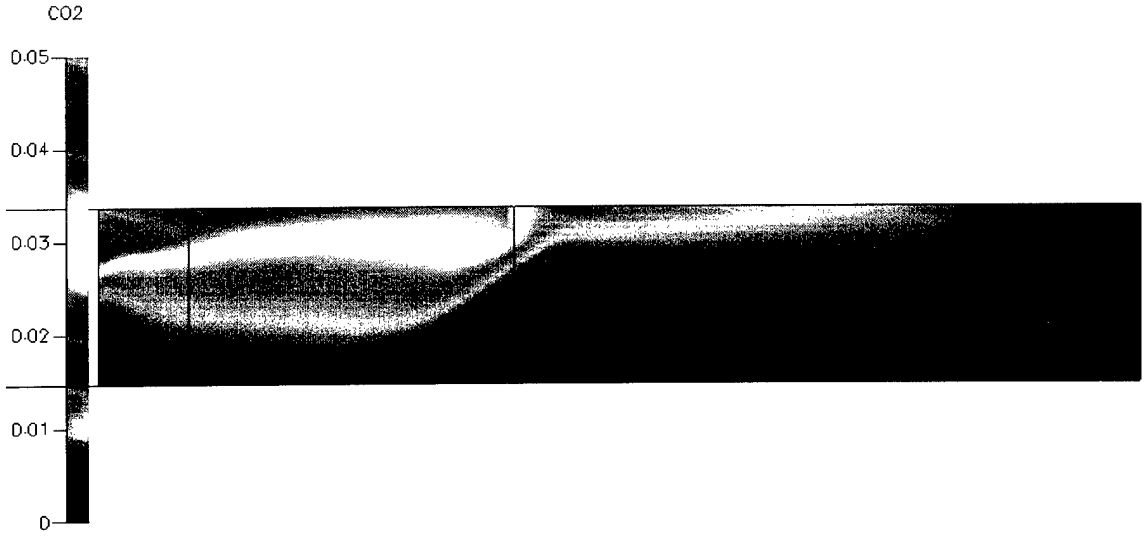

Figure 12. Simulation 1, elevation view (A-A) depicting CO_2 (mass fraction) distribution along the centerline of the longitudinal passageway.

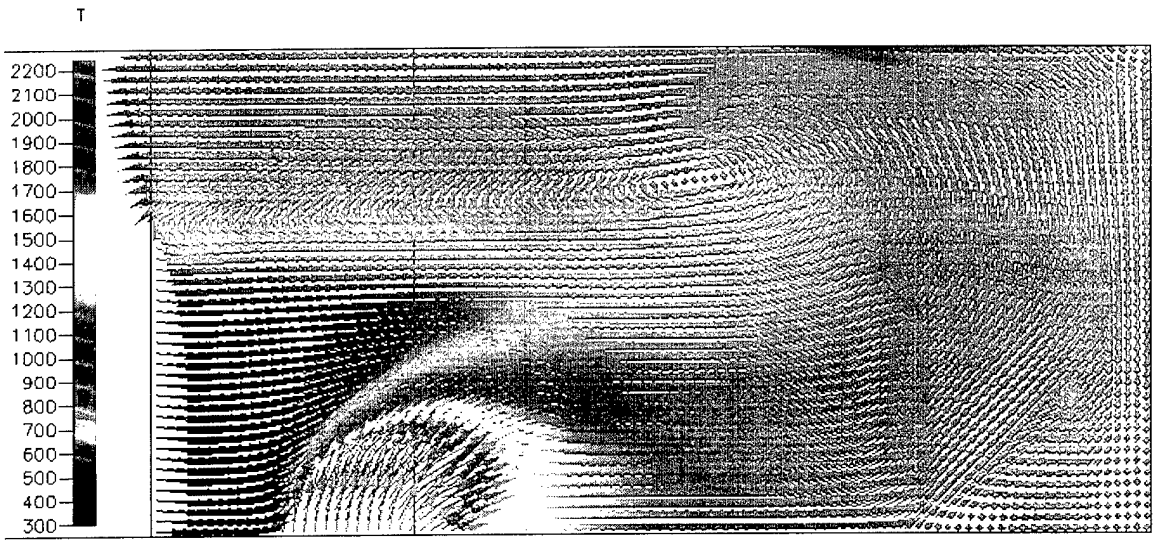

Figure 13. Simulation 1, partial elevation view (B-B) depicting temperature (K) distribution and fluid circulation pattern along the centerline of the transverse passageway on the port side of the structure.

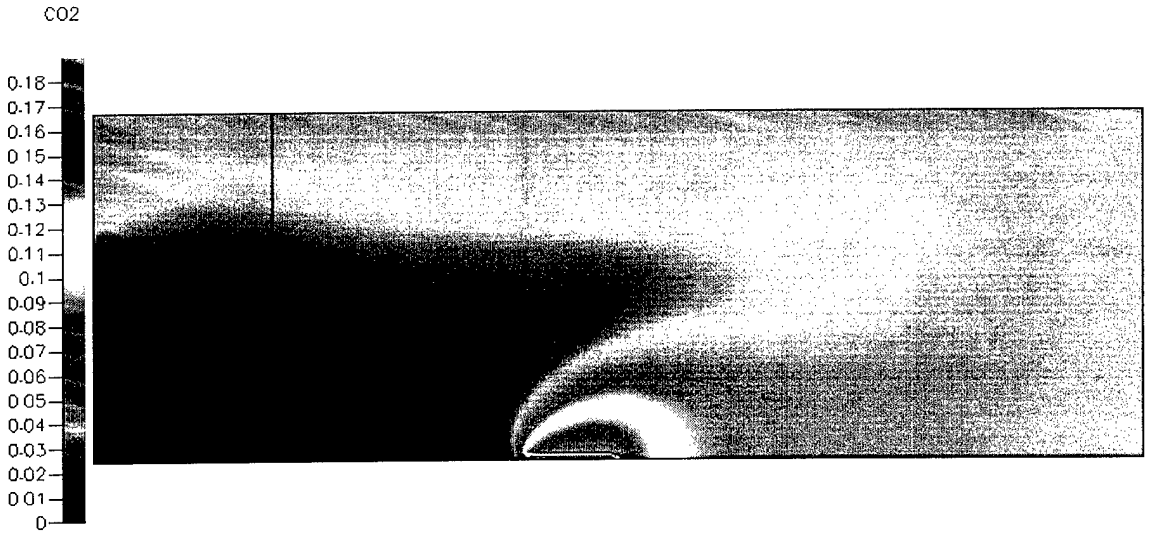

Figure 14. Simulation 1, elevation view (B-B) depicting CO_2 (mass fraction) distribution along the centerline of the transverse passageway.

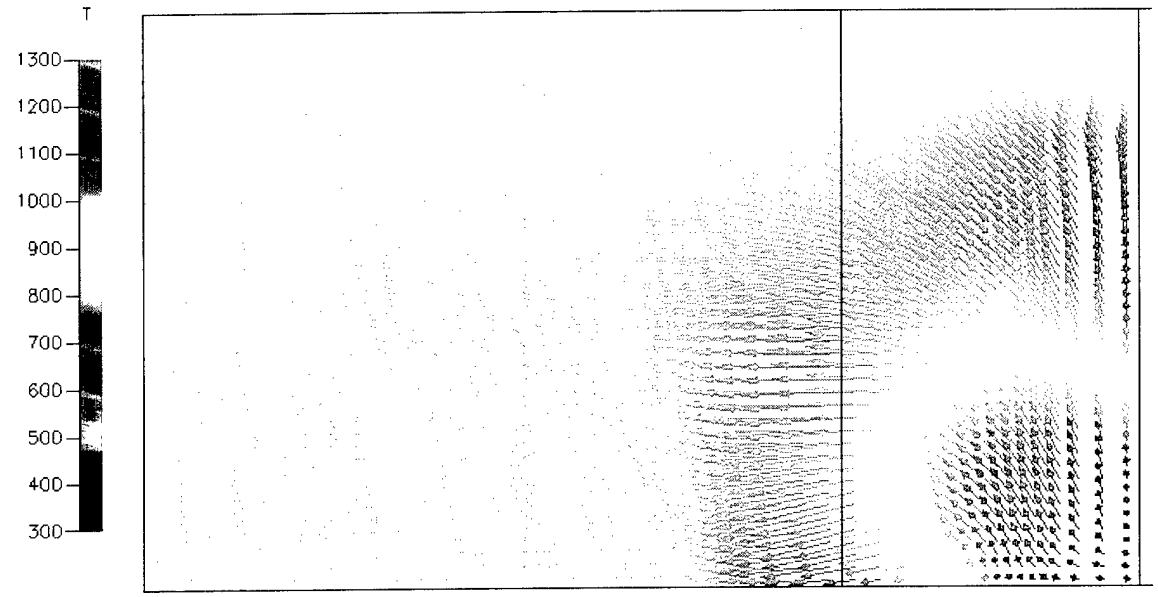

Figure 15. Simulation 1, partial elevation view (C-C) depicting temperature (K) distribution and fluid circulation pattern through the centerline of the stateroom door from the transverse passageway.

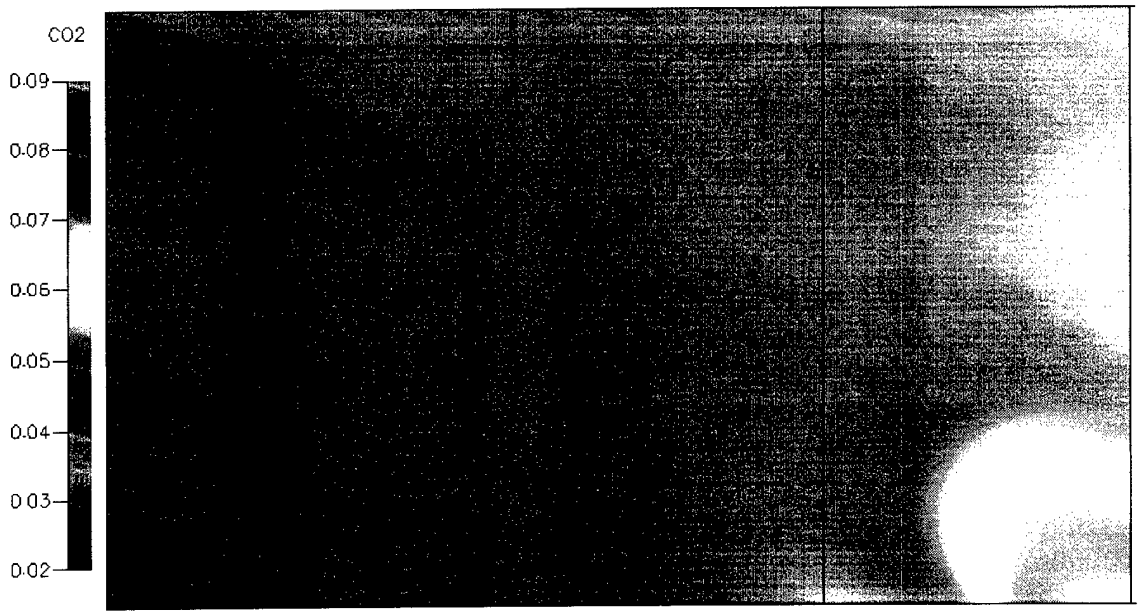

Figure 16. Simulation 1, partial elevation view (C-C) depicting CO_2 (mass fraction) distribution at the centerline of the stateroom door.

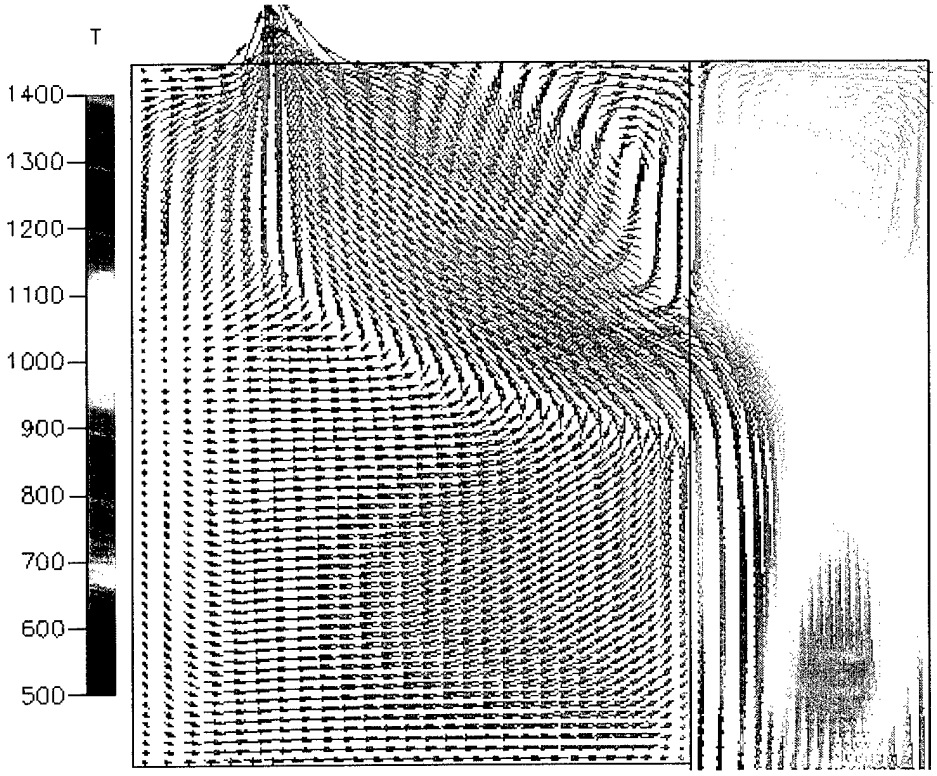

Figure 17. Simulation 1, partial plan view (D-D) depicting temperature (K) distribution and fluid circulation pattern from the transverse passageway through the door into the stateroom.

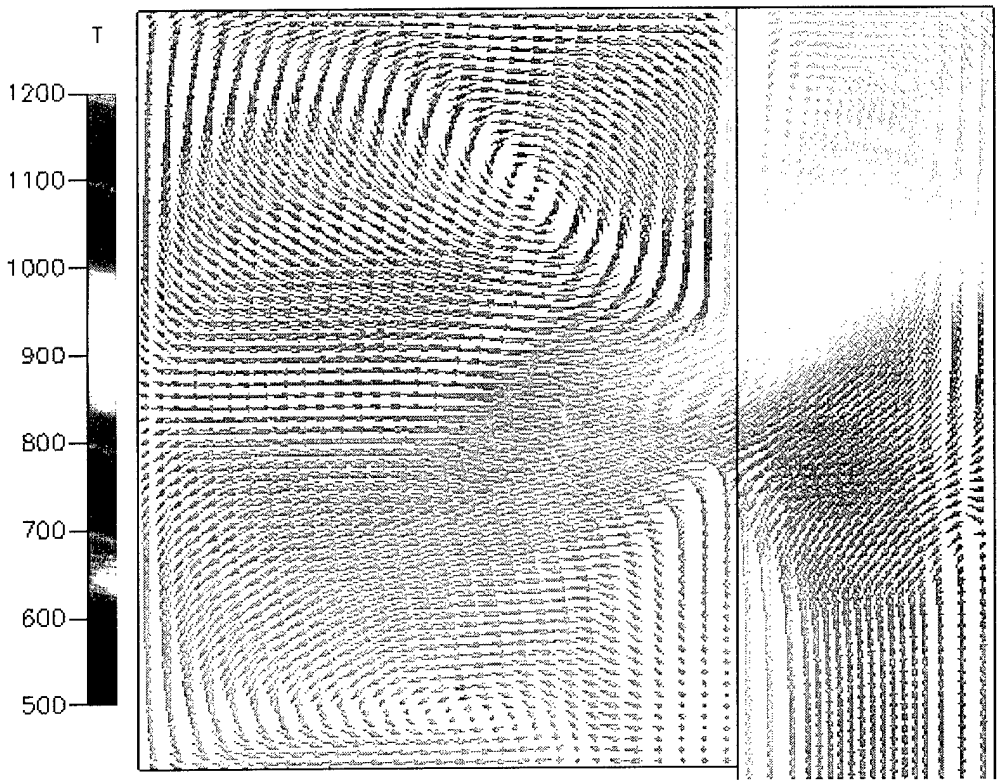

Figure 18. Simulation 1, partial plan view (E-E) depicting temperature (K) distribution and fluid circulation pattern from the transverse passageway through the door into the stateroom.

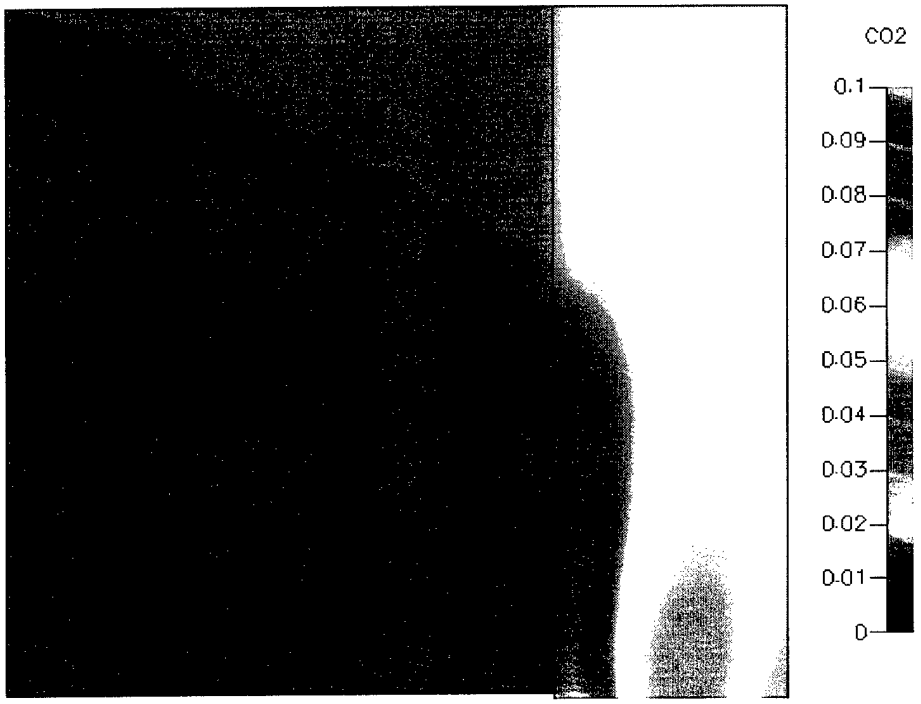

Figure 19. Simulation 1, partial plan view (D-D) depicting CO_2 (mass fraction) distribution in the stateroom and transverse passageway.

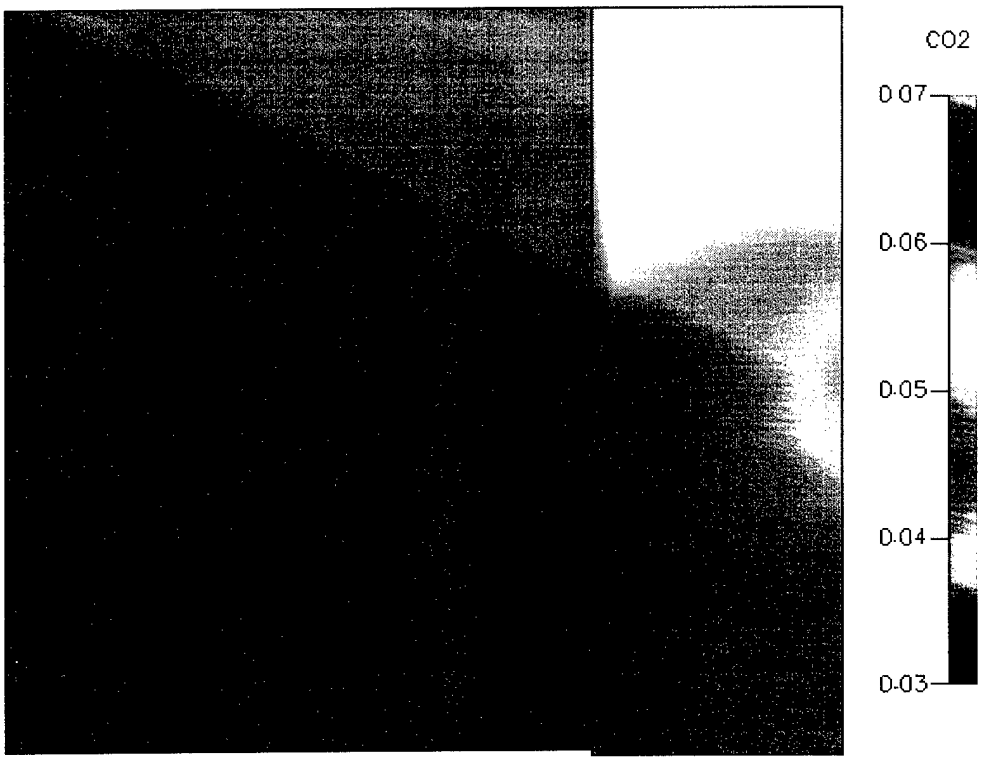

Figure 20. Simulation 1, partial plan view (E-E) depicting CO_2 (mass fraction) distribution in the stateroom and transverse passageway.

Figure 21. Simulation 1, plan view (D-D) depicting CO_2 (mass fraction) distribution throughout the structure.

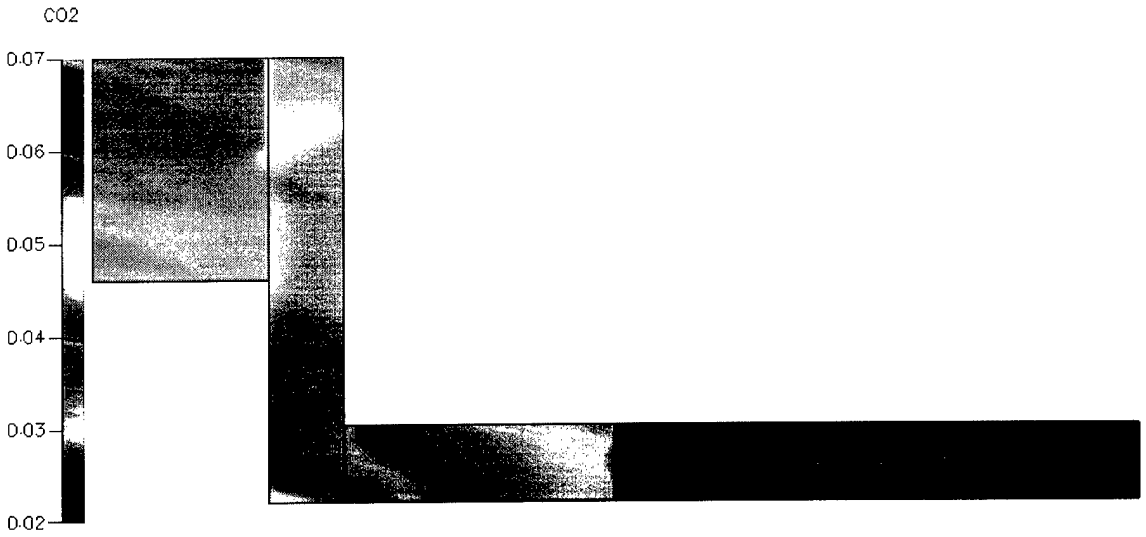

Figure 22. Simulation 1, plan view (E-E) depicting CO_2 (mass fraction) distribution throughout the structure.

APPENDIX B: SIMULATION 2

Simulation 2 uses the CFD combustion module to simulate a 620 kW fire. The overhead, deck and bulkheads of the structure are isothermal boundaries at 300 K. The inlet, burn pan and vent conditions are presented in Table 7. The gas mixtures for the inlet, burn pan and vent are shown in Table 8.

Inlet/ Outlet Boundary Conditions					
Location	U Velocity (m/s)	V Velocity (m/s)	W Velocity (m/s)	Relative Pressure (Pa)	Temperature (K)
Watertight Door Inlet	0	0	-1	0	300
Burn Pan	0	0.5	0	0	300
Vent	0	0	0	0	300
Bulkhead Boundary Conditions					
Location	U Velocity (m/s)	V Velocity (m/s)	W Velocity (m/s)	Wall Roughness (m)	Adiabatic / Isothermal
Interior Bulkheads	0	0	0	0.0005	Adiabatic
Exterior Bulkheads, Overheads, Deck	0	0	0	0.0005	Isothermal / 300 K

Table 7. Simulation 2, inlet, burn pan, vent and bulkhead boundary conditions.

	Inlet	Burn Pan	Vent
Mixture	Air	Propene/Air	Air

Table 8. Simulation 2, inlet, burn pan and vent mixture definition.

CFD program default solvers, inertial and linear relaxations, and variable limits are used to evaluate the model.

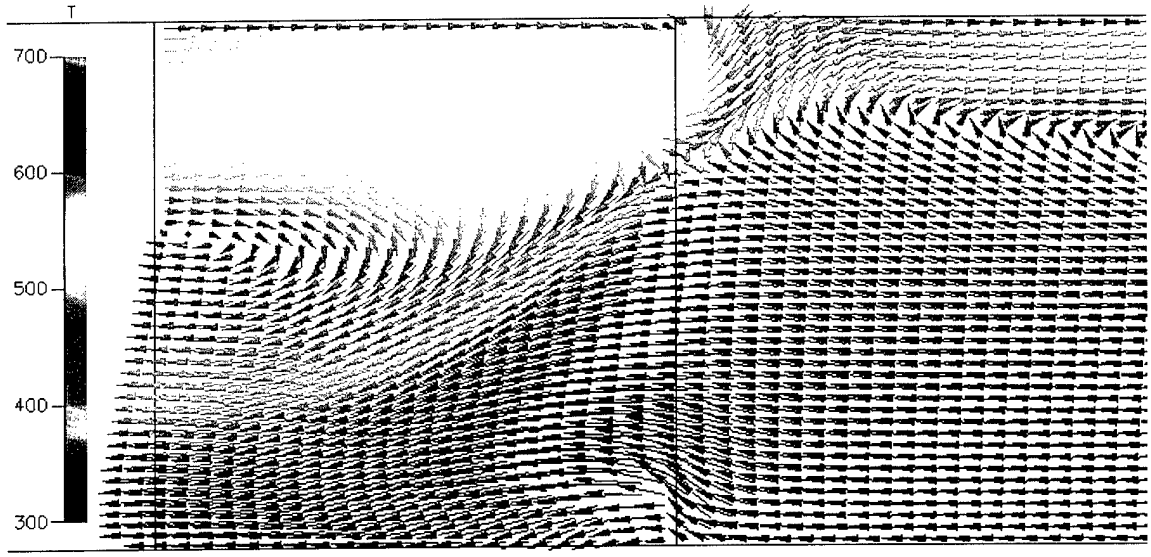

Figure 23. Simulation 2, partial elevation view (A-A) depicting temperature (K) distribution and fluid circulation pattern at the centerline of the longitudinal passageway in the vicinity of the watertight door.

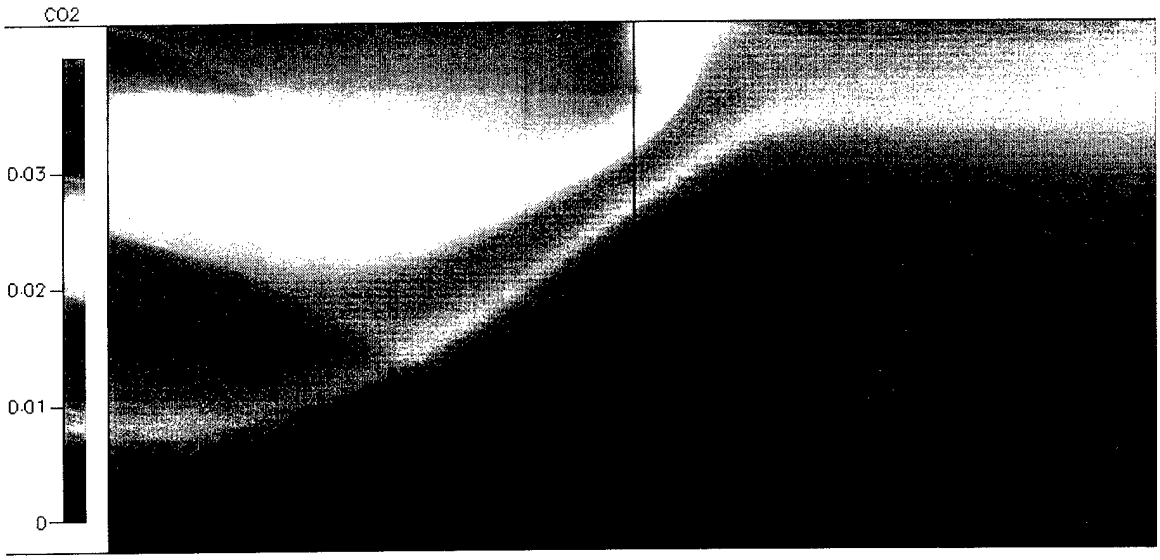

Figure 24. Simulation 2, partial elevation view (A-A) depicting CO_2 (mass fraction) distribution along the centerline of the longitudinal passageway in the vicinity of the watertight door.

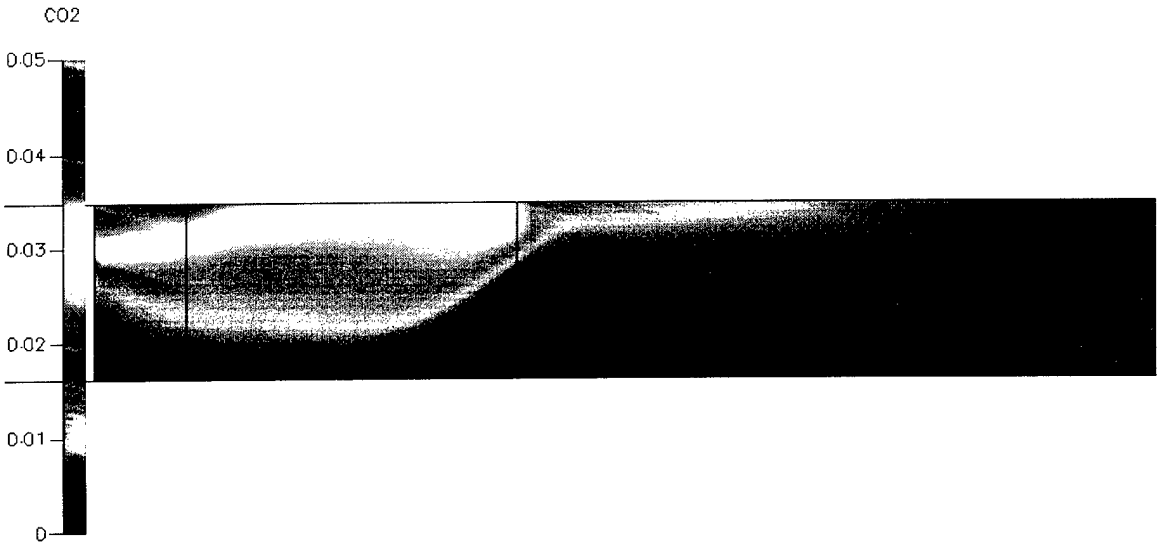

Figure 25. Simulation 2, partial elevation view (A-A) depicting CO_2 (mass fraction) distribution at the centerline of the longitudinal passageway.

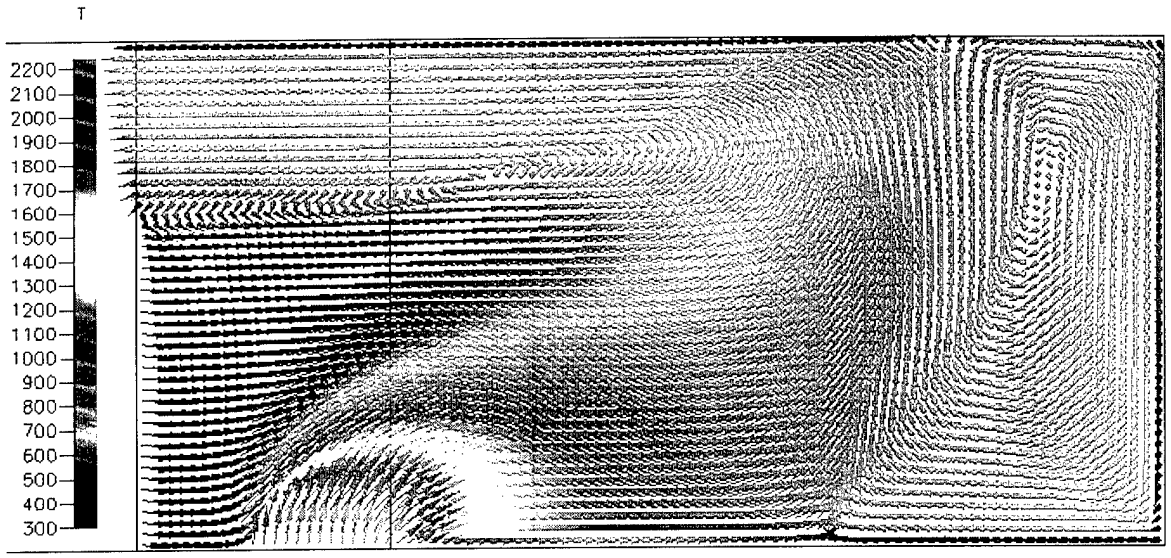

Figure 26. Simulation 2, partial elevation view (B-B) depicting temperature (K) distribution and fluid circulation pattern along the centerline of the transverse passageway on the port side of the structure.

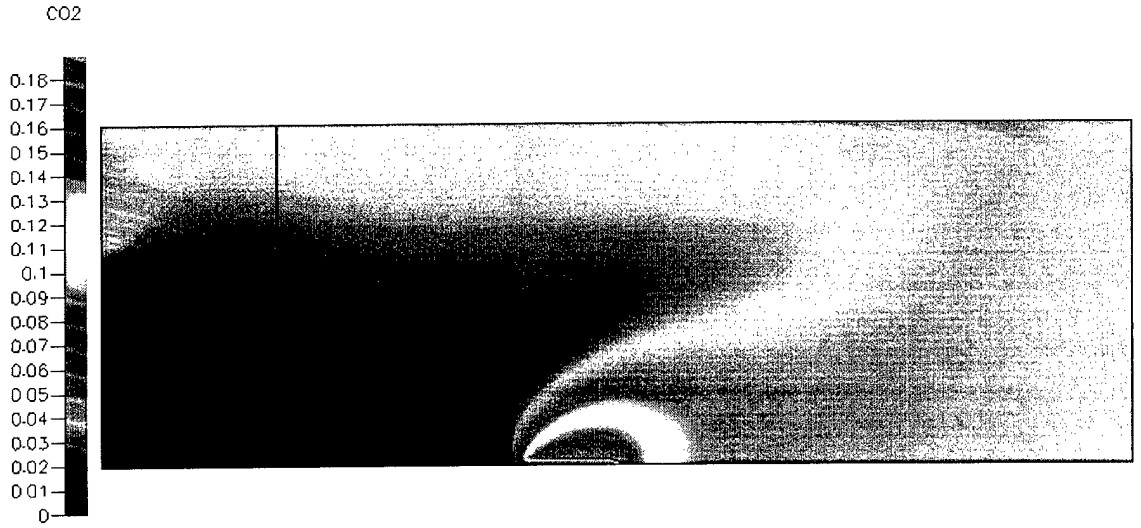

Figure 27. Simulation 2, elevation view (B-B) depicting CO_2 gas (mass fraction) distribution at the centerline of the transverse passageway.

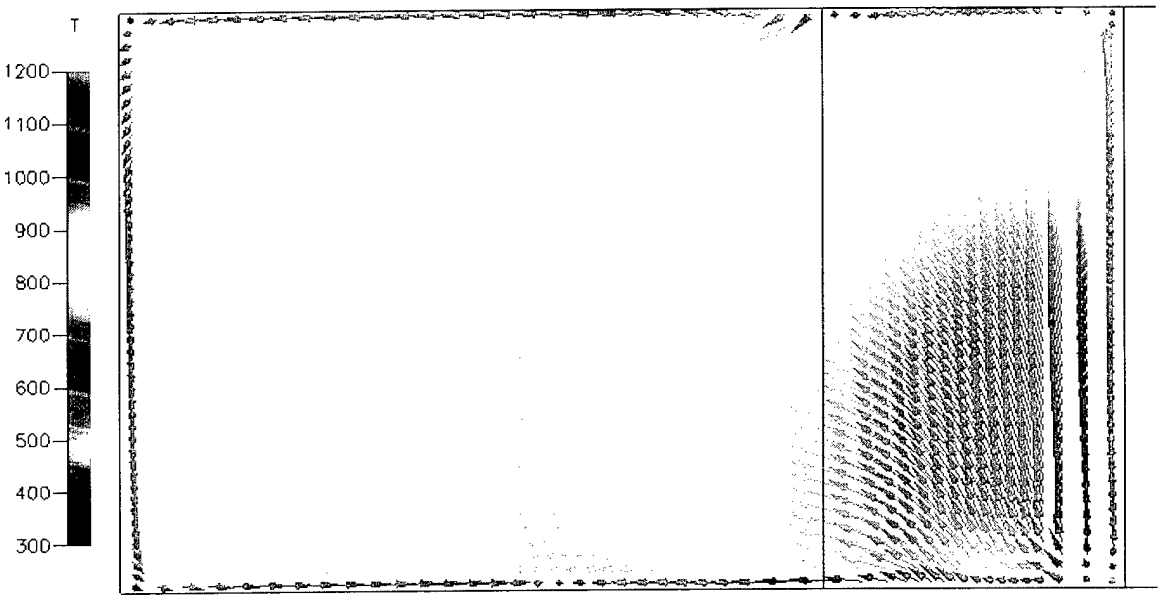

Figure 28. Simulation 2, partial elevation view (C-C) depicting temperature (K) distribution and fluid circulation pattern through the centerline of the stateroom door from the transverse passageway.

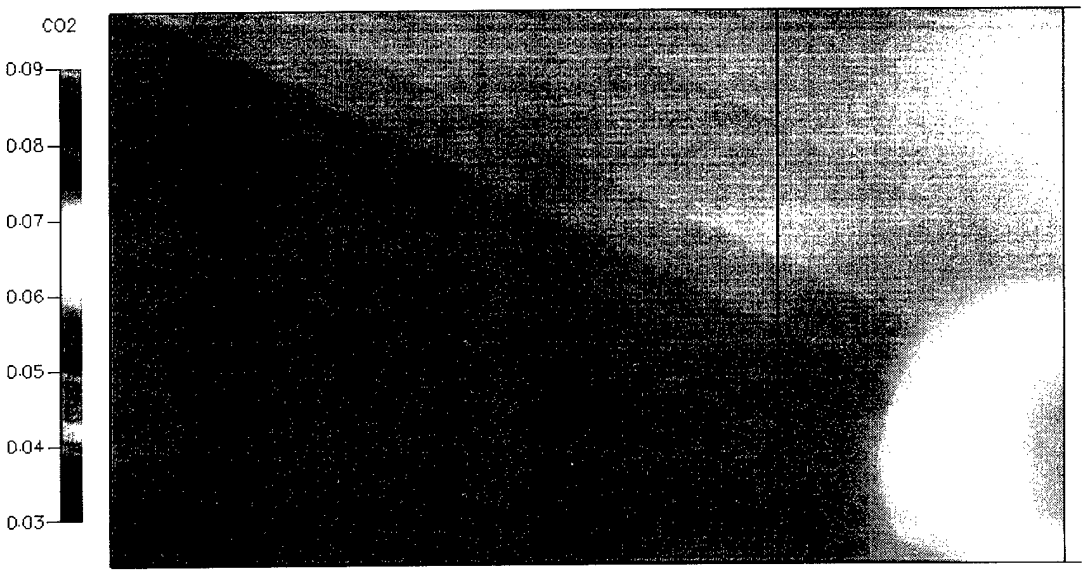

Figure 29. Simulation 2, partial elevation view (C-C) depicting CO_2 (mass fraction) distribution at the centerline of the stateroom door.

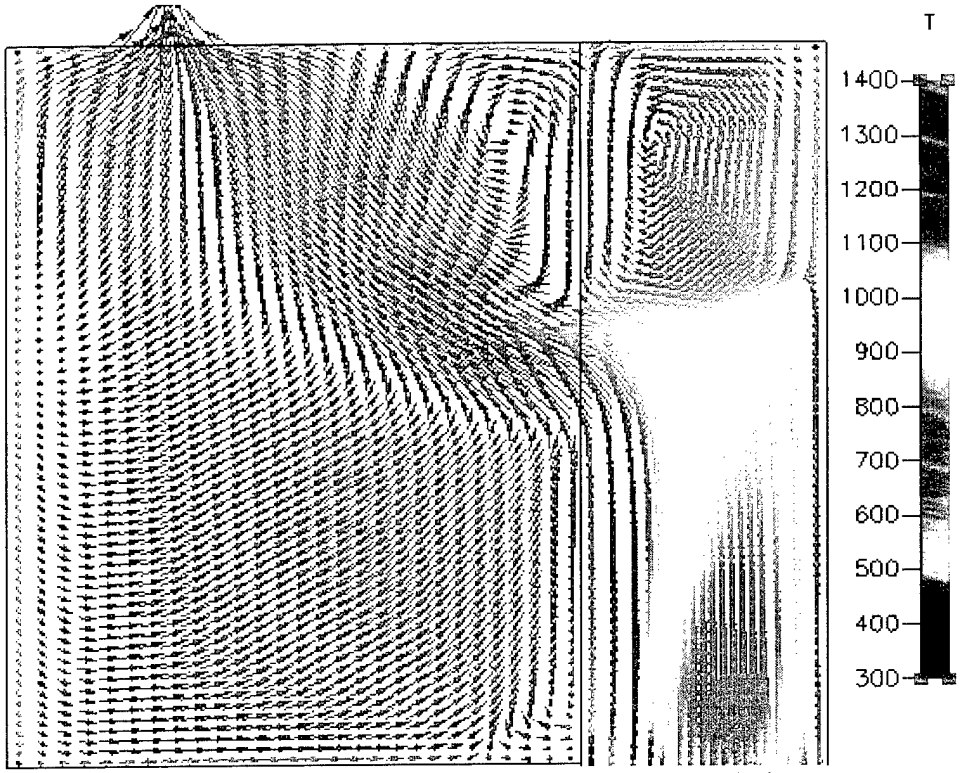

Figure 30. Simulation 2, partial plan view (D-D) depicting temperature (K) distribution and fluid circulation pattern from the transverse passageway through the door into the stateroom.

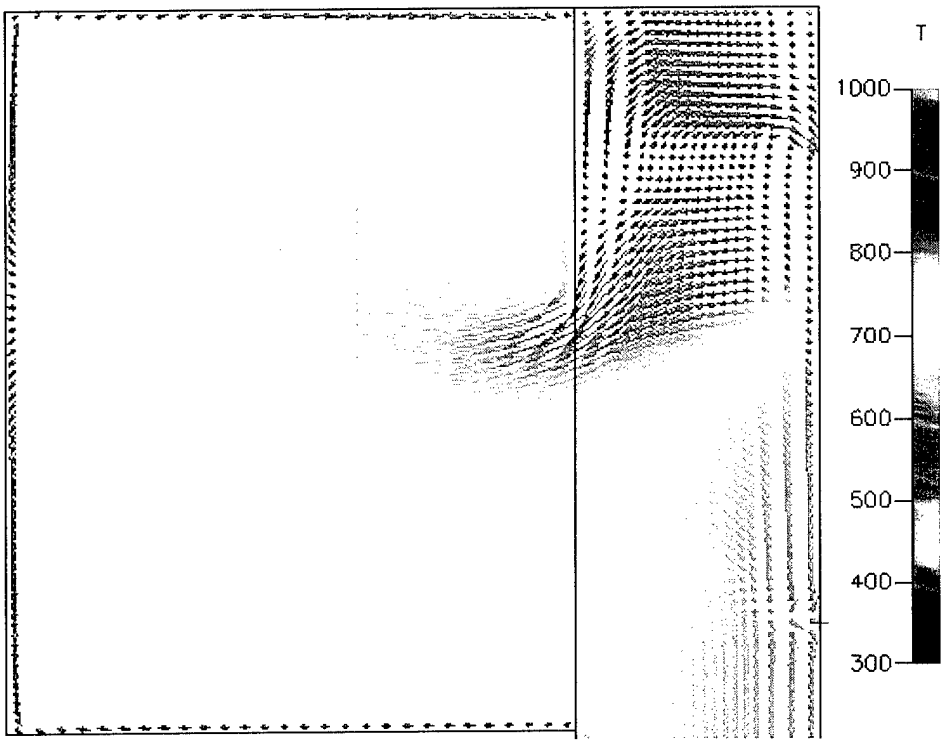

Figure 31. Simulation 2, partial plan view (E-E) depicting temperature (K) distribution and fluid circulation pattern from the transverse passageway through the door into the stateroom.

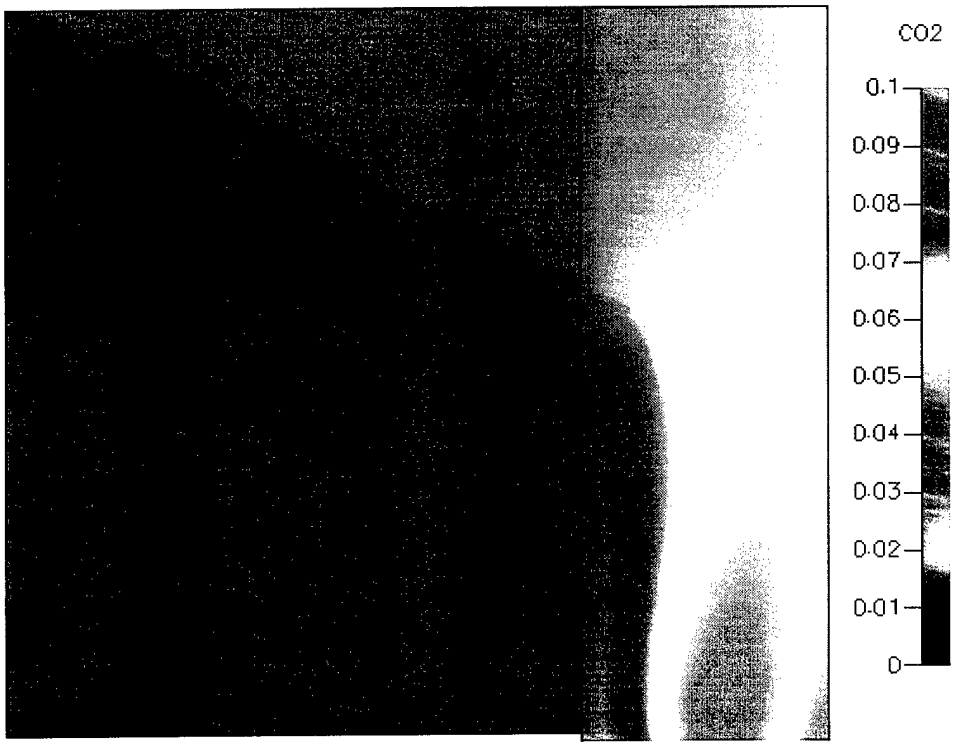

Figure 32. Simulation 2, partial plan view (D-D) depicting CO_2 (mass fraction) distribution in the stateroom and transverse passageway.

Figure 33. Simulation 2, partial plan view (E-E) depicting CO_2 (mass fraction) distribution in the stateroom and transverse passageway.

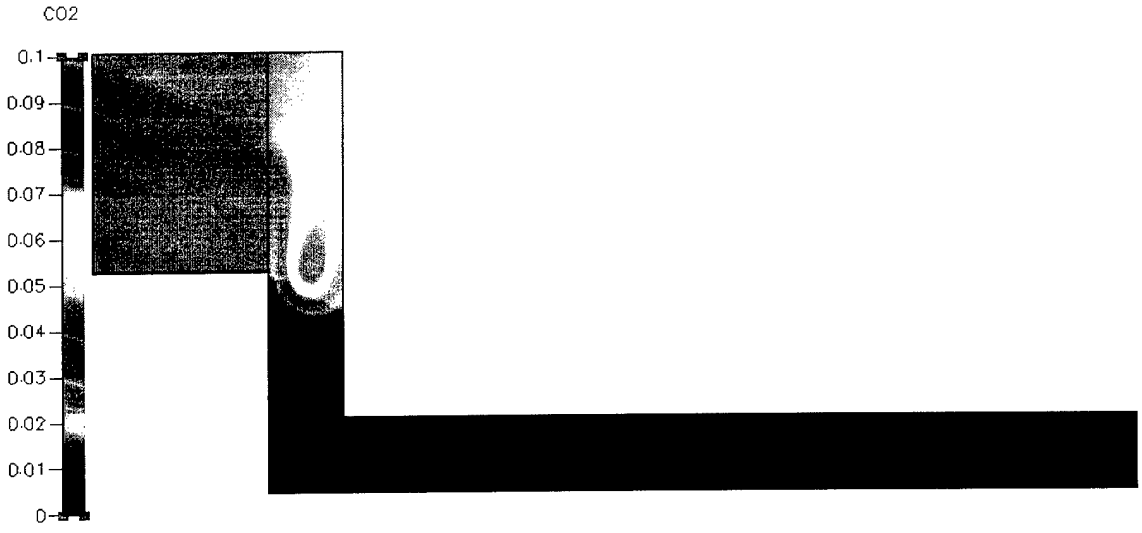

Figure 34. Simulation 2, plan view (D-D) depicting CO_2 (mass fraction) distribution throughout the structure.

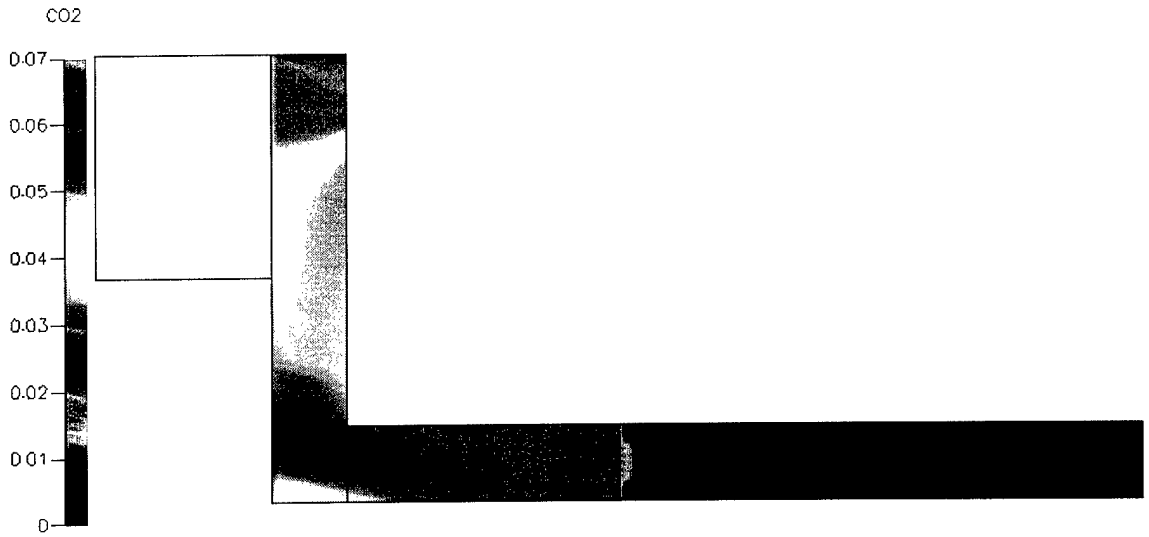

Figure 35. Simulation 2, plan view (E-E) depicting CO_2 (mass fraction) distribution throughout the structure.

APPENDIX C: SIMULATION 3

Simulation 3 does not use the CFD combustion module to simulate a 620 kW fire. The overhead, deck and bulkheads of the structure are isothermal boundaries at 300 K. The inlet, burn pan and vent conditions are presented in Table 9. The gas mixtures for the inlet, burn pan and vent are shown in Table 10.

Inlet/ Outlet Boundary Conditions					
Location	U Velocity (m/s)	V Velocity (m/s)	W Velocity (m/s)	Relative Pressure (Pa)	Temperature (K)
Watertight Door Inlet	0	0	-1	0	300
Burn Pan	0	4.08	0	0	2307
Vent	0	0	0	0	300
Bulkhead Boundary Conditions					
Location	U Velocity (m/s)	V Velocity (m/s)	W Velocity (m/s)	Wall Roughness (m)	Adiabatic / Isothermal
Interior Bulkheads	0	0	0	0.0005	Adiabatic
Exterior Bulkheads, Overheads, Deck	0	0	0	0.0005	Isothermal / 300K

Table 9. Simulation 3, inlet, burn pan, vent, bulkhead boundary conditions.

	Inlet	Burn Pan	Vent
Mixture	Air	CO_2, H_2O, N_2	Air

Table 10. Simulation 3, inlet, burn pan and vent mixture definition.

CFD program default solvers, inertial and linear relaxations, and variable limits are used to evaluate the model.

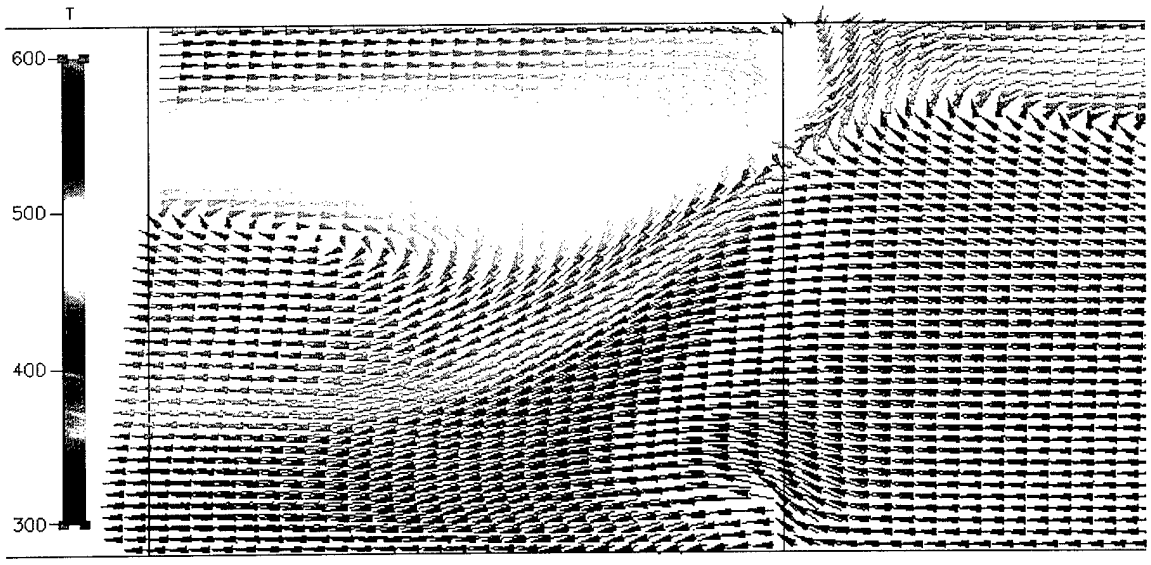

Figure 36. Simulation 3, partial elevation view (A-A) depicting temperature (K) distribution and fluid circulation pattern at the centerline of the longitudinal passageway in the vicinity of the watertight door.

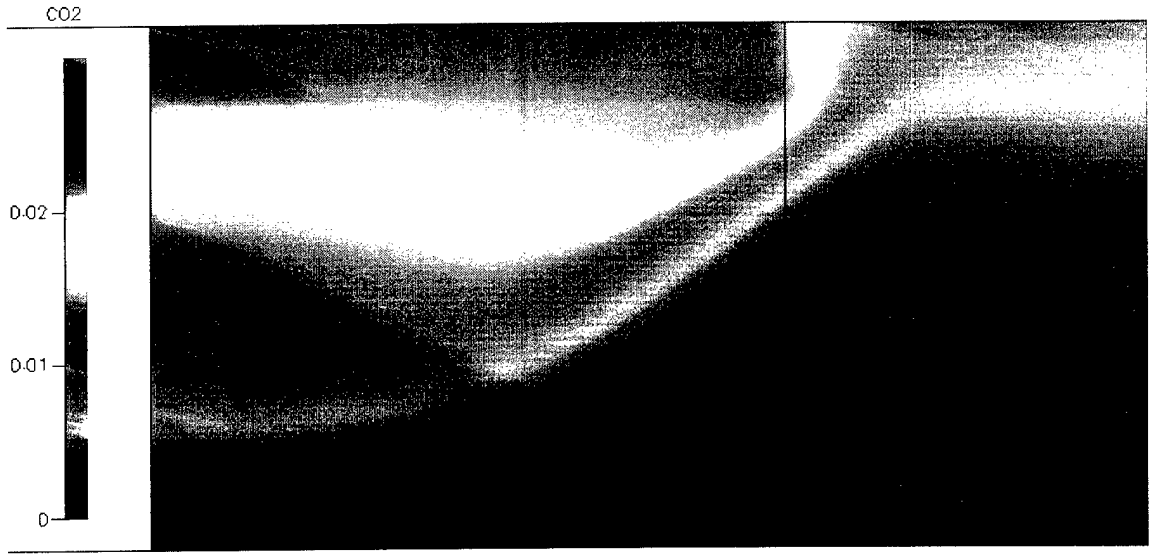

Figure 37. Simulation 3, partial elevation view (A-A) of CO_2 gas (mass fraction) propagation at the centerline of the longitudinal passageway in the vicinity of the watertight door.

Figure 38. Simulation 3, elevation view (A-A) of CO_2 gas (mass fraction) propagation at the centerline of the longitudinal passageway.

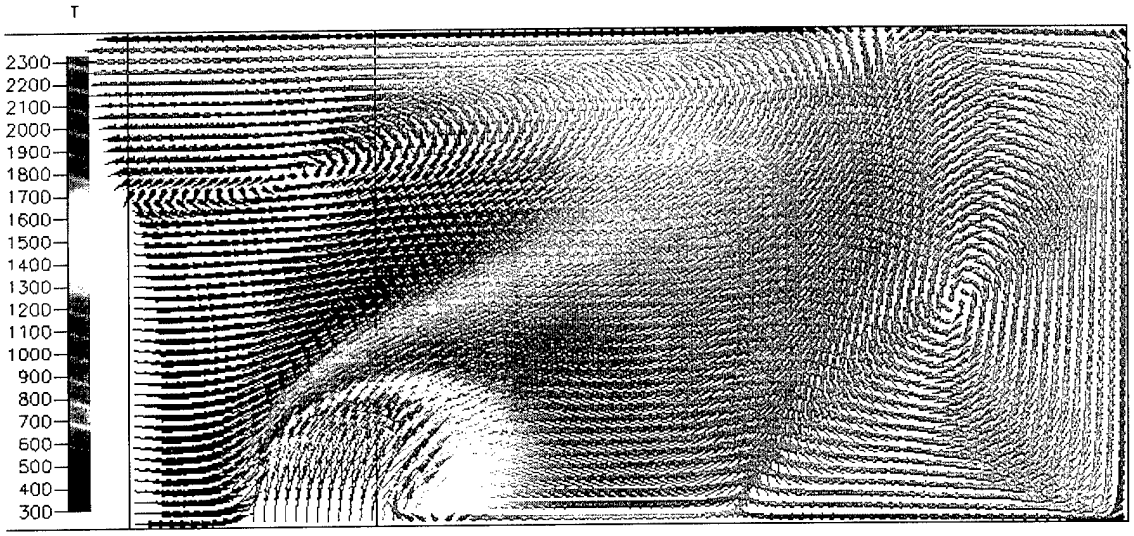

Figure 39. Simulation 3, partial elevation view (B-B) depicting temperature (K) distribution and fluid circulation pattern along the centerline of the transverse passageway on the port side.

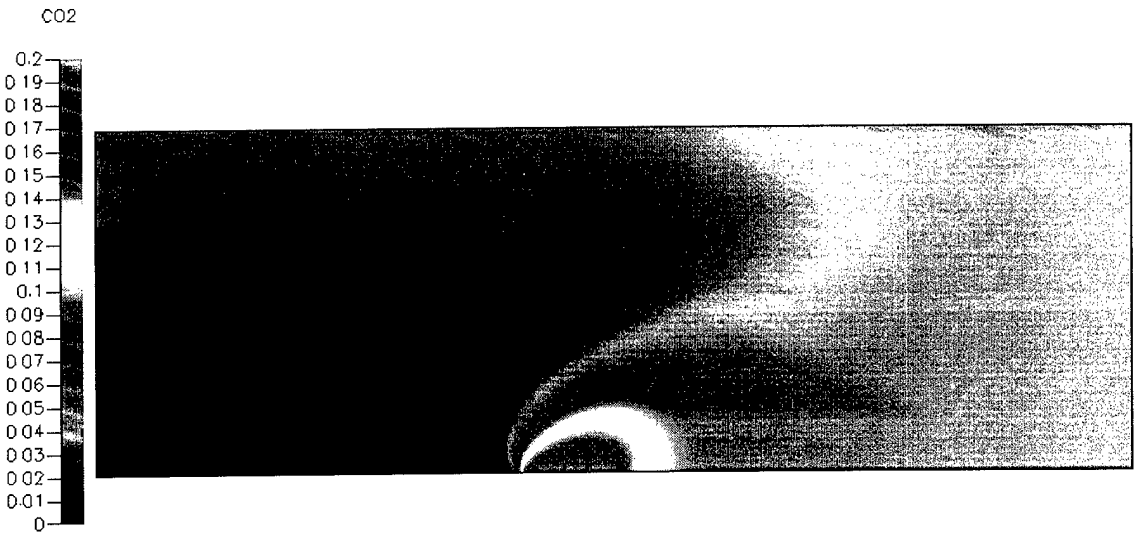

Figure 40. Simulation 3, elevation view (B-B) of CO_2 gas (mass fraction) propagation at the centerline of the transverse passageway.

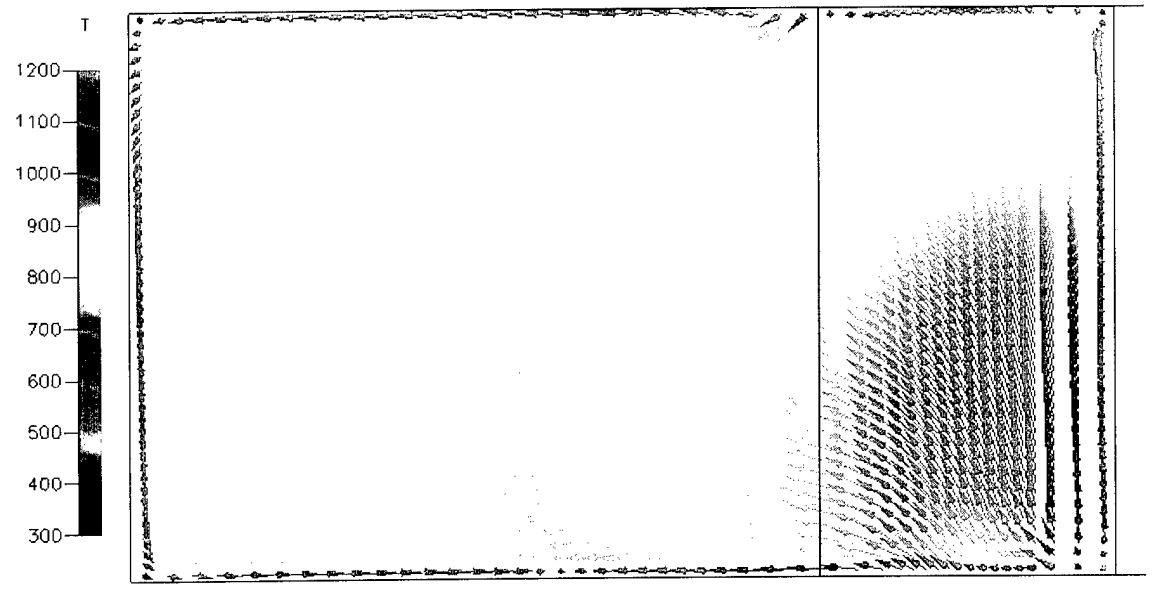

Figure 41. Simulation 3, elevation view (C-C) depicting the temperature (K) distribution and fluid circulation pattern through the centerline of the stateroom door from the transverse passageway.

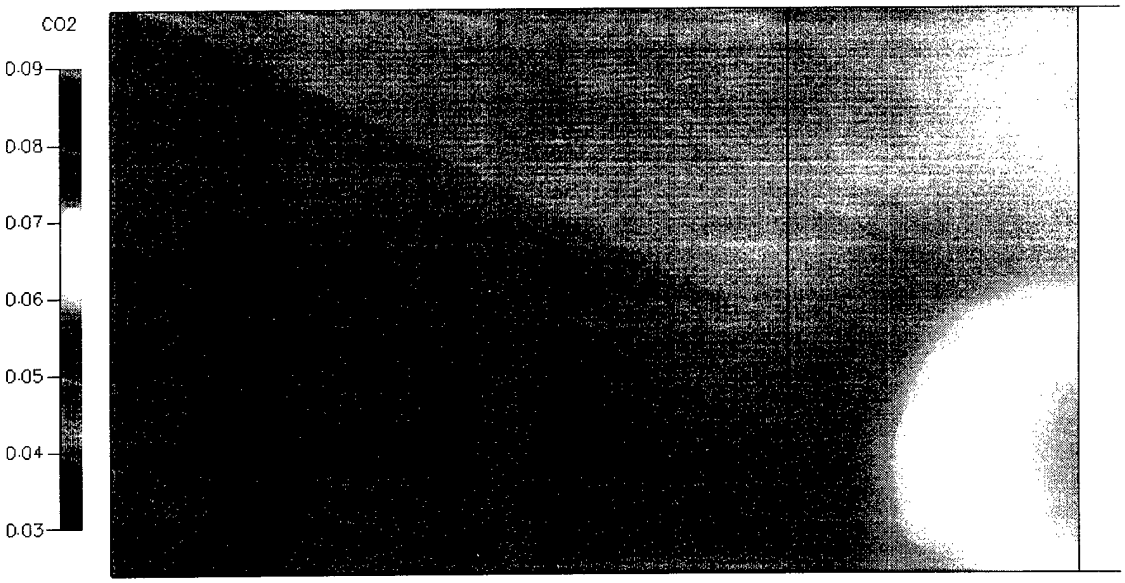

Figure 42. Simulation 3, elevation view (C-C) depicting CO_2 (mass fraction) distribution at the centerline of the stateroom door.

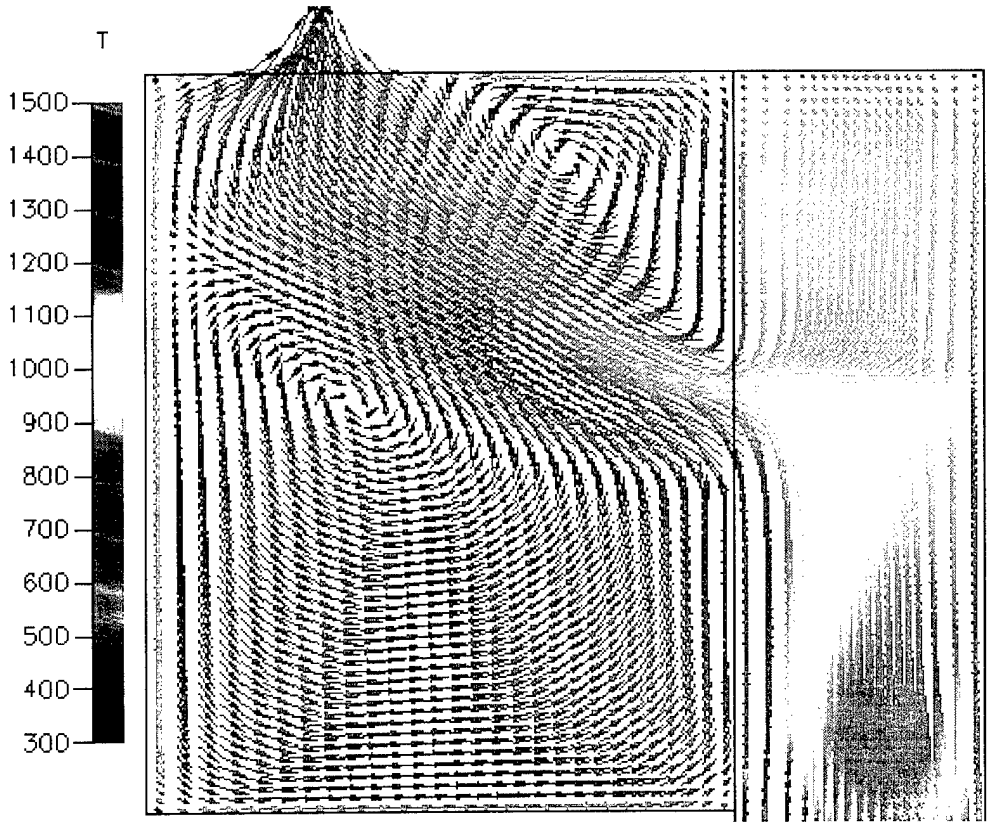

Figure 43. Simulation 3, partial plan view (D-D) depicting temperature (K) distribution and fluid circulation pattern from the transverse passageway through the door into the stateroom.

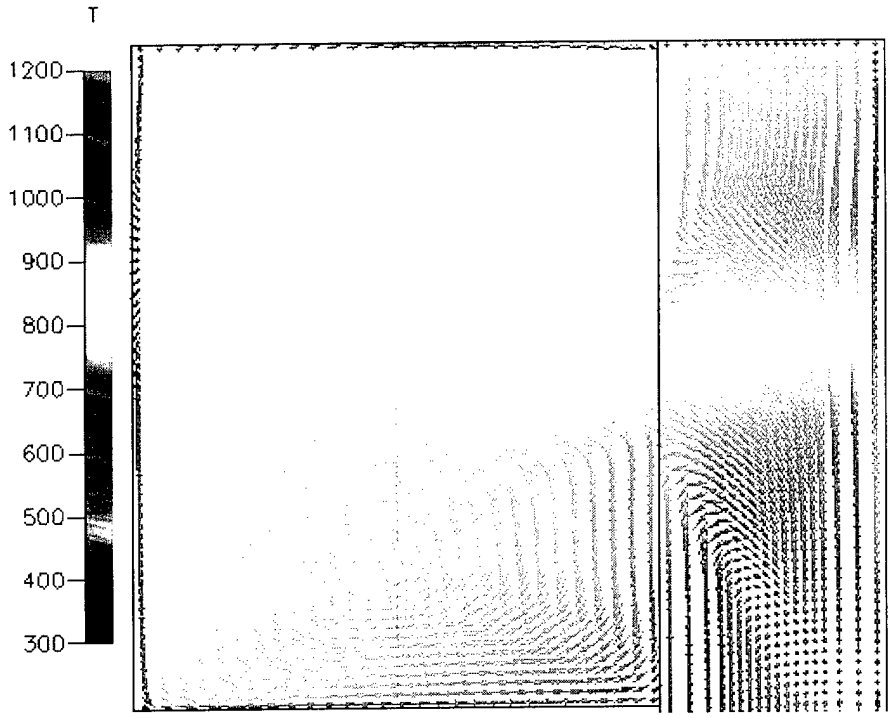

Figure 44. Simulation 3, partial plan view (E-E) depicting temperature (K) distribution and fluid circulation pattern from the transverse passageway through the door into the stateroom.

Figure 45. Simulation 3, partial plan view (D-D) depicting CO_2 (mass fraction) distribution in the stateroom and transverse passageway.

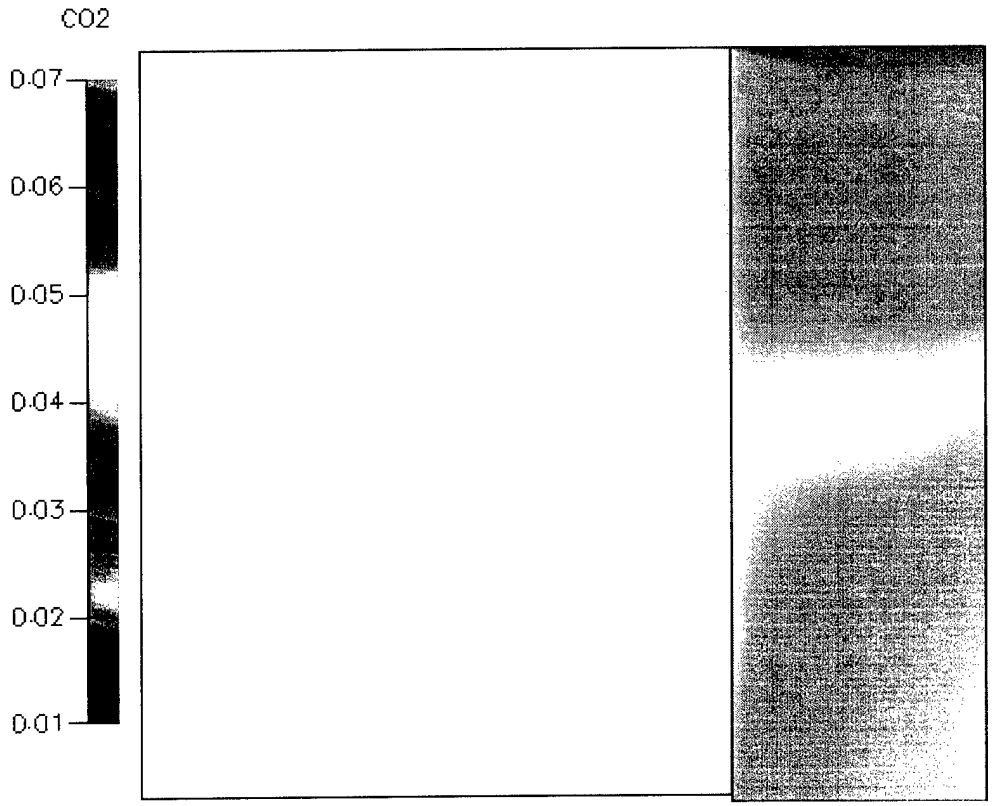

Figure 46. Simulation 3, partial plan view (E-E) depicting CO_2 (mass fraction) distribution in the stateroom and transverse passageway.

Figure 47. Simulation 3, plan view (D-D) depicting CO_2 (mass fraction) distribution throughout the structure.

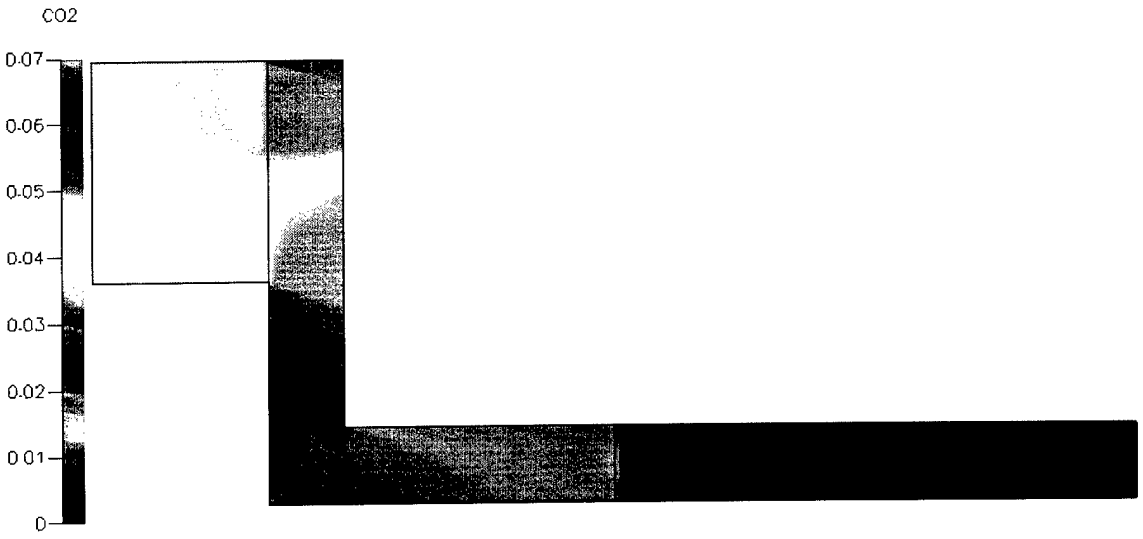

Figure 48. Simulation 3, plan view (E-E) depicting CO_2 (mass fraction) distribution throughout the structure.

APPENDIX D: SIMULATION 4

Simulation 4 uses the CFD combustion module to simulate a 620 kW fire. The overhead, deck and bulkheads of the structure were isothermal boundaries at 300 K. The inlet, burn pan and vent conditions are presented in Table 11. The gas mixtures for the inlet, burn pan and vent are shown in Table 12.

Inlet/ Outlet Boundary Conditions					
Location	U Velocity (m/s)	V Velocity (m/s)	W Velocity (m/s)	Relative Pressure (Pa)	Temperature (K)
Watertight Door Inlet	0	0	-0.5	0	300
Burn Pan	0	0.5	0	0	300
Vent	0	0	0	0	300
Bulkhead Boundary Conditions					
Location	U Velocity (m/s)	V Velocity (m/s)	W Velocity (m/s)	Wall Roughness (m)	Adiabatic / Isothermal
Interior Bulkheads	0	0	0	0.0005	Adiabatic
Exterior Bulkheads, Overheads, Deck	0	0	0	0.0005	Isothermal / 300 K

Table 11. Simulation 4, inlet, burn pan, vent and bulkhead boundary conditions.

	Inlet	Burn Pan	Vent
Mixture	Air	Propene/Air	Air

Table 12. Simulation 4, inlet, burn pan and vent mixture definition.

CFD program default solvers, inertial and linear relaxations, and variable limits were used to evaluate the model.

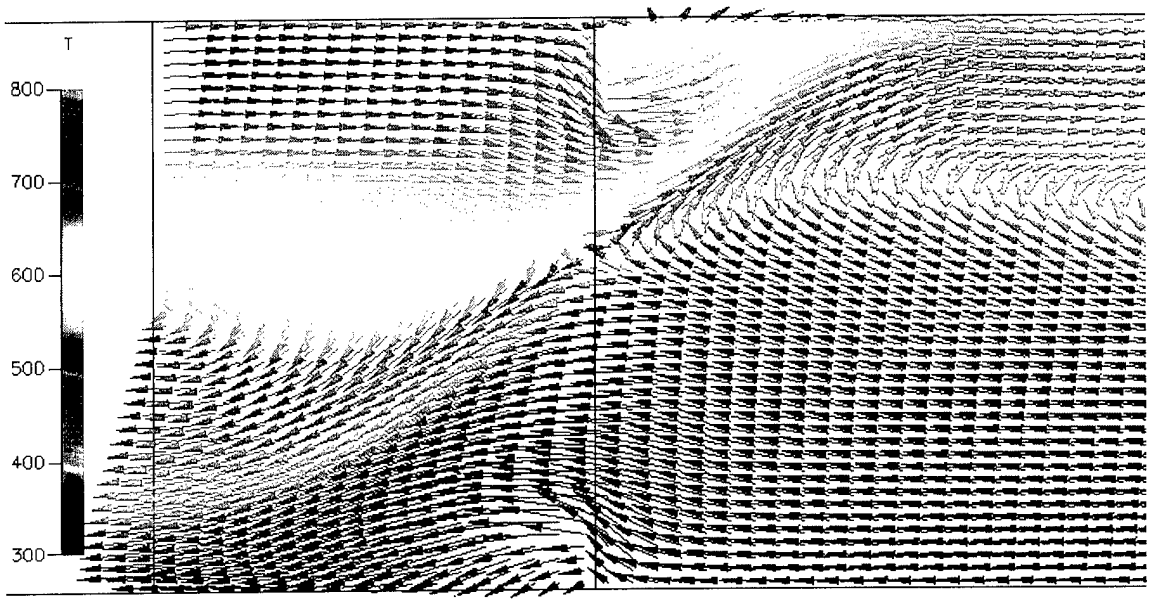

Figure 49. Simulation 4, partial elevation view (A-A) depicting temperature (K) distribution and fluid circulation pattern at the centerline of the longitudinal passageway in the vicinity of the watertight door.

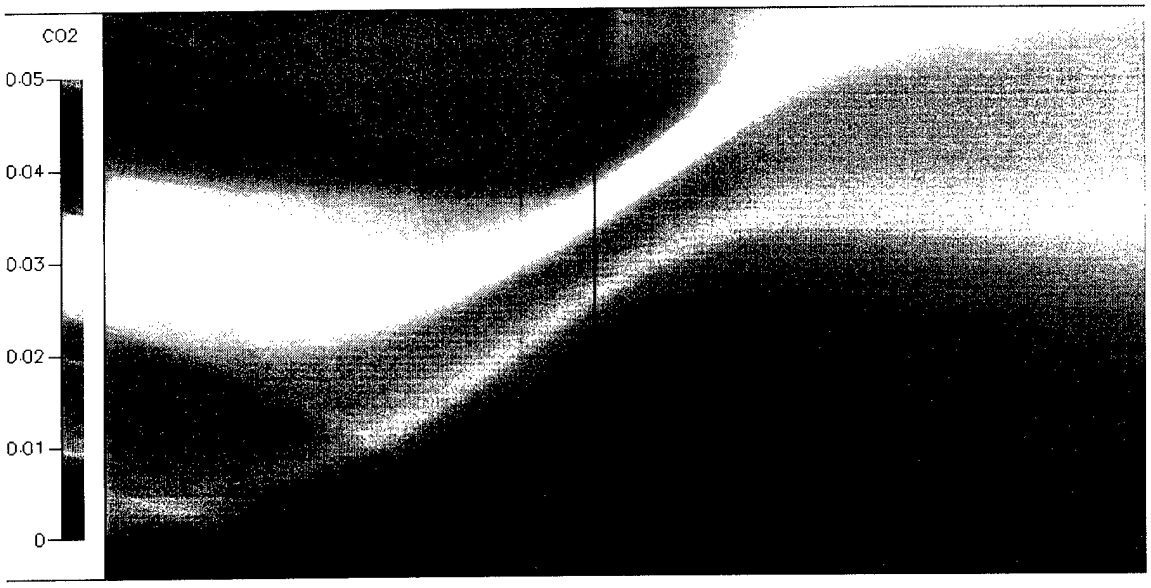

Figure 50. Simulation 4, partial elevation view (A-A) of CO_2 gas (mass fraction) propagation at the centerline of the longitudinal passageway in the vicinity of the watertight door.

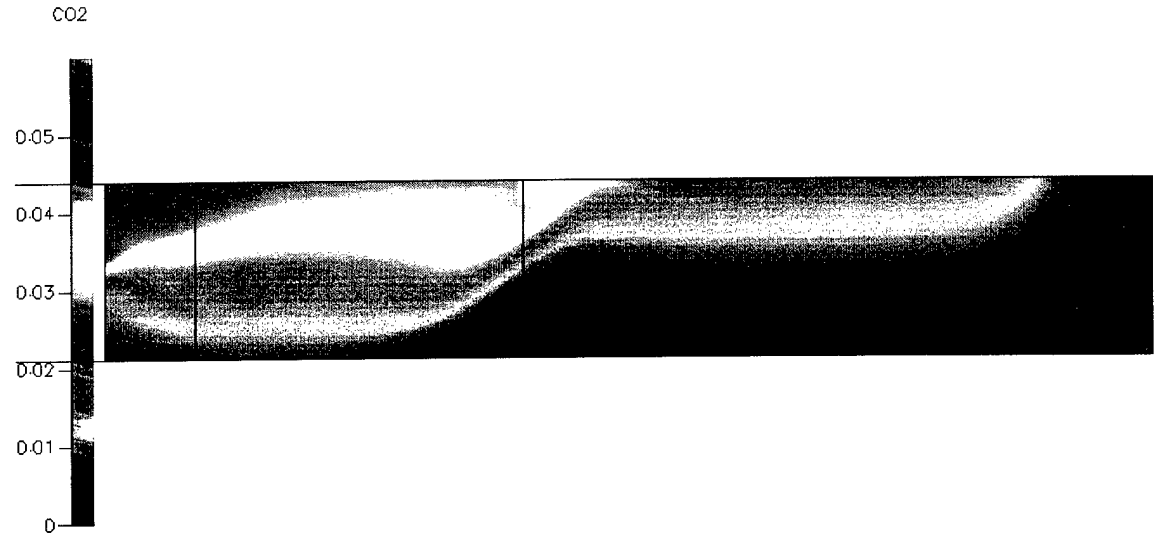

Figure 51. Simulation 4, elevation view (A-A) of CO_2 gas (mass fraction) propagation at the centerline of the longitudinal passageway.

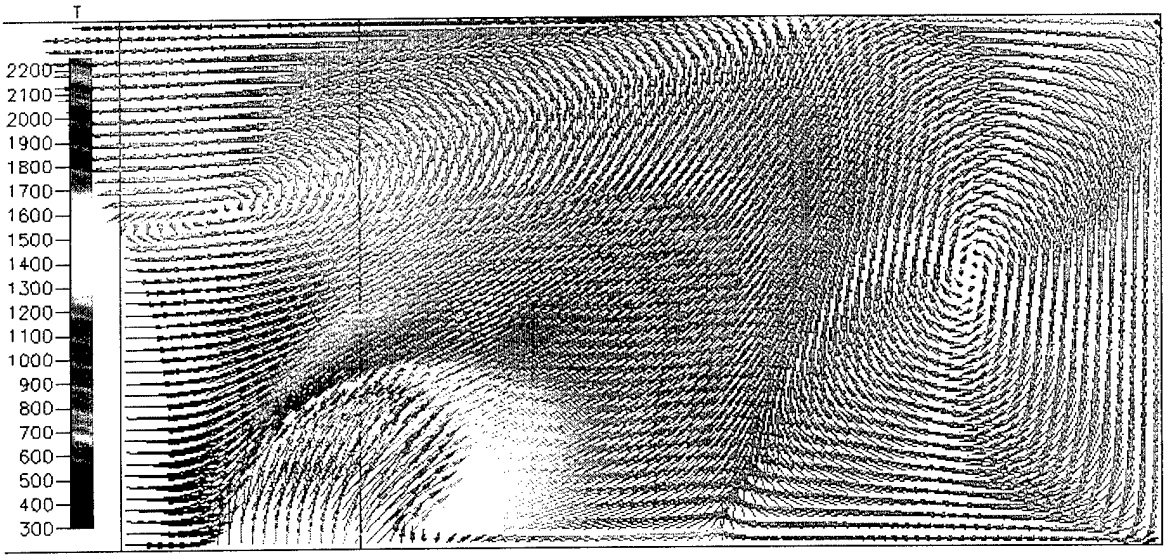

Figure 52. Simulation 4, partial elevation view (B-B) depicting temperature (K) distribution and fluid circulation pattern along the centerline of the transverse passageway on the port side.

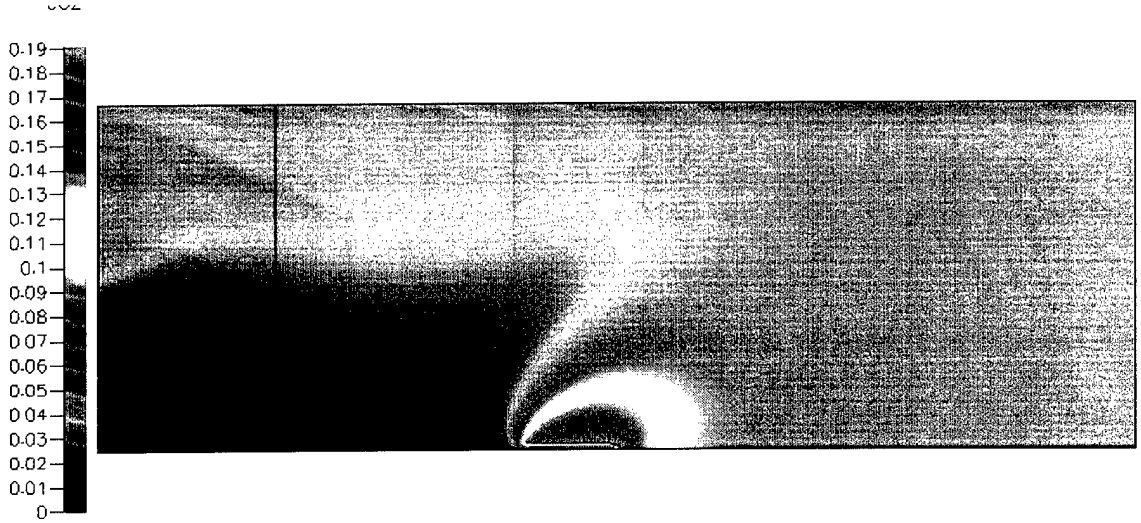

Figure 53. Simulation 4, elevation view (B-B) of CO_2 gas (mass fraction) propagation at the centerline of the transverse passageway.

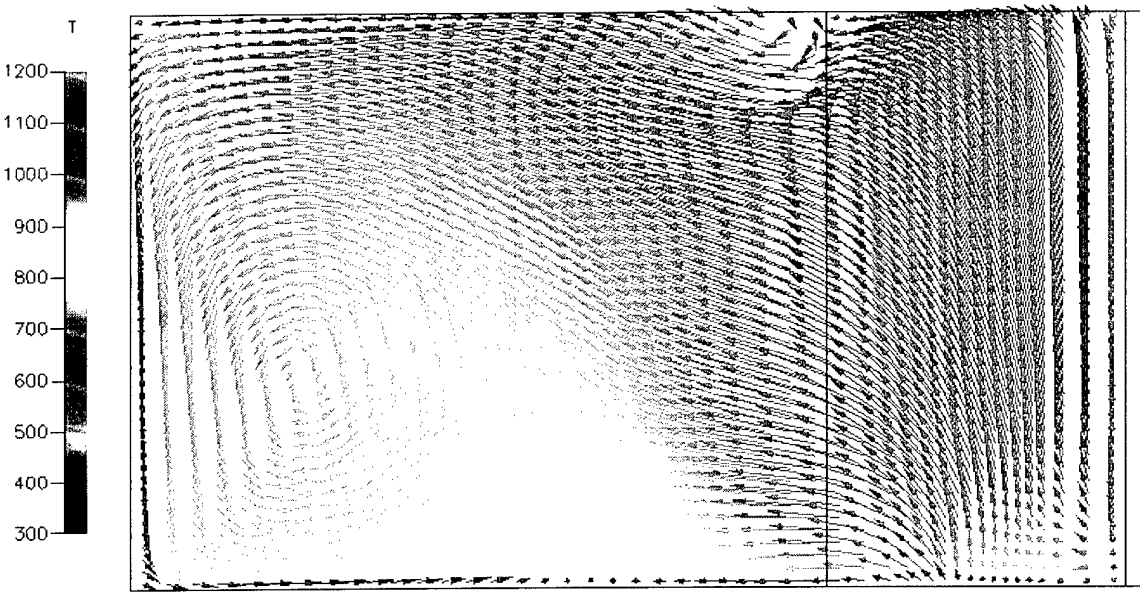

Figure 54. Simulation 4, elevation view (C-C) depicting the temperature (K) distribution and fluid circulation pattern through the centerline of the stateroom door from the transverse passageway.

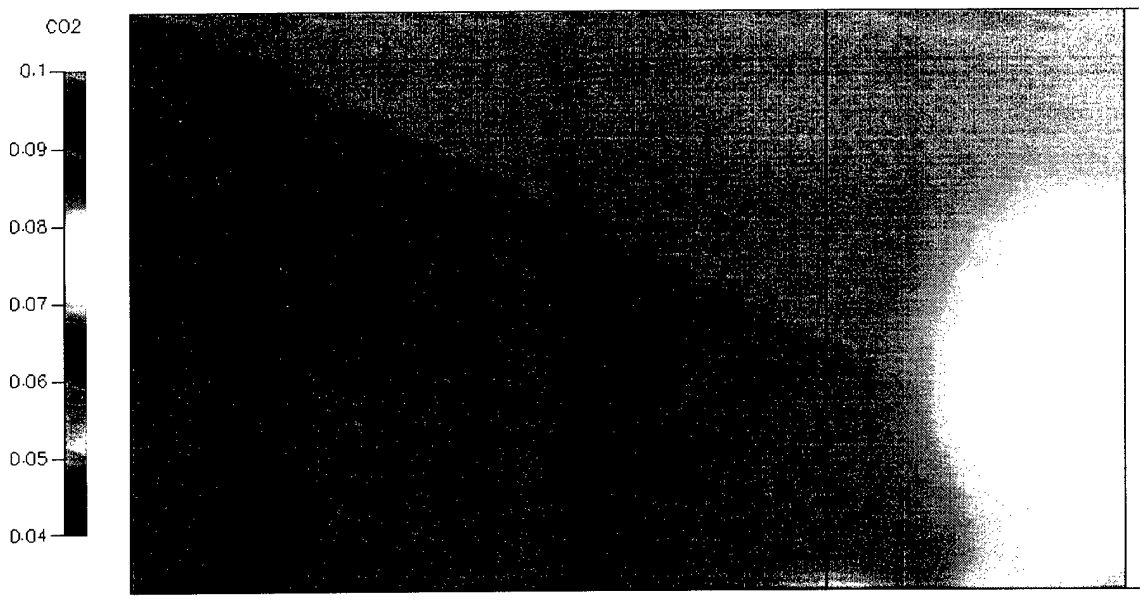

Figure 55. Simulation 4, elevation view (C-C) depicting CO_2 (mass fraction) distribution at the centerline of the stateroom door.

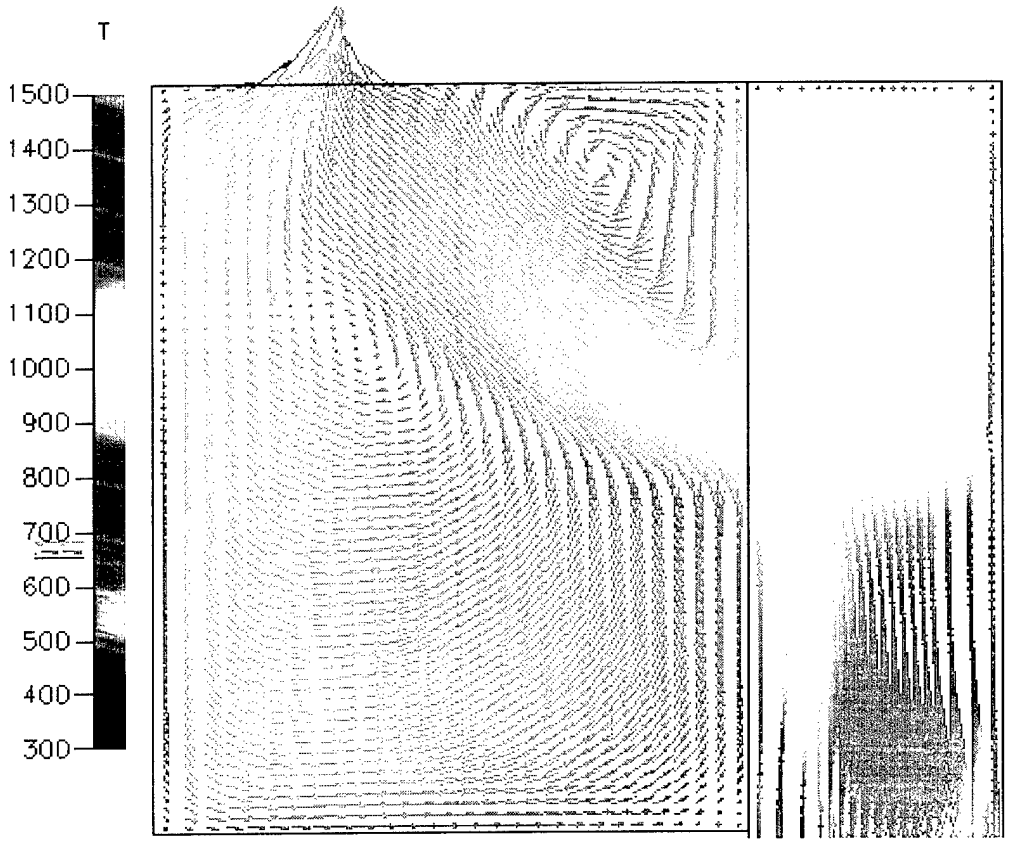

Figure 56. Simulation 4, partial plan view (D-D) depicting temperature (K) distribution and fluid circulation pattern from the transverse passageway through the door into the stateroom.

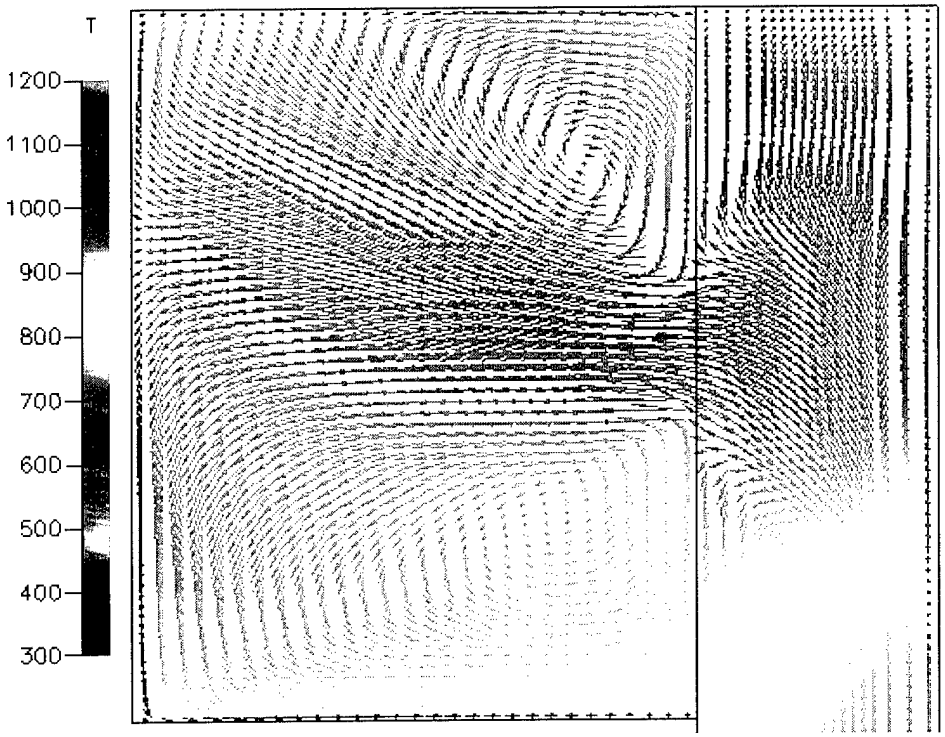

Figure 57. Simulation 4, partial plan view (E-E) depicting temperature (K) distribution and fluid circulation pattern from the transverse passageway through the door into the stateroom.

Figure 58. Simulation 4, partial plan view (D-D) depicting CO_2 (mass fraction) distribution in the stateroom and transverse passageway.

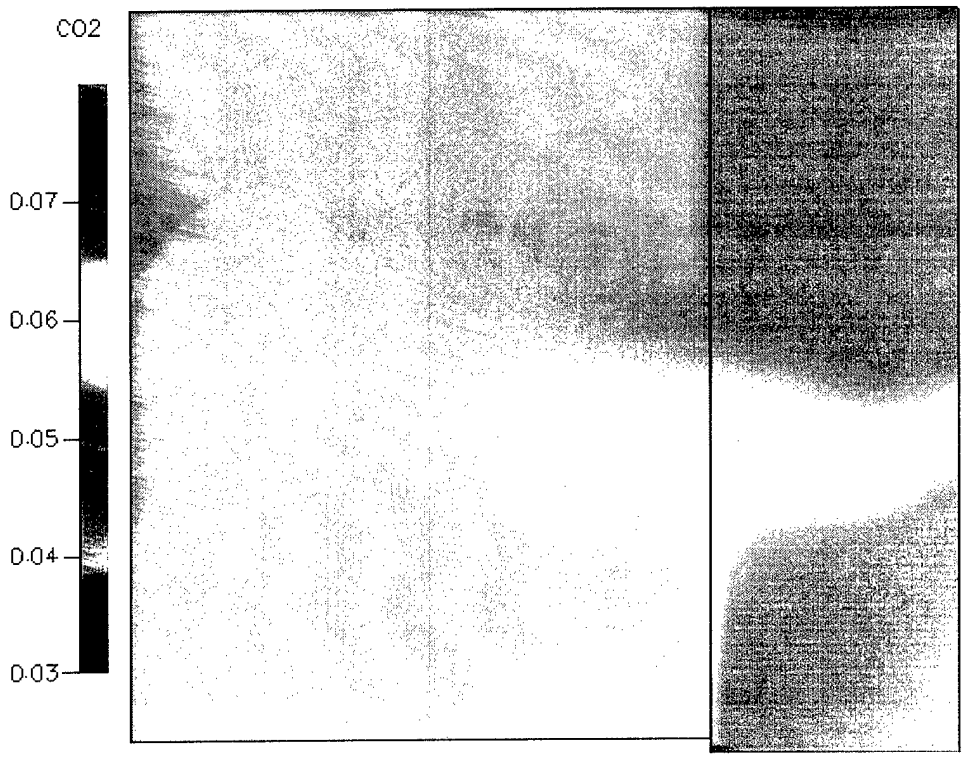

Figure 59. Simulation 4, partial plan view (E-E) depicting CO_2 (mass fraction) distribution in the stateroom and transverse passageway.

Figure 60. Simulation 4, plan view (D-D) depicting CO_2 (mass fraction) distribution throughout the structure.

Figure 61. Simulation 4, plan view (E-E) depicting CO_2 (mass fraction) distribution throughout the structure.

APPENDIX E: SIMULATION 5

Simulation 5 uses the CFD combustion module to simulate a 620 kW fire. The overhead, deck and bulkheads of the structure are isothermal boundaries at 300 K. The inlet, burn pan and vent conditions are presented in Table 13. The gas mixtures for the inlet, burn pan and vent are shown in Table 14.

Inlet/ Outlet Boundary Conditions					
Location	U Velocity (m/s)	V Velocity (m/s)	W Velocity (m/s)	Relative Pressure (Pa)	Temperature (K)
Watertight Door Inlet	0	0	-2	0	300
Burn Pan	0	0.5	0	0	300
Vent	0	0	0	0	300
Bulkhead Boundary Conditions					
Location	U Velocity (m/s)	V Velocity (m/s)	W Velocity (m/s)	Wall Roughness (m)	Adiabatic / Isothermal
Interior Bulkheads	0	0	0	0.0005	Adiabatic
Exterior Bulkheads, Overheads, Deck	0	0	0	0.0005	Isothermal / 300 K

Table 13. Simulation 5, inlet, burn pan, vent, bulkhead boundary conditions.

	Inlet	Burn Pan	Vent
Mixture	Air	Propene/Air	Air

Table 14. Simulation 5, inlet, burn pan and vent mixture definition.

CFD program default solvers, inertial and linear relaxations, and variable limits are used to evaluate the model.

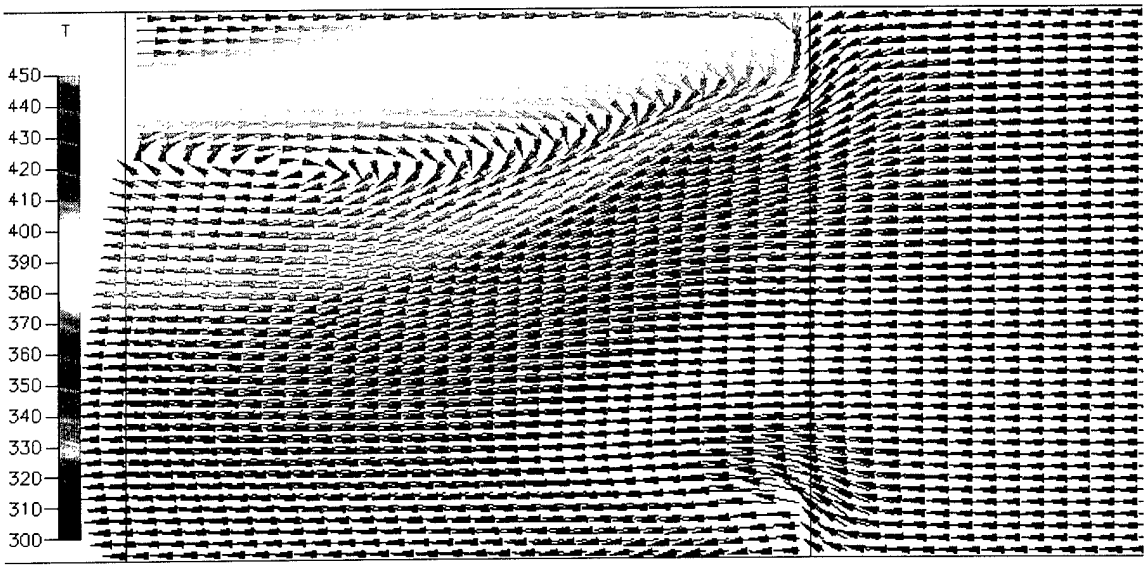

Figure 62. Simulation 5, partial elevation view (A-A) depicting temperature (K) distribution and fluid circulation pattern at the centerline of the longitudinal passageway in the vicinity of the watertight door.

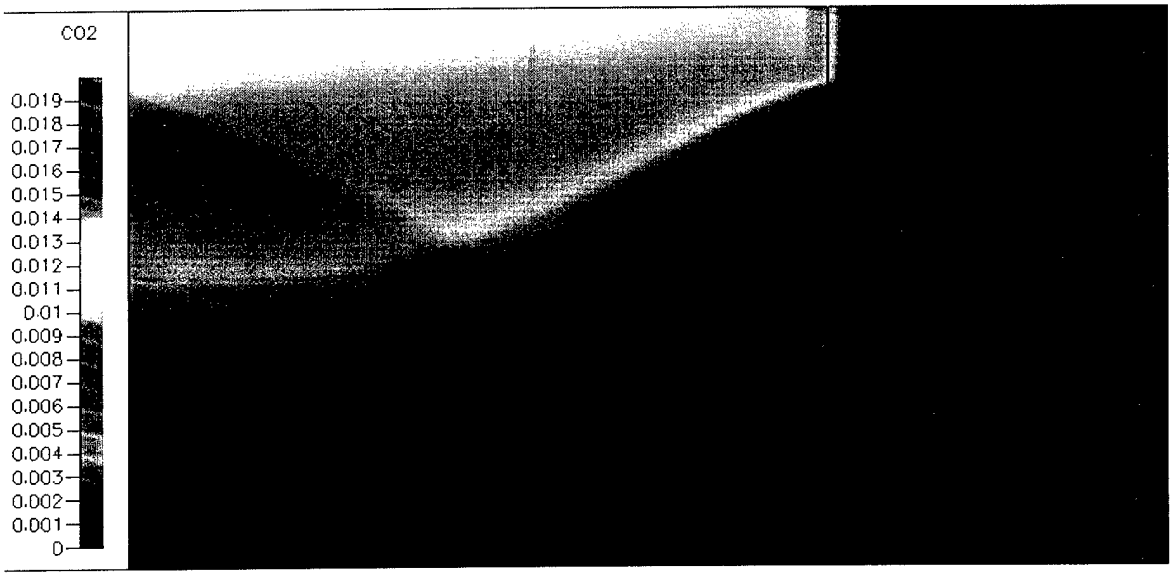

Figure 63. Simulation 5, partial elevation view (A-A) of CO_2 gas (mass fraction) propagation at the centerline of the longitudinal passageway in the vicinity of the watertight door.

Figure 64. Simulation 5, elevation view (A-A) of CO_2 gas (mass fraction) propagation at the centerline of the longitudinal passageway.

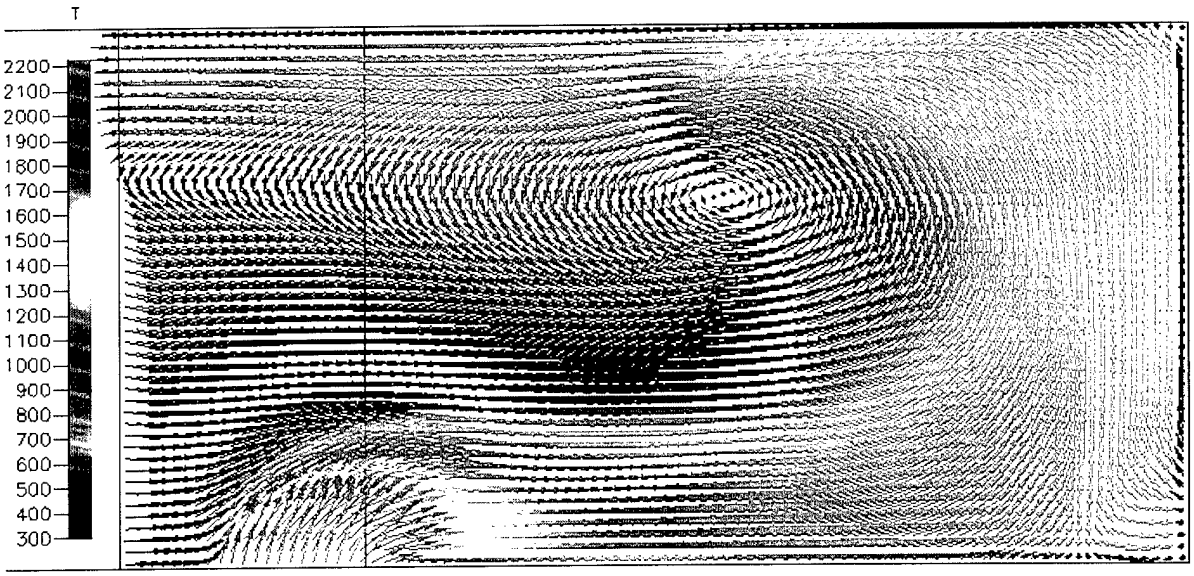

Figure 65. Simulation 5, partial elevation view (B-B) depicting temperature (K) distribution and fluid circulation pattern along the centerline of the transverse passageway on the port side.

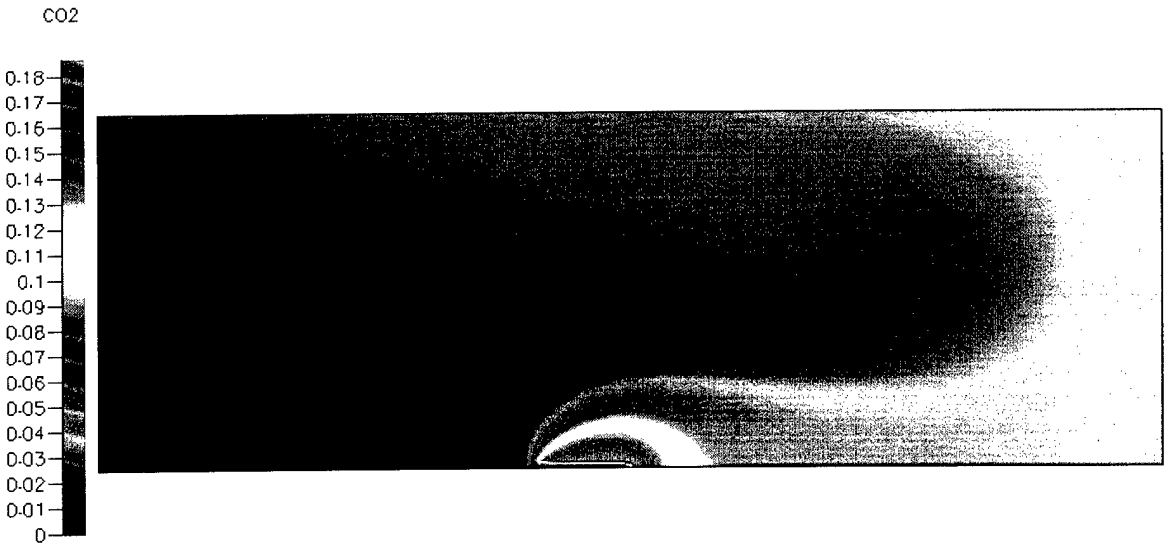

Figure 66. Simulation 5, elevation view (B-B) of CO_2 gas (mass fraction) propagation at the centerline of the transverse passageway.

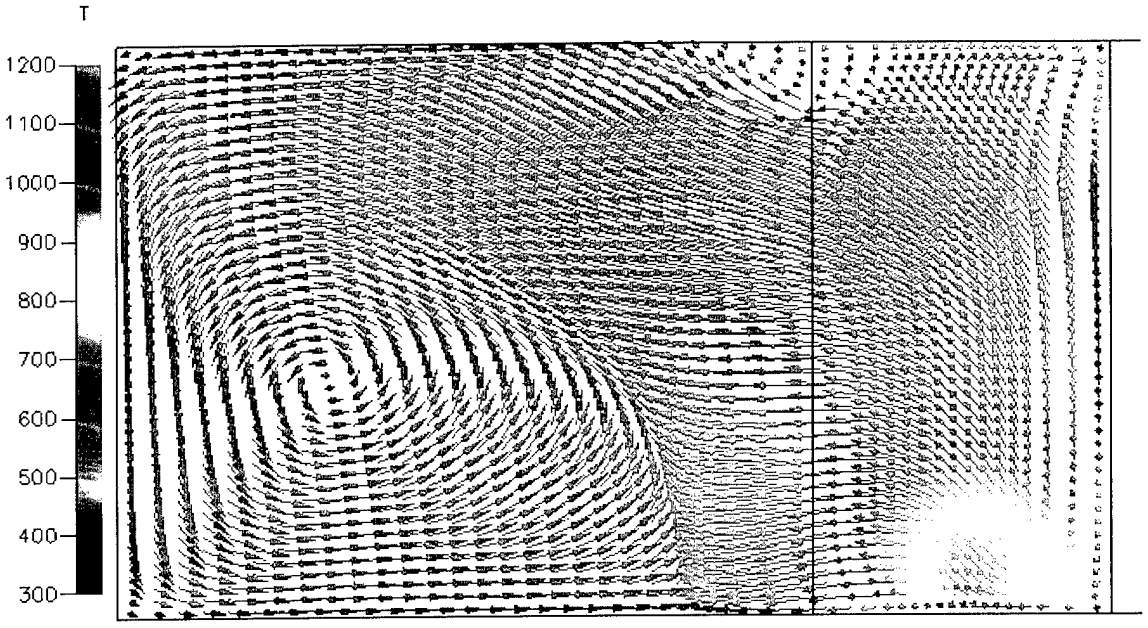

Figure 67. Simulation 5, elevation view (C-C) depicting the temperature (K) distribution and fluid circulation pattern through the centerline of the stateroom door from the transverse passageway.

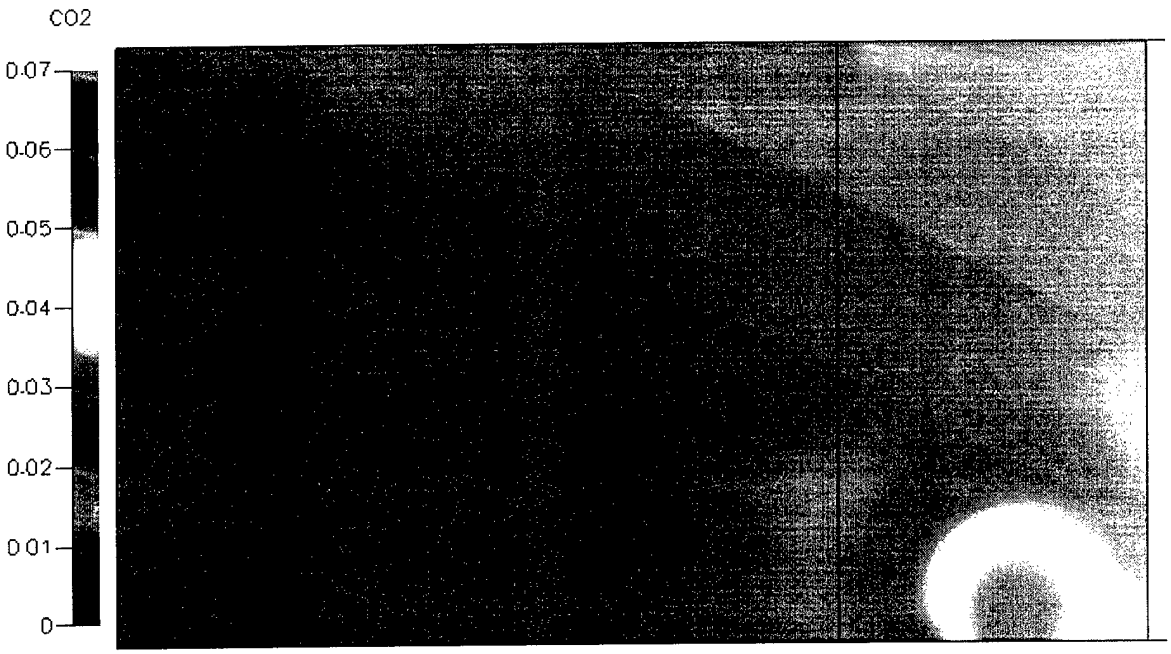

Figure 68. Simulation 5, elevation view (C-C) depicting CO_2 (mass fraction) distribution at the centerline of the stateroom door.

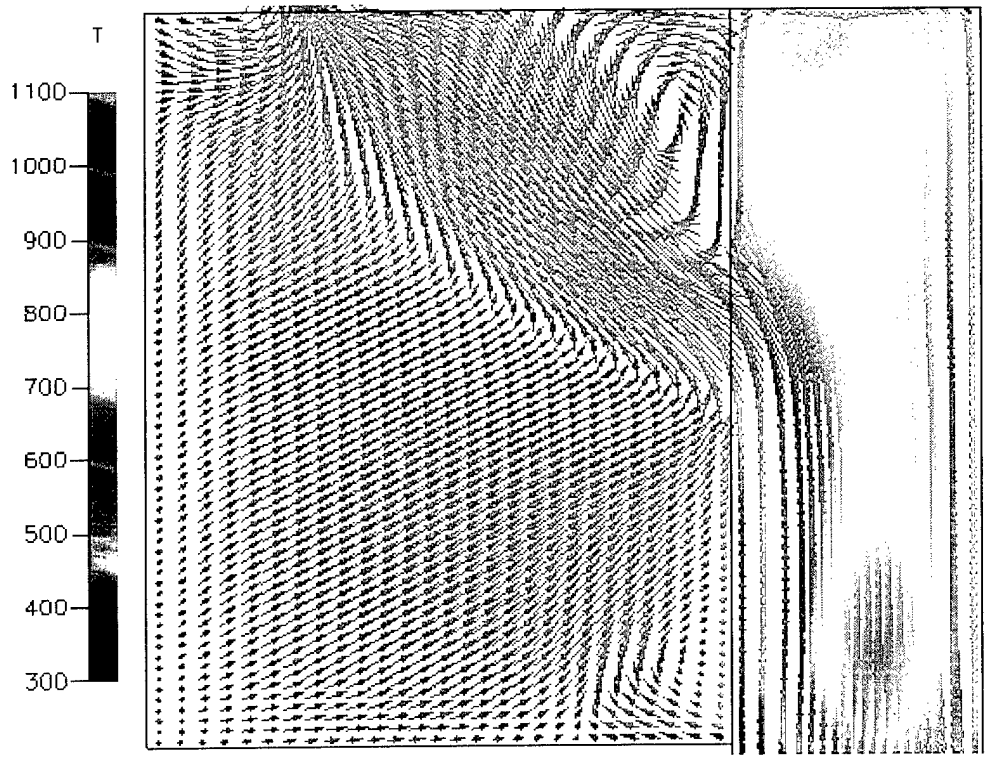

Figure 69. Simulation 5, partial plan view (D-D) depicting the temperature (K) distribution and fluid circulation pattern from the transverse passageway through the door into the stateroom.

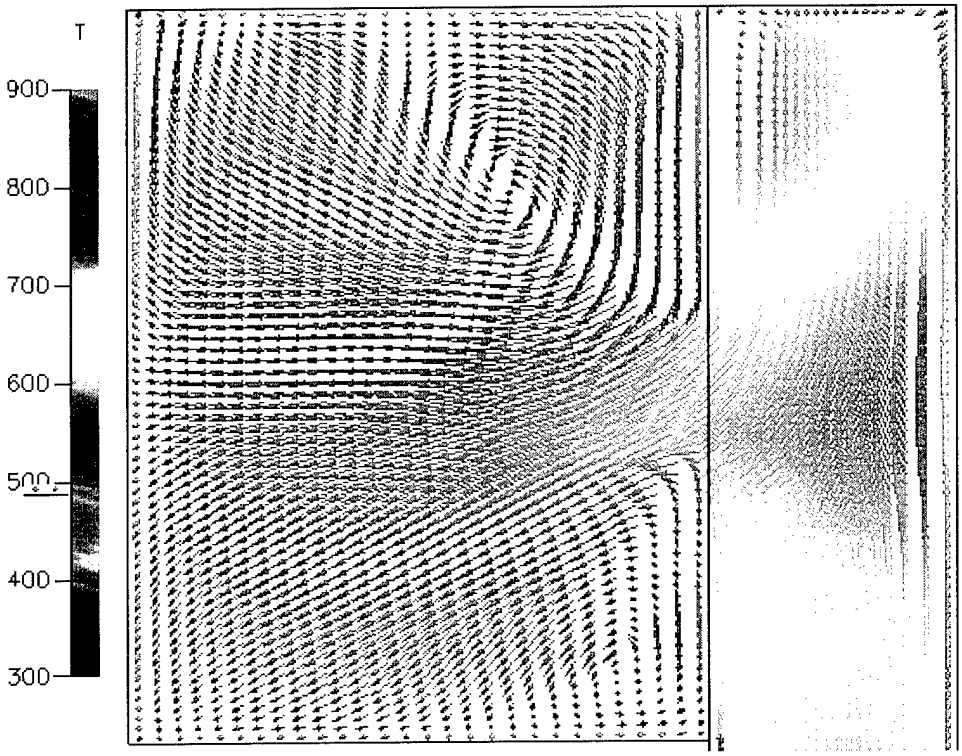

Figure 70. Simulation 5, partial plan view (E-E) depicting the temperature (K) distribution and fluid circulation pattern from the transverse passageway through the door into the stateroom.

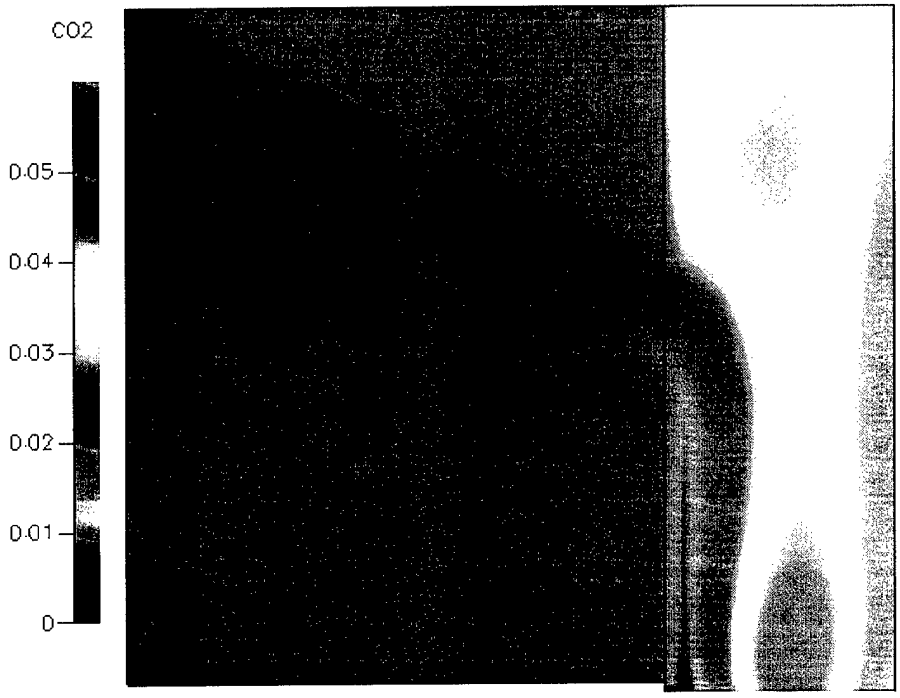

Figure 71. Simulation 5, partial plan view (D-D) depicting CO_2 (mass fraction) distribution in the stateroom and transverse passageway.

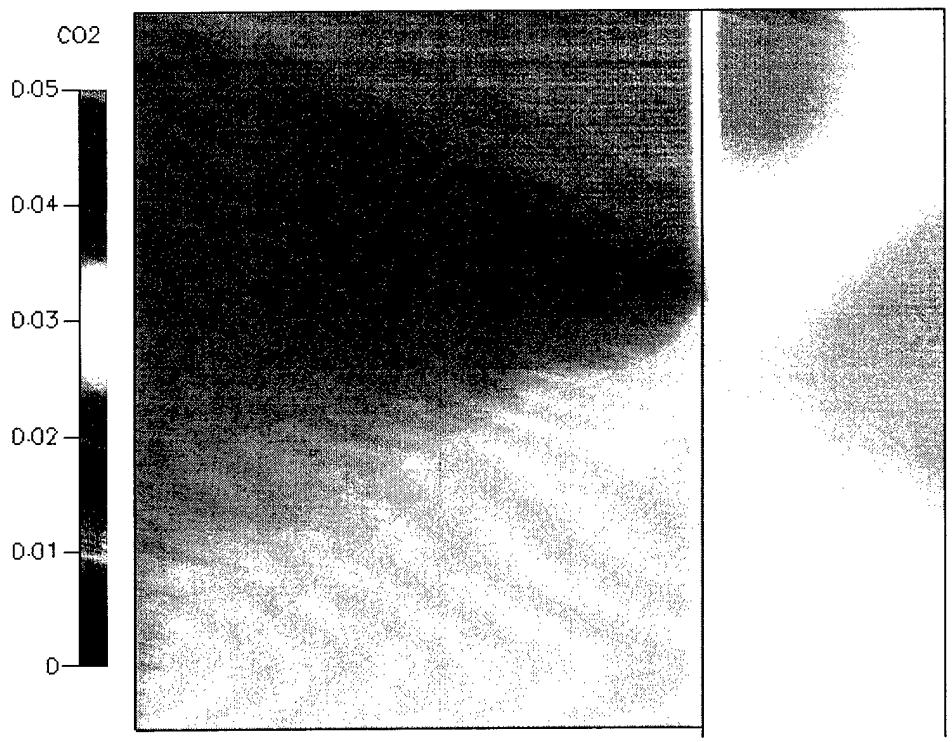

Figure 72. Simulation 5, partial plan view (E-E) depicting CO_2 (mass fraction) distribution in the stateroom and transverse passageway.

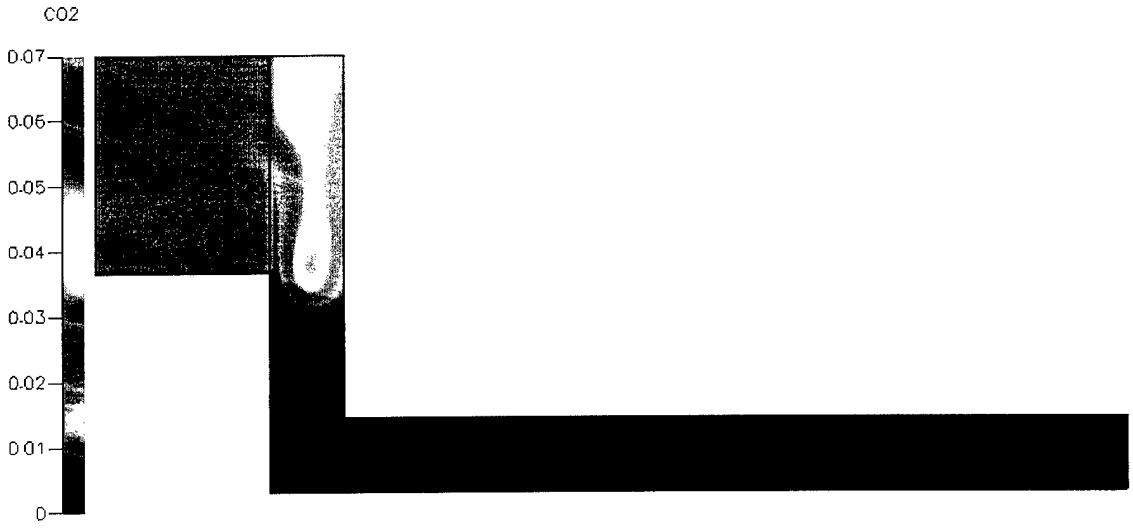

Figure 73. Simulation 5, plan view (D-D) depicting CO_2 (mass fraction) distribution throughout the structure.

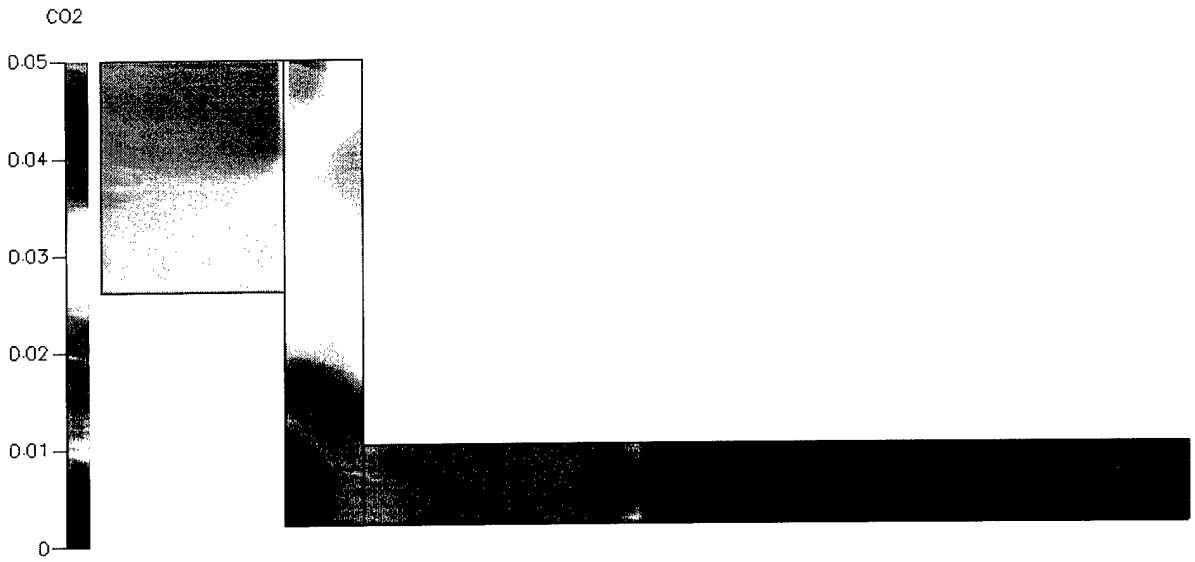

Figure 74. Simulation 5, plan view (E-E) depicting CO_2 (mass fraction) distribution throughout the structure.

APPENDIX F: SIMULATION 6

Simulation 6 uses the CFD combustion module to simulate a 620 kW fire. The overhead, deck and bulkheads of the structure are adiabatic. The inlet, burn pan and vent conditions are presented in Table 15. The gas mixtures for the inlet, burn pan and vent are shown in Table 16.

Inlet/ Outlet Boundary Conditions					
Location	U Velocity (m/s)	V Velocity (m/s)	W Velocity (m/s)	Relative Pressure (Pa)	Temperature (K)
Watertight Door Inlet	0	0	-0.5	0	300
Burn Pan	0	0.5	0	0	300
Vent	0	0	0	0	300
Bulkhead Boundary Conditions					
Location	U Velocity (m/s)	V Velocity (m/s)	W Velocity (m/s)	Wall Roughness (m)	Adiabatic / Isothermal
Interior Bulkheads	0	0	0	0.0005	Adiabatic
Exterior Bulkheads, Overheads, Deck	0	0	0	0.0005	Adiabatic

Table 15. Simulation 6, inlet, burn pan, vent, bulkhead boundary conditions.

	Inlet	Burn Pan	Vent
Mixture	Air	Propene/Air	Air

Table 16. Simulation 6, inlet, burn pan and vent mixture definition.

CFD program default solvers, inertial and linear relaxations, and variable limits are used to evaluate the model.

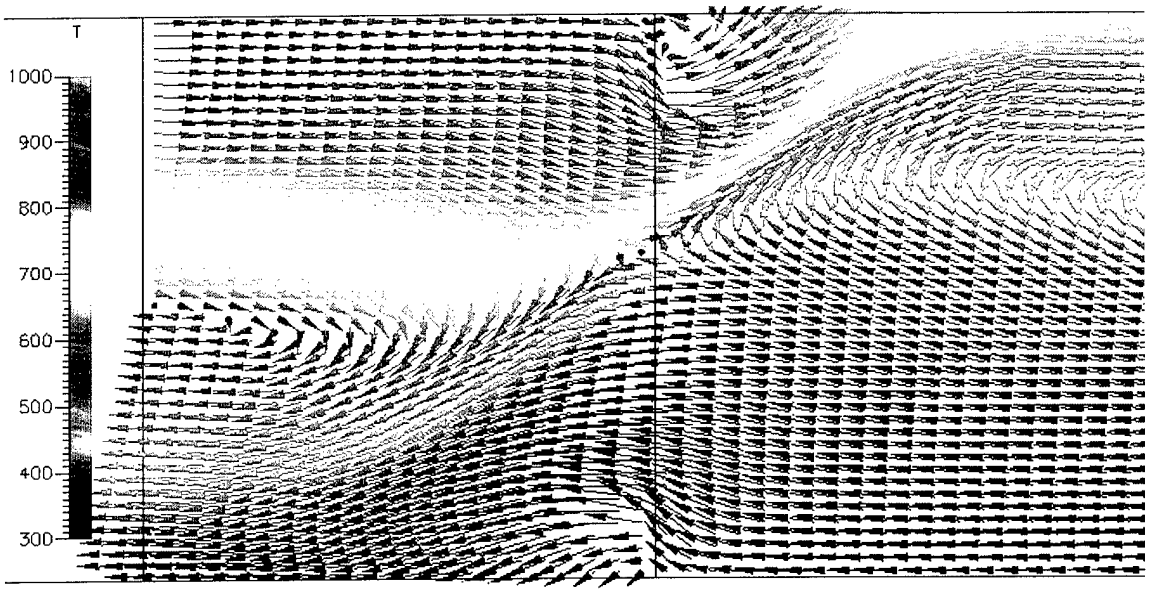

Figure 75. Simulation 6, partial elevation view (A-A) depicting temperature (K) distribution and fluid circulation pattern at the centerline of the longitudinal passageway in the vicinity of the watertight door.

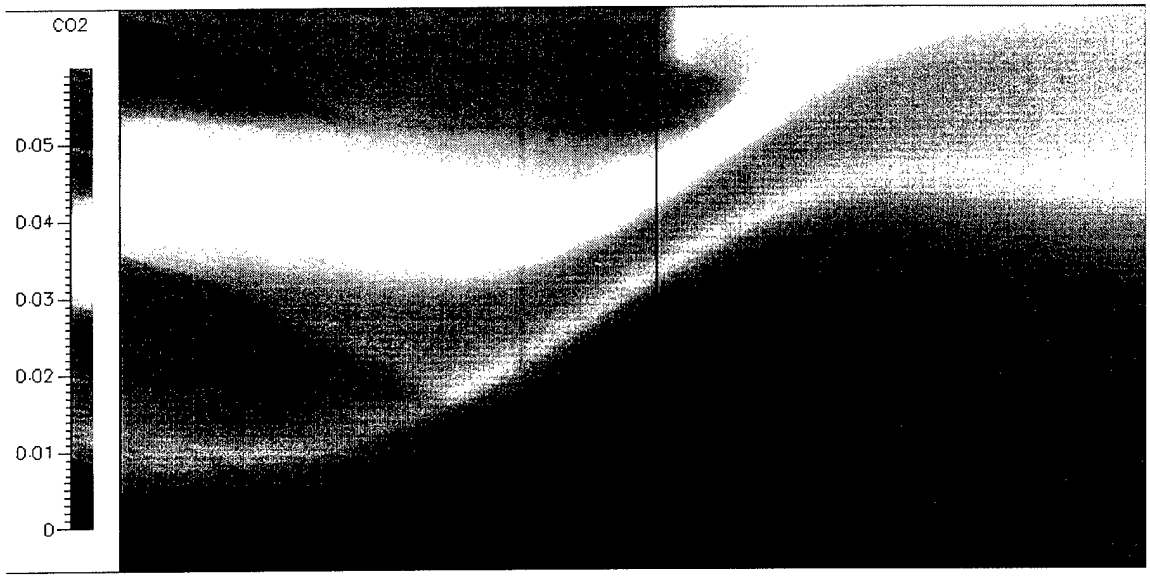

Figure 76. Simulation 6, partial elevation view (A-A) of CO_2 gas (mass fraction) propagation at the centerline of the longitudinal passageway in the vicinity of the watertight door.

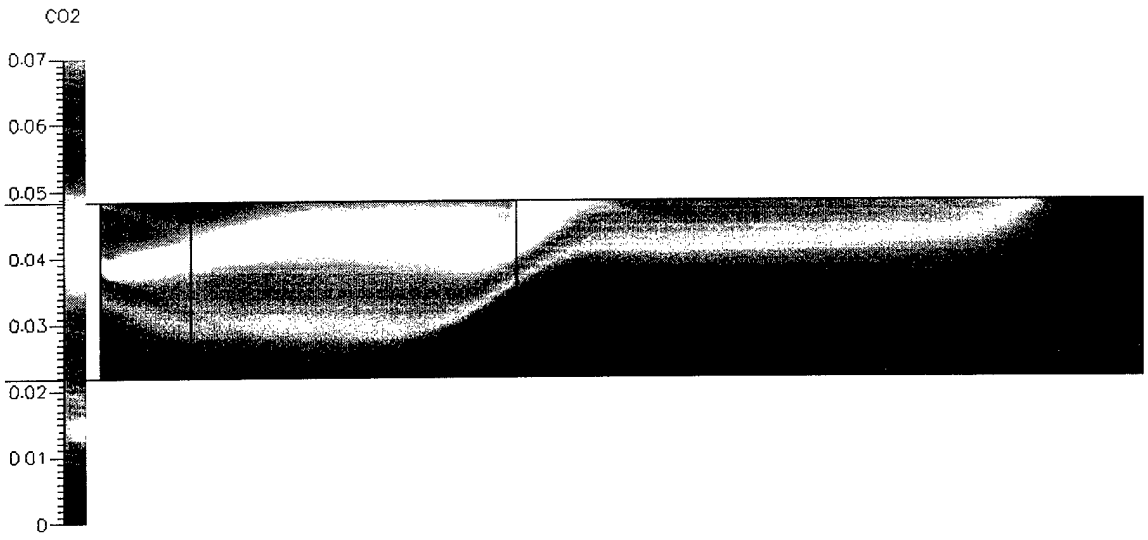

Figure 77. Simulation 6, elevation view (A-A) of CO_2 gas (mass fraction) propagation at the centerline of the longitudinal passageway.

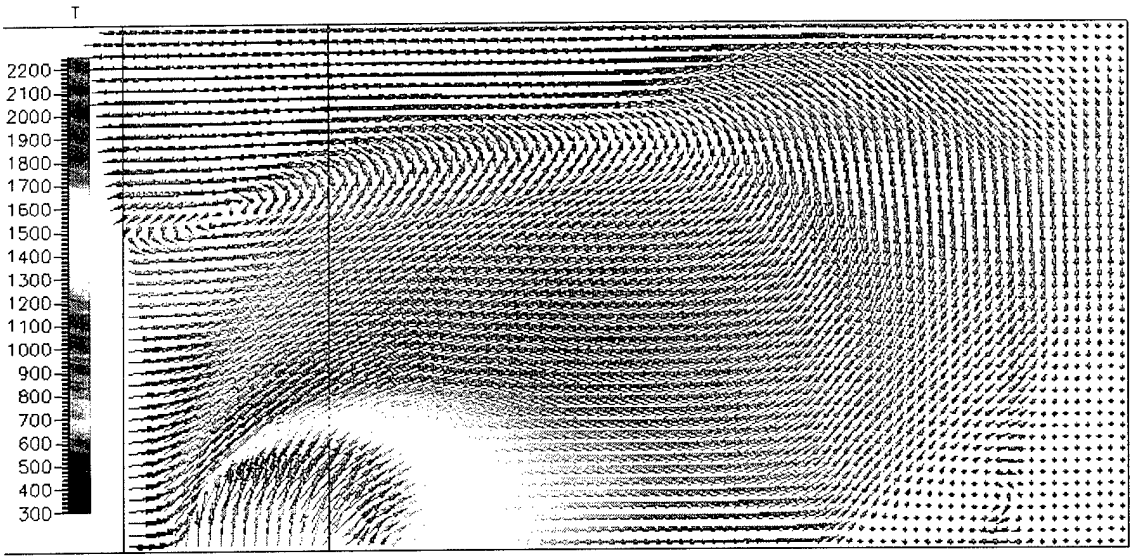

Figure 78. Simulation 6, partial elevation view (B-B) depicting temperature (K) distribution and fluid circulation pattern along the centerline of the transverse passageway on the port side.

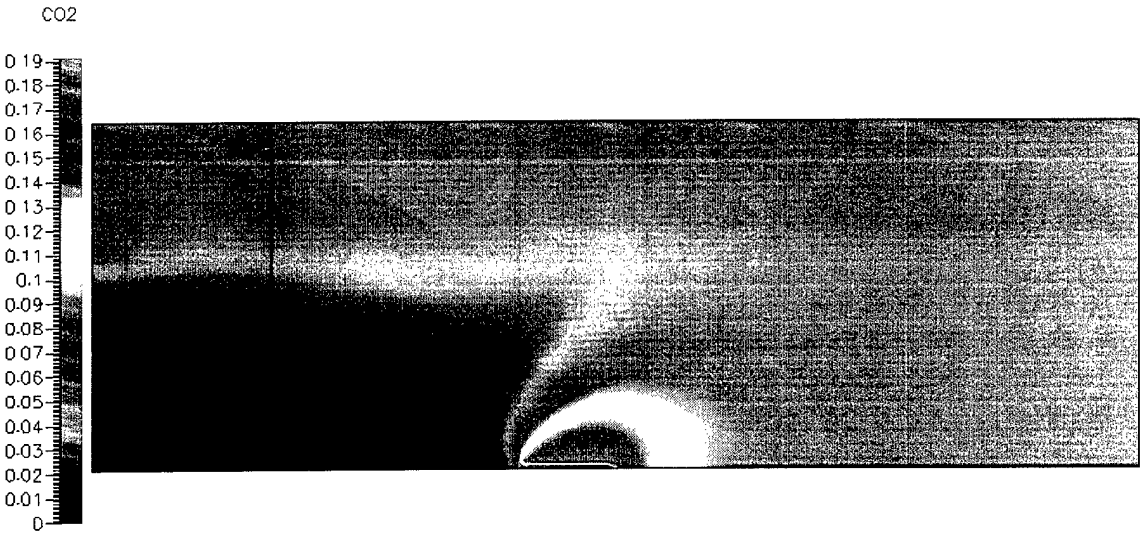

Figure 79. Simulation 6, elevation view (B-B) of CO_2 gas (mass fraction) propagation at the centerline of the transverse passageway.

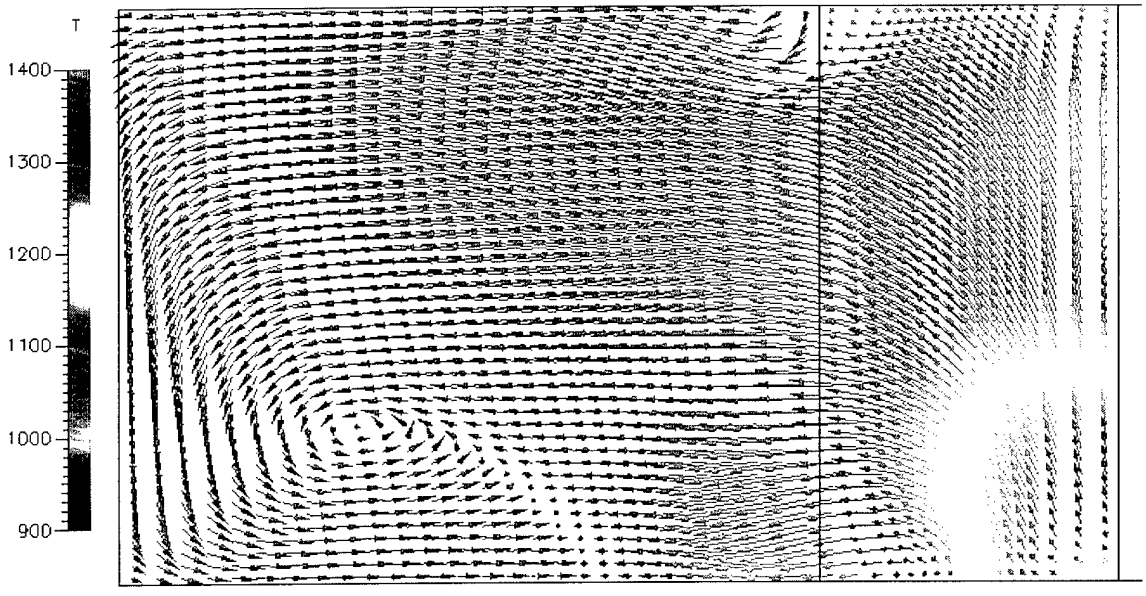

Figure 80. Simulation 6, elevation view (C-C) depicting the temperature (K) distribution and fluid circulation pattern through the centerline of the stateroom door from the transverse passageway.

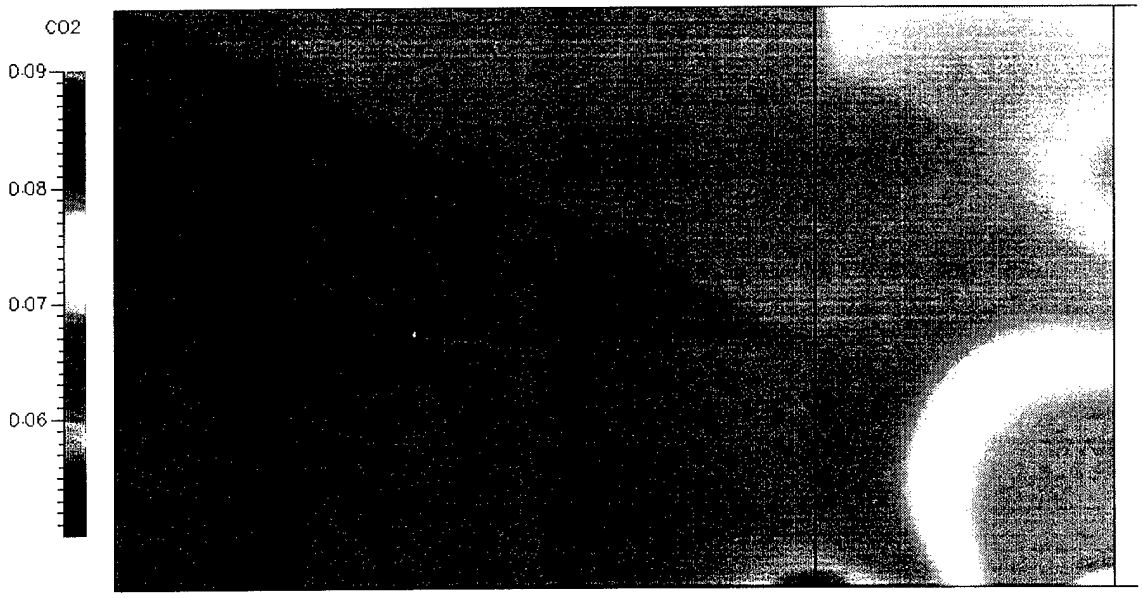

Figure 81. Simulation 6, elevation view (C-C) depicting CO_2 (mass fraction) distribution at the centerline of the stateroom door.

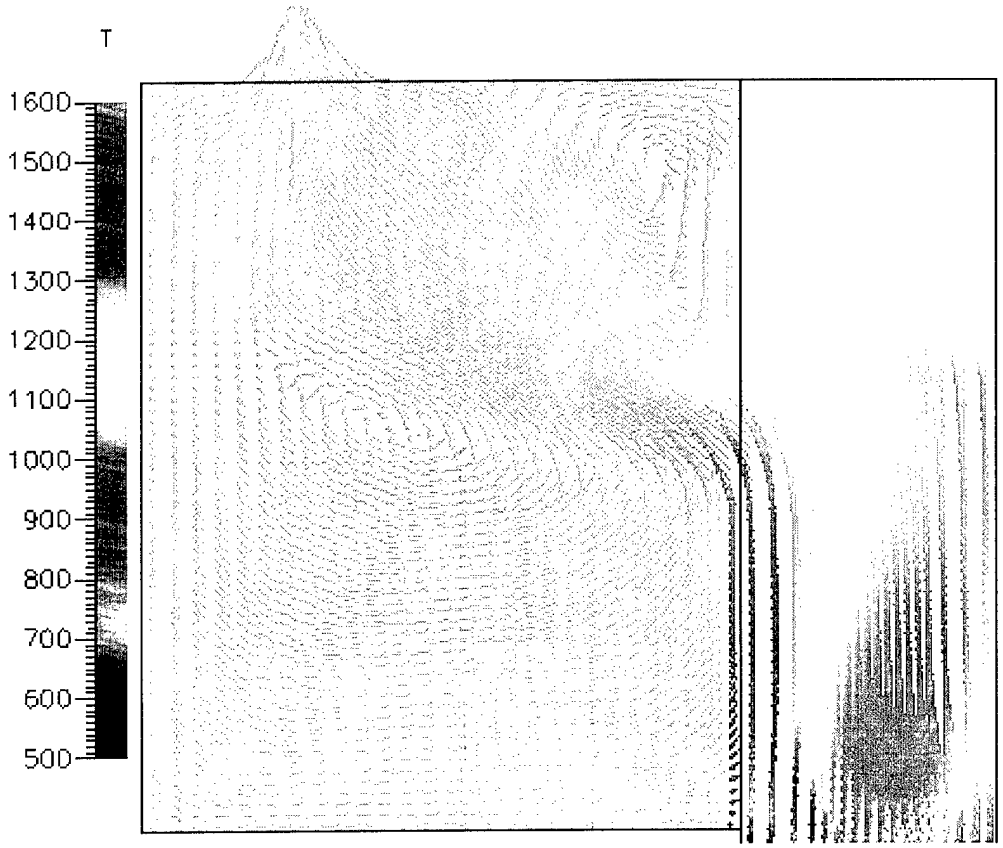

Figure 82. Simulation 6, partial plan view (D-D) depicting the temperature (K) distribution and fluid circulation pattern from the transverse passageway through the door into the stateroom.

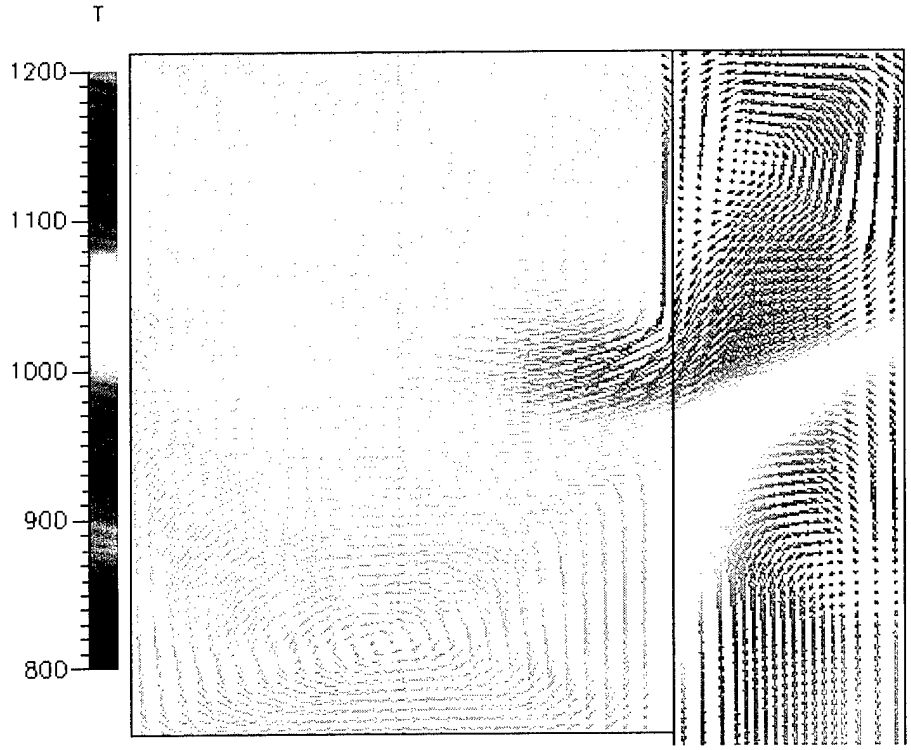

Figure 83. Simulation 6, partial plan view (E-E) depicting the temperature (K) distribution and fluid circulation pattern from the transverse passageway through the door into the stateroom.

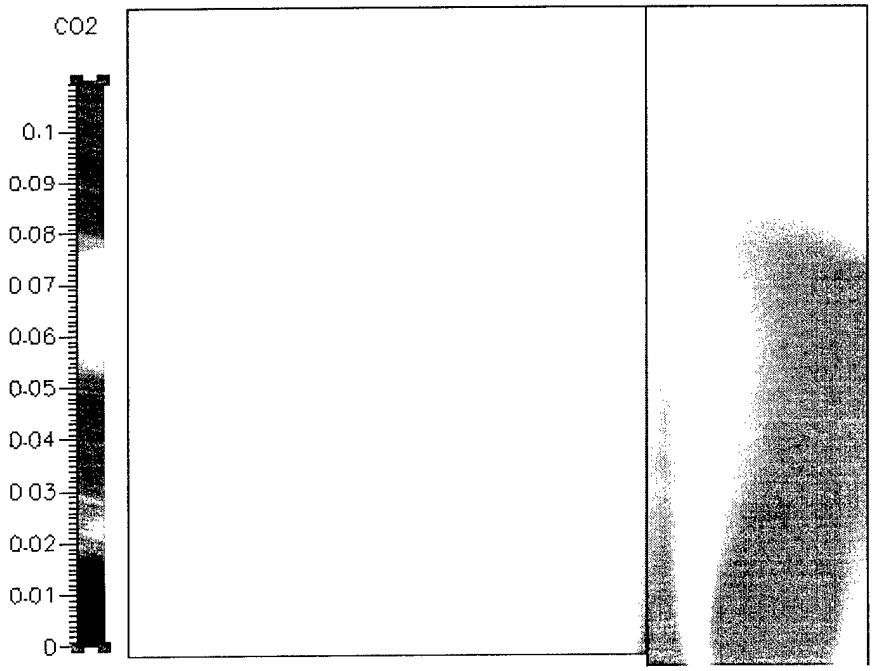

Figure 84. Simulation 6, partial plan view (D-D) depicting CO_2 (mass fraction) distribution in the stateroom and transverse passageway.

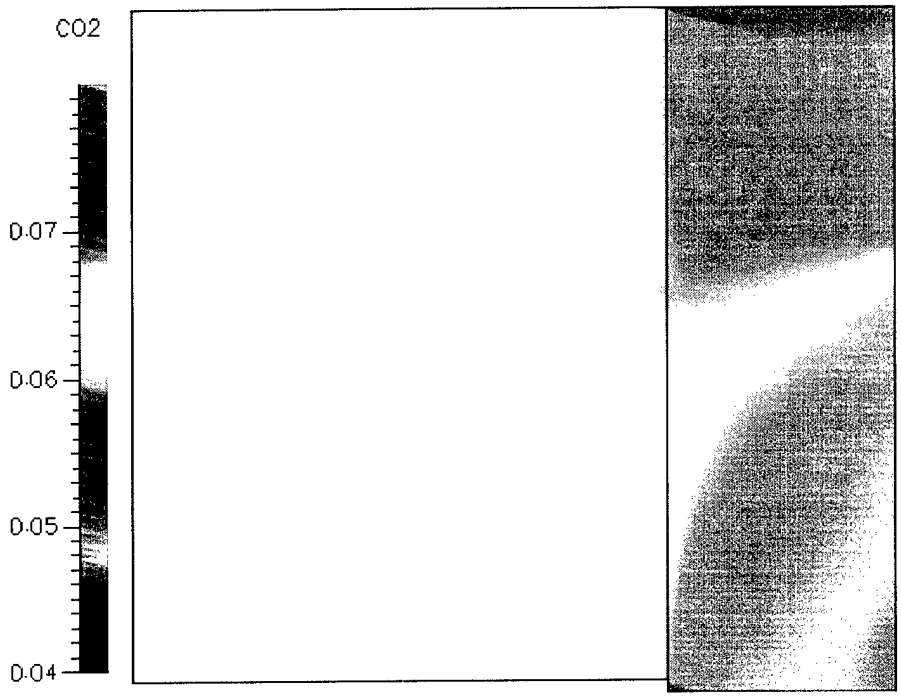

Figure 85. Simulation 6, partial plan view (E-E) depicting CO_2 (mass fraction) distribution in the stateroom and transverse passageway.

Figure 86. Simulation 6, plan view (D-D) depicting CO_2 (mass fraction) distribution throughout the structure.

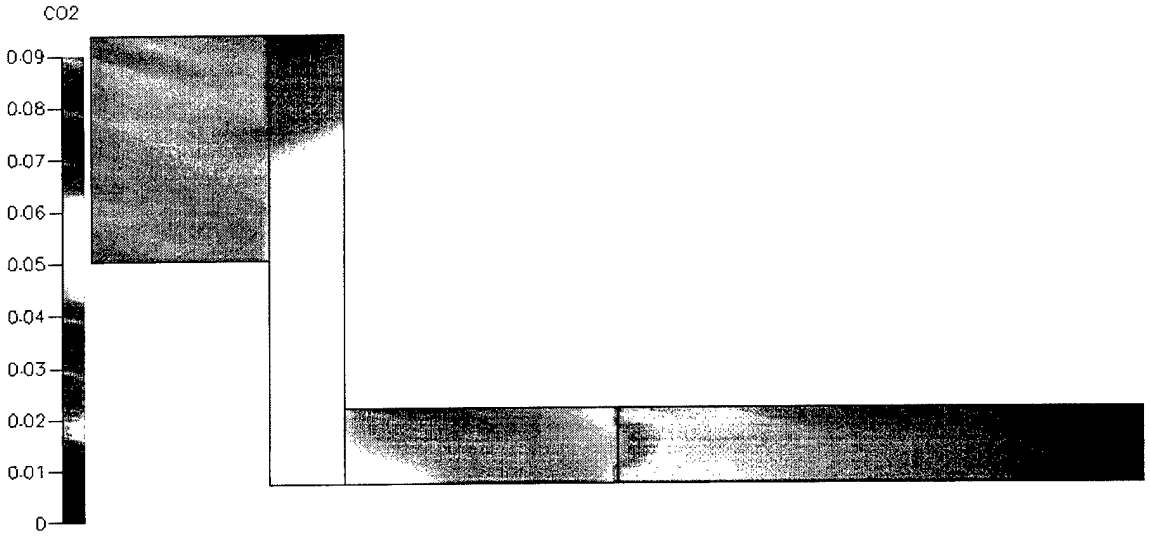

Figure 87. Simulation 6, plan view (E-E) depicting CO_2 (mass fraction) distribution throughout the structure.

APPENDIX G: SIMULATION 7

Simulation 7 uses the CFD combustion module to simulate a 620 kW fire. The overhead, deck and bulkheads of the structure are adiabatic. The inlet, burn pan and vent conditions are presented in Table 17. The gas mixtures for the inlet, burn pan and vent are shown in Table 18.

Inlet/ Outlet Boundary Conditions					
Location	U Velocity (m/s)	V Velocity (m/s)	W Velocity (m/s)	Relative Pressure (Pa)	Temperature (K)
Watertight Door Inlet	0	0	-2	0	300
Burn Pan	0	0.5	0	0	300
Vent	0	0	0	0	300
Bulkhead Boundary Conditions					
Location	U Velocity (m/s)	V Velocity (m/s)	W Velocity (m/s)	Wall Roughness (m)	Adiabatic / Isothermal
Interior Bulkheads	0	0	0	0.0005	Adiabatic
Exterior Bulkheads, Overheads, Deck	0	0	0	0.0005	Adiabatic

Table 17. Simulation 7, inlet, burn pan, vent, bulkhead boundary conditions.

	Inlet	Burn Pan	Vent
Mixture	Air	Propene/Air	Air

Table 18. Simulation 7, inlet, burn pan and vent mixture definition.

CFD program default solvers, inertial and linear relaxations, and variable limits are used to evaluate the model.

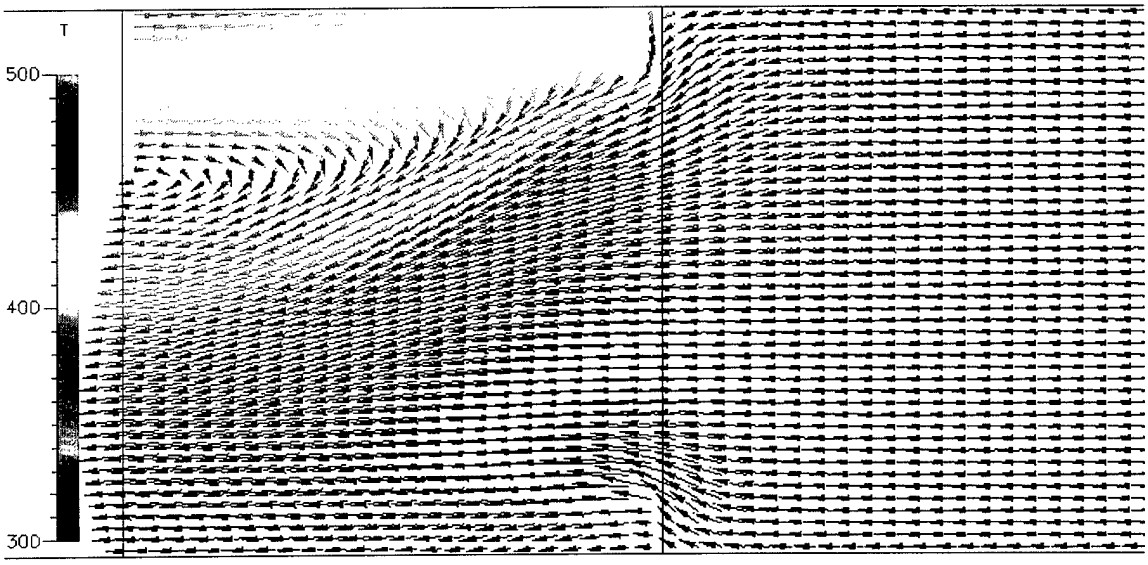

Figure 88. Simulation 7, partial elevation view (A-A) depicting temperature (K) distribution and fluid circulation pattern at the centerline of the longitudinal passageway in the vicinity of the watertight door.

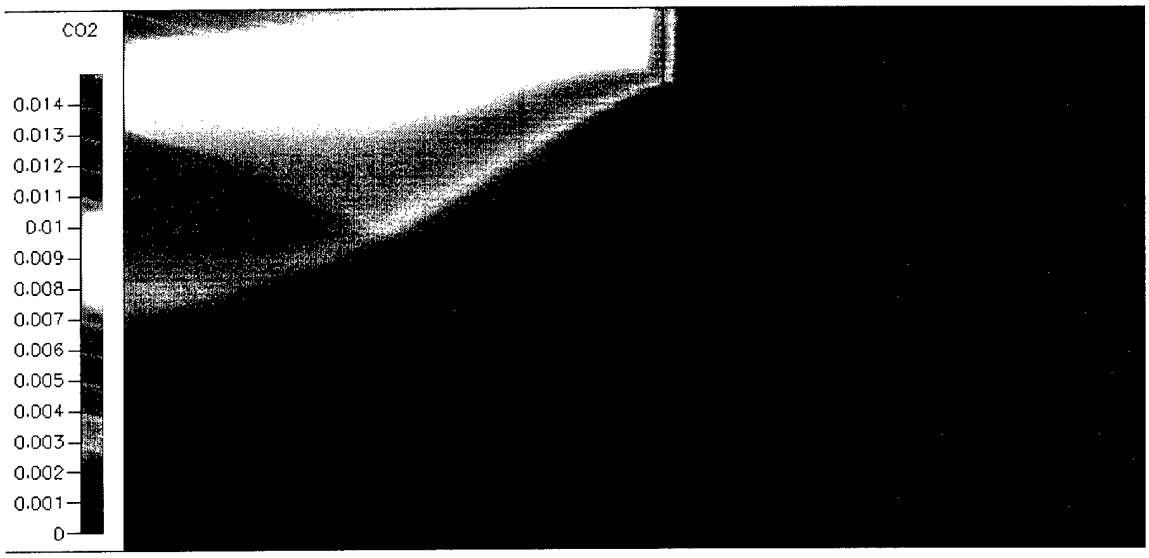

Figure 89. Simulation 7, partial elevation view (A-A) of CO_2 gas (mass fraction) propagation at the centerline of the longitudinal passageway in the vicinity of the watertight door.

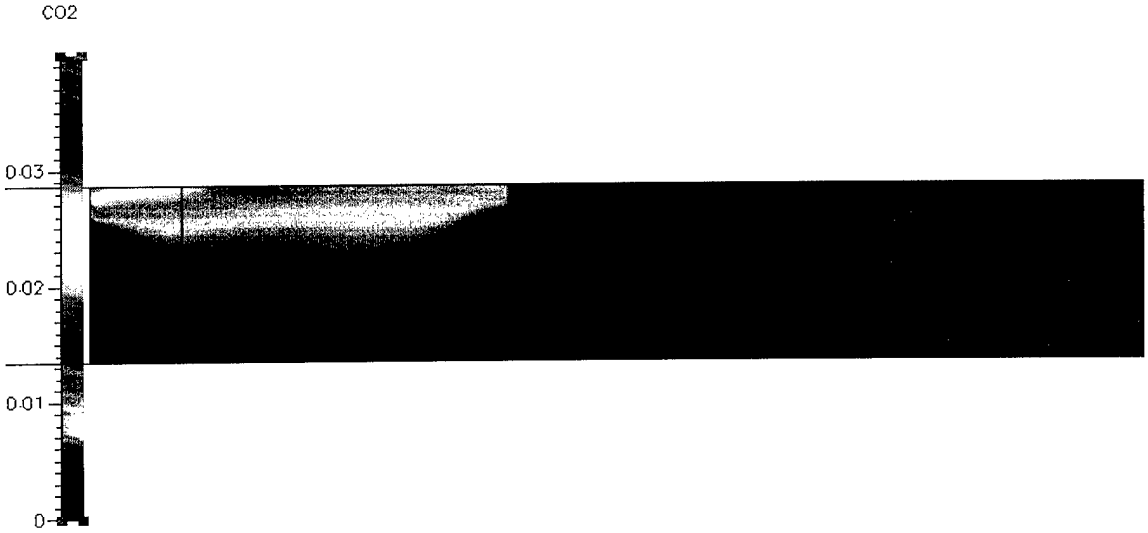

Figure 90. Simulation 7, elevation view (A-A) of CO_2 gas (mass fraction) propagation at the centerline of the longitudinal passageway.

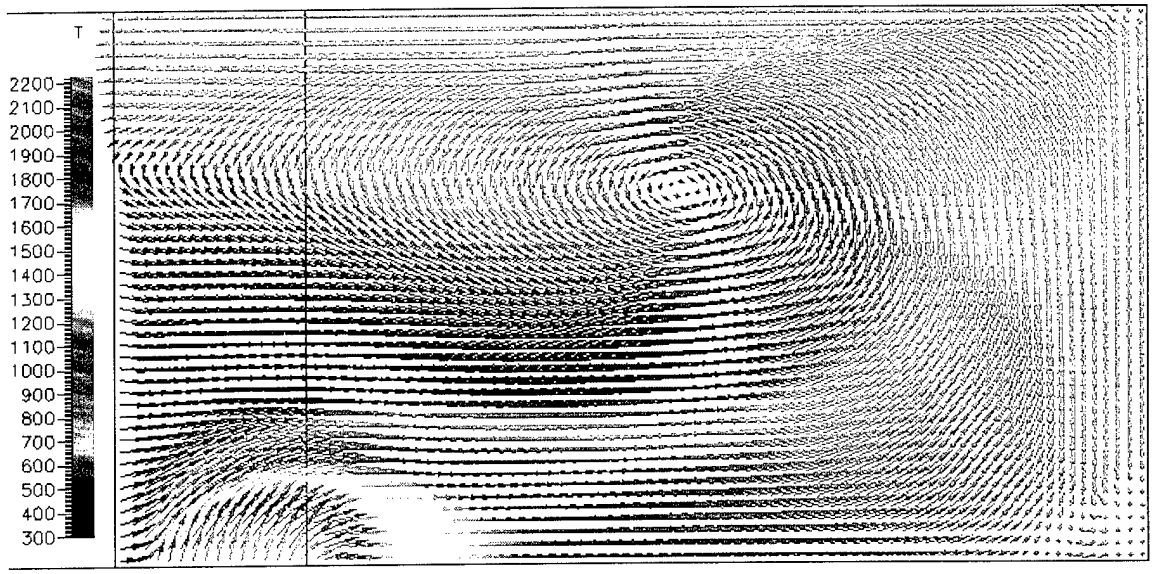

Figure 91. Simulation 7, partial elevation view (B-B) depicting temperature (K) distribution and fluid circulation pattern along the centerline of the transverse passageway on the port side.

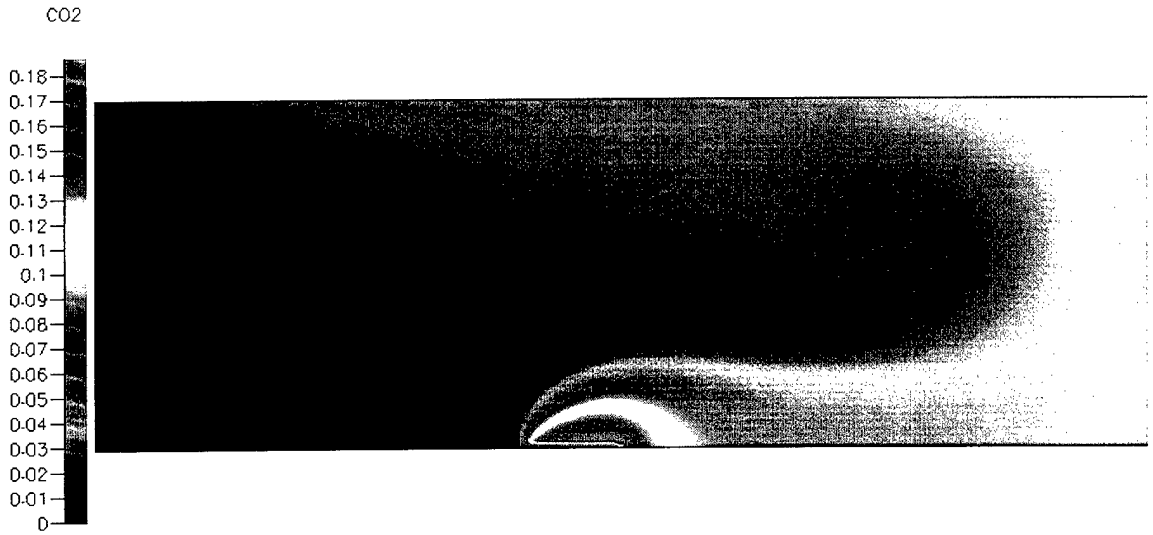

Figure 92. Simulation 7, elevation view (B-B) of CO_2 gas (mass fraction) propagation at the centerline of the transverse passageway.

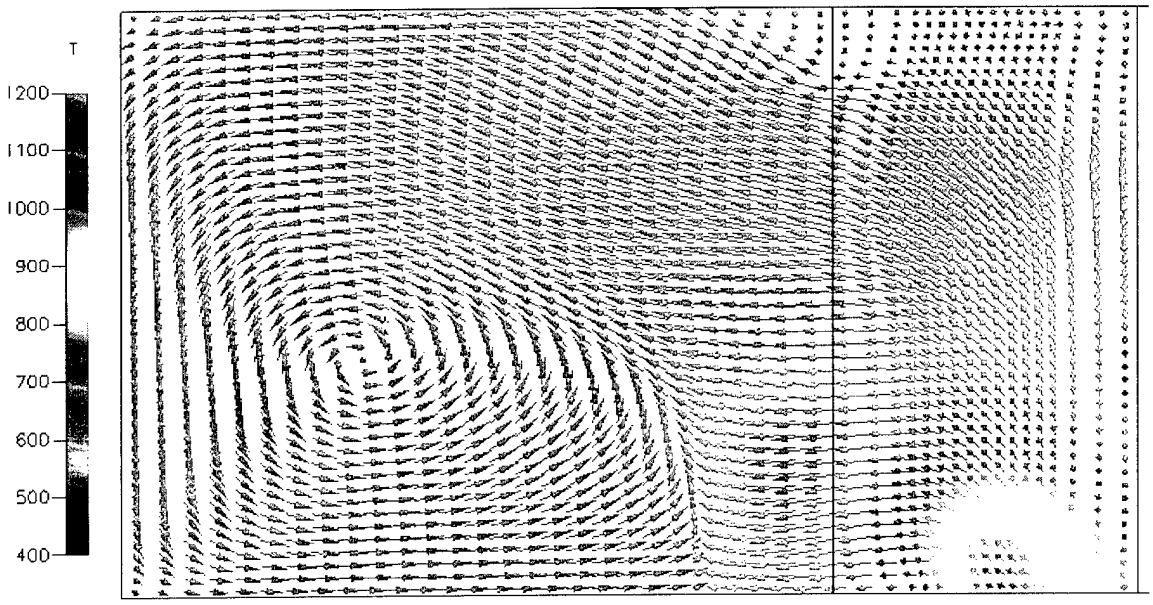

Figure 93. Simulation 7, elevation view (C-C) depicting the temperature (K) distribution and fluid circulation pattern through the centerline of the stateroom door from the transverse passageway.

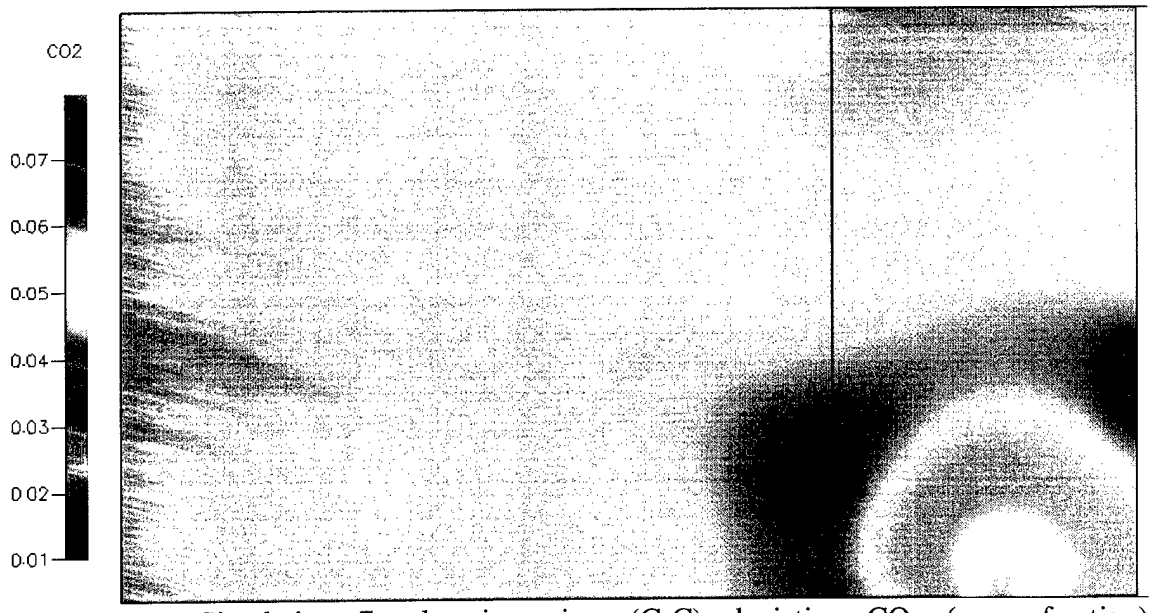

Figure 94. Simulation 7, elevation view (C-C) depicting CO_2 (mass fraction) distribution at the centerline of the stateroom door.

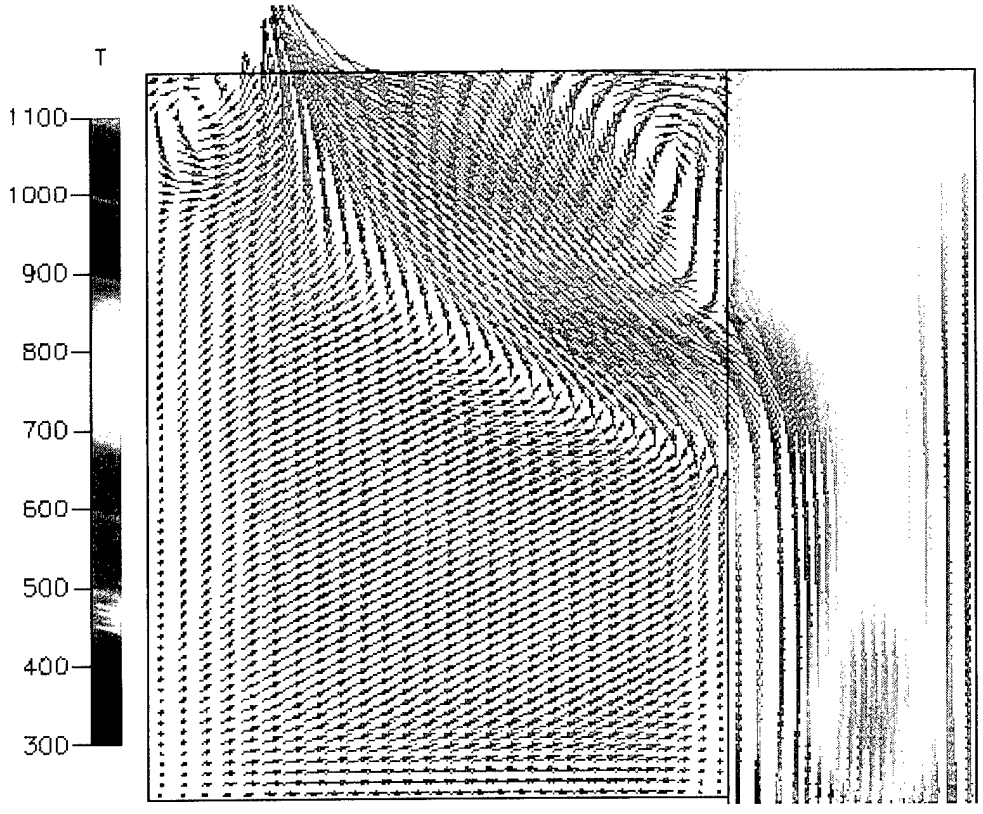

Figure 95. Simulation 7, partial plan view (D-D) depicting the temperature (K) distribution and fluid circulation pattern from the transverse passageway through the door into the stateroom.

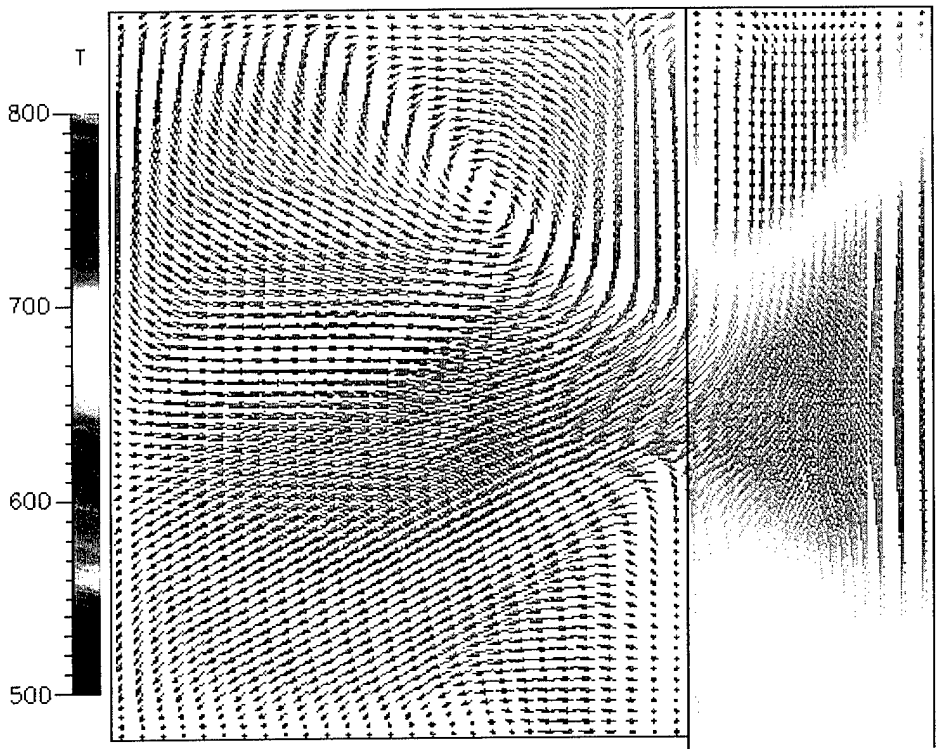

Figure 96. Simulation 7, partial plan view (E-E) depicting the temperature (K) distribution and fluid circulation pattern from the transverse passageway through the door into the stateroom.

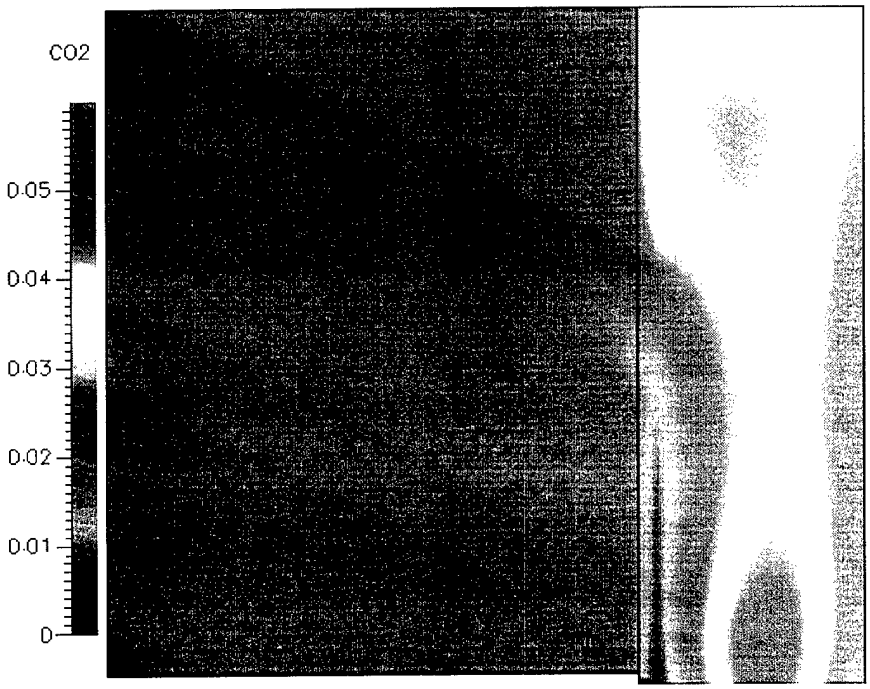

Figure 97. Simulation 7, partial plan view (D-D) depicting CO_2 (mass fraction) distribution in the stateroom and transverse passageway.

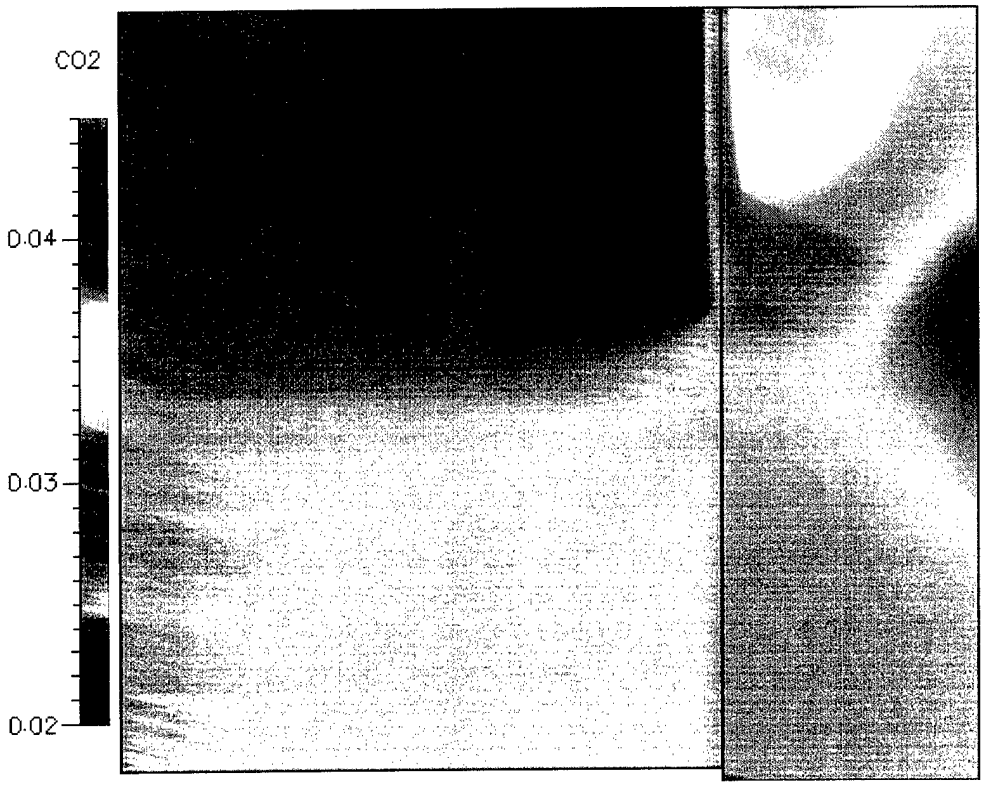

Figure 98. Simulation 7, partial plan view (E-E) depicting CO_2 (mass fraction) distribution in the stateroom and transverse passageway.

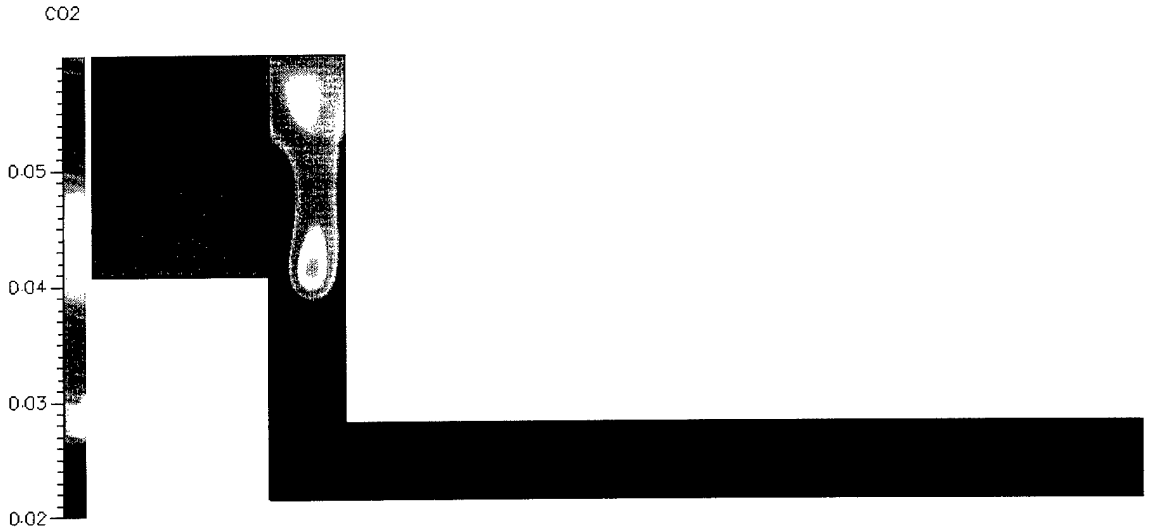

Figure 99. Simulation 7, plan view (D-D) depicting CO_2 (mass fraction) distribution throughout the structure.

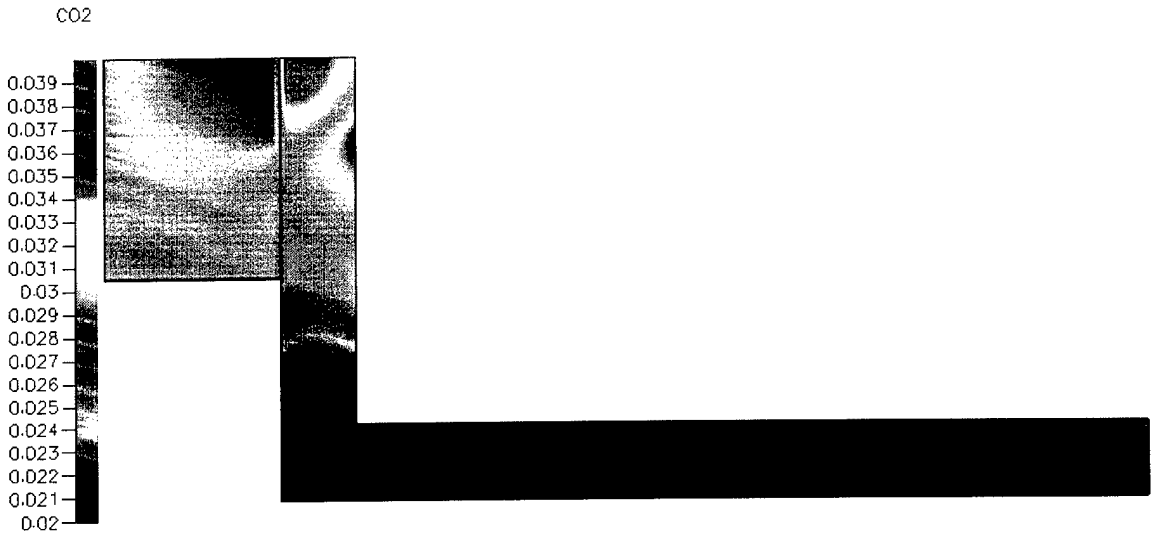

Figure 100. Simulation 7, plan view (D-D) depicting CO_2 (mass fraction) distribution throughout the structure.

INITIAL DISTRIBUTION LIST

1. Defense Technical Information Center 2
   8725 John J. Kingman Road, Suite 0944
   Ft. Belvoir, VA 22060-6218

2. Dudley Knox Library 2
   Naval Postgraduate School
   411 Dyer Road
   Monterey, CA 93943-5101

3. Engineering & Technology Curricular Office, Code 34 1
   Naval Postgraduate School
   Monterey, Ca 93943-5101

4. Department of Mechanical Engineering, Code ME 1
   Naval Postgraduate School
   Monterey, Ca 93943-5101

5. Professor Matthew D. Kelleher 1
   Mechanical Engineering Department, Code ME/KK
   Naval Postgraduate School
   Monterey, Ca 93943-5101

6. Garrett J. Farman 1
   227 West Center St.
   Medina, NY 14103

7. CFD Research Corporation 1
   Cummings Research Park
   215 Wynn Drive
   Huntsville, Alabama 35805

8. Dr. Fredrick W. Williams 1
   Navy Technology Center for Safety and Survivability
   Code 6180
   Naval Research Laboratory
   Washington, DC 20375

9. Dr. Patricia A. Tatem 1
   Navy Technology Center for Safety and Survivability
   Code 6183
   Naval Research Laboratory
   Washington, DC 20375